Durham E-Theses

Trimethylsilyl Substituent Effects on the Triazolium-catalysed Benzoin Condensation

MACRAE, HECTOR,IAN

Trimethylsilyl Substituent Effects on the Triazolium-catalyzed Benzoin Condensation

Hector Ian Macrae

A thesis submitted to the Durham University for the degree of Master of Science in the Department of Chemistry. 2021.

Table of Contents

Statement of copywrite

Acknowledgements

Dedication

To Bruce, Vanessa and Frankie Macrae with my heartfelt thanks.

Abbreviations

Ac	acetyl	m.	multiplet (spectral)
Ad	adamantly	*m-*	*meta*
Ar	aryl	Me	methyl
br.	Broad (spectral)	MS	mass spectrometry
Bu	butyl	m.p.	melting point
°C	degree centigrade	min	minute(s)
δ	chemical shift	mL	mililitre(s)
d	doublet (spectral)	mmol	millimole(s)
DBAD	di-tert-butyl azodicarboxylate	mol	mole(s)
		m/z	mass /unit charge
DCM	dichloromethane	NaOH	sodium hydroxide
Dip	diindenoperylene	NHC	N-heterocyclic carbene
DMSO	dimethylsulfoxide	NMR	nuclear magnetic resonance
D2O	deuterium oxide	NOE	nuclear overhauser effect
EA	elemental analysis	*o-*	*ortho*
Et	ethyl	*p-*	*para*
EtOAc	ethyl acetate	Ph	phenyl
g	gram(s)	PhCHO	benzaldehyde
GC-MS	gas chromatography with mass spectrometry	ppm	parts per million
		R	alkyl substituents
HCl	hydrochloric acid	Rt	retention time
1H NMR	proton nuclear magnetic resonance	r.t.	room temperature
		R_f	retention factor
H	hour(s)	ρ	reaction constant
HPLC	high performance liquid chromatography	σ	substituent constant
		s	second(s)
Hz	hertz	t	triplet (spectral)
^{i}Pr	isopropyl	TBAF	tetrabutylammonium fluoride
J	coupling constant		
J	joule(s)	t-, tert-	tertiary
K	rate constant	THF	tetrahydrofuran
K	equilibrium constant	TLC	thin layer chromatography
K_a	acidity constant	TMEDA	tetramethylethylene diamine
K_{ex}	experimental rate of reaction		
		UV	ultraviolet
λ	wavelength	Vis	visible
L	litre(s)		
LC-MS	liquid chromatography with mass spectrometry		
ln	natural logarithm		
log	logarithm (base 10)		
M	molar (moles/litre)		

Abstract

In the benzoin condensation catalysed by N-heterocyclic carbenes (NHCs) there exists a unique 2-substituent effect. 2-Substituted aldehydes with 2-Lewis basic substituents will preferentially take part in the first addition step of NHC to aldehyde, though the relative contributions of steric and electronic factors are unknown. The aim of this project was to further probe the origin of this 2-substituent effect, and to investigate the influences of sterics and Lewis acidity on the N-aryl substituent of pyrrolidine derived triazolium NHCs. By substituting trimethylsilyl groups into the 2-position of benzaldehyde we sought to identify the nature of the 2-substituent effect. The substituent effect was investigated by examining 2-silyl substituent effects on homo and cross benzoin type condensations. It was discovered that a 2-substituent reduces the rate of the benzoin condensation in the case of a 2-trimethylsilyl substituent. Thus, it appears that the 2-substituent effect varies depending on electronic nature, as benzaldehyde with sterically crowded and Lewis acidic 2-positions have reduced activity in the benzoin condensation, as opposed to what has been observed for the 2-substituent effect with Lewis basic substituents.

Two NHC precursors, 6,7-Dihydro-2-(3-chlorophenyl)-5*H*-pyrrolo[2,1-*c*]-1,2,4-triazolium tetrafluoroborate **142** and 6,7-Dihydro-2-(4-bromophenyl)-5*H*-pyrrolo[2,1-*c*]-1,2,4-triazolium tetrafluoroborate **144**, were isolated with the intent to substitute trimethylsilyl groups onto the N-aryl group.

The pK_as of the novel NHCs were identified, and efforts to substitute trimethylsilyl groups onto these are ongoing. These results indicate that that silyl groups present challenges for examining the benzoin condensation, and that the 2-silyl substituent effect differs from other 2-heteroatoms examined to date. Further work is necessary to explore the origin of this difference in behaviour.

1   Introduction

1.1   Early work in the field of carbene chemistry

Carbenes are a diverse group of functionalised formally divalent carbon centres, with uses in a variety of reactions. Through careful choice of substituents the carbenes can be tuned to exhibit either ambiphilic or diradical character. This permits nucleophilic function or insertion across σ- or π-bonds, respectively. Carbenes can be electrophilic or nucleophilic in nature. Carbenes can be either singlet or triplet, **Figure 1.1**.
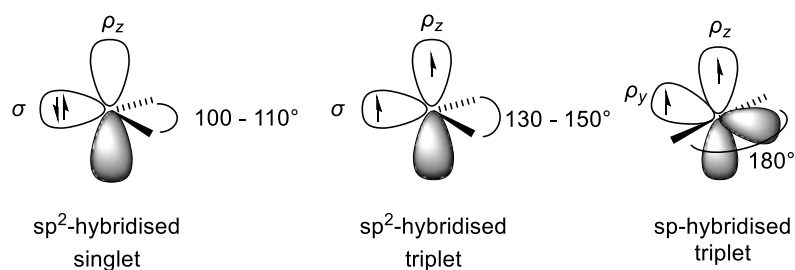
Figure 1.1   Hybridisation of carbenes showing singlet and triplet carbene states.

During a discussion of the nomenclature of carbenes (specifically methylenes) Hine[1] suggested that the definition of carbene could include carbon centres where the carbene reactivity has been masked by multiple bonding between neighbouring centres, if there exists a stable analogous dimer, or a 4-coordinate system that appears to have arisen from the insertion of a carbene into a sigma bond.

This definition was later expanded upon by Vasiliu *et al.*[2] by characterising carbenes by their hydrogenation energies. The most stable carbenes have both large singlet-triplet splittings and low hydrogenation energies. In this study it was identified that imidazolium-derived N-heterocyclic carbenes (NHCs) have the most stable singlet ground states, with both the lowest hydrogenation energies, and the largest singlet-triplet gap.

The seminal discovery of a stable N-heterocyclic carbene (NHC) **1** was in 1991 by Arduengo *et al.*[3] This carbene has a core of an imidazolium heterocycle, with two N-adamantyl groups. This carbene was stable to heating, water, oxygen, and could be formed from **2** by deprotonation, and reprotonated without degradation of the structure. It was the first "bottle-able", bench stable NHC and could be fully characterised.
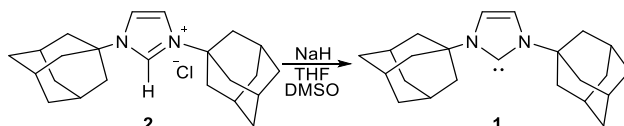
Scheme 1.1 Formation of 1,3-di-1-adamantylimidazolylidene 1 from 1,3-di-1-adamantylimidazolium chloride 2 by deprotonation.

Three years prior to this, a stable phosphinosilyl carbene **3** was isolated by Bertrand and co-workers[4]. This carbene was isolated as a red oil and was stable for weeks at room temperature when solvated in benzene. However, it lacked the central heterocyclic core of the NHCs. The surprising stability of both this carbene, and of the synthetically produced NHC **1** allowed for closer scrutiny of related structures and their potential in the fields of both catalysis and metal ligands.
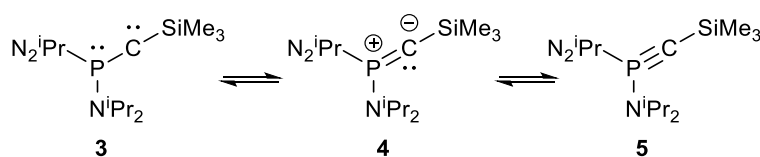
Scheme 1.2 Resonance structures of phosphinocarbene **3**, **4**, **5**.

In contrast to these findings about N-heterocyclic carbenes, the phosphinosilyl carbene **3, 4, 5**[5], with phosphorus substituents on the carbon centre, display higher hydrogenation energies and smaller singlet-triplet gaps, showing lower stability than the imidazolyl analogues. Planarity around the adjacent heteroatom is required to allow

donation of electron density into the empty p-orbital at the carbon centre to stabilise the singlet state and allow for hydrogenation, which is more difficult to achieve for P- relative to N-heterocyclic analogues. For example, in 1,3-di-1-adamantylimidazolylidene **1**, the lone pairs of the nitrogen atom can donate into the unoccupied p-orbital of the carbene, stabilising the singlet state.

Seppelt thiaacetylene/sulfauranyl carbenes[6], **Figure 1.2**, appear to be energetically similar to the Bertrand carbenes, requiring adjustments of the calculations for altered geometries at the sulfur centre[2].

6
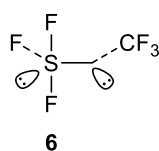
Figure 1.2 Lone pair oribitals of trifluoroethyldynesulfur trifluoride, **6**, identified by Pötter and Seppelt in 1984**[6]**.

With the (phosphino)(aryl) carbenes[7] (Bertrand carbenes) the phosphino group brings enough stabilisation to the molecule to allow for characterisation under standard laboratory conditions, **Figure 1.3**. The phosphino group functions as a weak σ-, and π-donor substituent, whereas the function of the aryl group within the molecule depends largely on the sterics and electronics of this substituent. The more sterically hindered aryl groups, particularly ones that sterically crowd the carbene carbon centre, have a larger propensity to form a stabilised push pull structure. In contrast to this, aryl substituents, with less steric hindrance, behave more as spectator substituents. If the aryl ring is electronically enriched with amino derived groups, to have an electron donating effect, a push-push system is formed instead. However in this scenario, the π-donation effects of the phosphino and aryl groups are not additive, but instead have an overall destabilising effect

on the molecule[8]. This causes the resultant carbene to be highly reactive and unstable although this destabilisation with resonance donation is initially counterintuitive, due to opposing inductive effects of the substituents. The phosphino groups function as σ-donors and the amino groups as σ-acceptors.
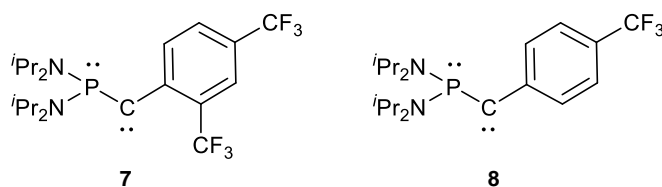
Figure 1.3   Example structures of (Phosphino)(aryl) carbenes[7].

The first carbene transition-metal complex was discovered in 1925 by Chugaev[7], predating these stable carbenes by over six decades, though it was not recognised as such at the time of its discovery. Since then, carbenes have become very attractive as ligands for transition metal complexes, to a greater extent than in their use as catalytic molecules.

The direct reactivity of carbenes as catalysts was initially studied by Breslow in 1958[9]. The mechanism of catalysis of the benzoin condensation by the cofactor thiamine **9** was identified, as was the key catalytic intermediate, enaminol **10**. This structure would later become known as the Breslow intermediate, **Figure 1.4**. Following this it was not until 1991[3] that the azolium derived NHCs would again come under scrutiny, this time with the imidazolium skeleton. Research into azolium derived carbenes has grown to include imidazolinium, triazolium and, to a lesser extent, piperazine derived triazoliums, as well as the previously mentioned thiazolium and imidazolium derived carbenes[10].
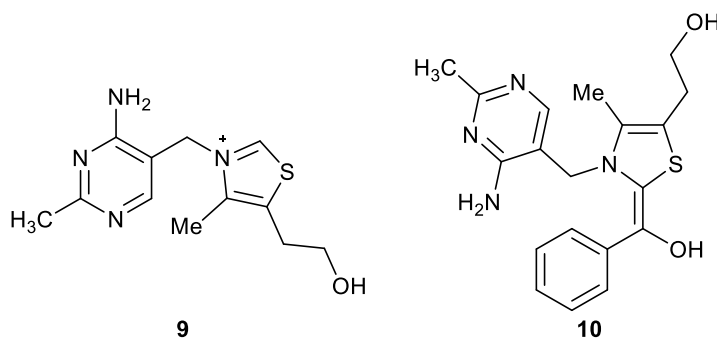
Figure 1.4 Structures of the thiamine cation **9** and proposed thiamine-derived Breslow intermediate **10**.

Though the imidazolium derived carbenes have found most use as metal ligands[10], the thiazolium and triazolium derived carbenes have seen much more use in the field of small molecule organic catalysis, *e.g.* in the benzoin and Stetter condensations[10]. The more acidic nature of the triazolyl and thiazolyl species facilitates the formation of the NHC-aldehyde complex required for these reactions. Triazoliums typically display a much higher reactivity than other carbene precursors in this reaction pathway. The central heterocycle in NHCs allow for sensitive modifications to be made to the reactivity of the carbene with changes to the substituents on the ring. This allows for fine tuning of the reactivity with regard to stereoselectivity and regioselectivity for the formation of the desired product, making these heterocycles a very attractive option for designing catalyst structures.

The NHC-catalysed reaction of an aldehyde with a Michael acceptor was later documented, and has since been known as the Stetter reaction[11]. Other potential routes for reaction have been researched more recently, such as the functionalisation of epoxy aldehydes into activated carboxylates (by Chow and Bode)[12] with stereoselective formation of the *anti*-aldol product, the formation of α-amido ketones from acylimines (Murry,

Frantz and co-workers)[13], oxidative esterification (Connon and co-workers)[14], and the sila-Stetter reaction using acylsilanes as aldehyde surrogates (Scheidt and co-workers)[15,16].

Of particular success in this area have been triazolyl N-heterocyclic carbenes derived from triazolium ions by deprotonation, which will be the subject of this thesis.

1.2　The electronic properties of carbenes

Carbenes are neutral divalent carbon species. Of the six valence electrons on the carbenic carbon, four are involved in bonding to substituents, with the other two electrons in non-bonding orbitals. The non-bonding electrons can either be paired in an orbital, or can be unpaired, occupying separate orbitals. Carbenes can exist in one of two states: the singlet state, where the non-bonding electrons are paired in one orbital, or the triplet state, where the electrons are unpaired in two separate orbitals. Carbenes can occupy either bent or linear geometries and, though the geometry of the carbene affects multiplicity, there are carbenes of both geometries in each state. The geometry of the carbene is largely determined by the extent of hybridisation at the carbon centre[17].

Linear carbene systems are less common than other geometries. The sp hybridisation state is the basis of these bonding orbitals of these carbenes, with two bonding σ orbitals. There are also two non-bonding orbitals, p_y and p_z[17]. In this geometry the degeneracy of the orbitals ensures the non-bonding electrons remain unpaired, with each occupying a separate p orbital to mitigate electrostatic repulsive forces of the electrons. This geometry of a carbene is generally an extreme case, limited to highly sterically hindered carbenes, because of the highly reactive nature of the unpaired electrons. Furthermore, the substituents bonded to the carbon centre in these carbene systems do not generally provide any electronic stabilisation to the carbene[17].

Nonlinear carbenes are the most common of the possible geometries of carbenes. These are based upon the trigonal sp^2-hybridisation state of the carbon centre. This results in a bent geometry, with bond angles between 100˚ - 150˚. In this geometry the non-bonding σ and p_z are not degenerate, so the carbenes can have either a singlet state, with the non-bonding electrons paired in the same orbital, or triplet ground state multiplicity, with the non-bonding electrons occupying separate orbitals. The multiplicity of the carbene is highly dependent on the substituents bound to the carbon centre. The ground state multiplicity of carbenes strongly dictates their reactivity, with triplet carbenes exhibiting diradical behaviour with their two singly occupied p-orbitals. Conversely, singlet state carbenes possess ambiphilic character, due to having an orbital filled with a lone pair as well as a vacant orbital.

The ground state multiplicity of carbenes is determined by the relative energy of the σ and p_z orbitals. The singlet state is favoured when the gap between these two energy levels exceeds the pairing energy for the electrons. If the energy gap between these energy levels exceeds this value, the carbene is more likely to exhibit singlet ground state multiplicity. The size of the σ-p_z is influenced by the electronic characteristics of neighbouring substituents. The type and extent of these influences can be divided into two broad categories: inductive and mesomeric[17].

1.3   Inductive and mesomeric substituent effects

Inductive effects interact with the σ orbital, without affecting the p_z orbital. Inductively electron withdrawing groups stabilise the σ orbital increasing the σ-p_z gap, and therefore favour the singlet state. Conversely, inductively electron donating groups destabilise the σ orbital, increasing the energy level of the σ orbital. This causes a decrease in the σ-p_z energy gap, and so the triplet state is more likely to be favoured.

Bent singlet carbenes are strongly stabilised by resonance effects owing to interactions between the empty p_z orbital on the carbon, and the lone pairs on adjacent atoms. Mesomeric substituents for carbenes include amines, alkoxides, halides and sulphides. The π-donation from adjacent atoms increases the electron density in p_z, destabilising this energy level and thus increasing the σ-p_z gap. As such, π-donation from adjacent atoms favours singlet ground state multiplicity and examples include dihalocarbenes, dimethoxycarbenes and diaminocarbenes[18–20].

One of the earlier classes of carbenes to be studied was dihalocarbenes. These carbenes are predominantly formed transiently in insertion reactions from relatively accessible starting materials in most cases. Difluorocarbenes were studied by Mitsch *et al*[18] using both photolytic and pyrolytic methods of formation to generate the difluorocarbene **12** from the relevant difluorodiazirine **11** (**Scheme 1.3**). A high propensity to insert into double bonds in a stereospecific fashion was demonstrated indicating singlet carbene character, as was suggested by the substitution of the carbenic carbon. These singlet carbenes display an affinity for reactions with styrenes[19].
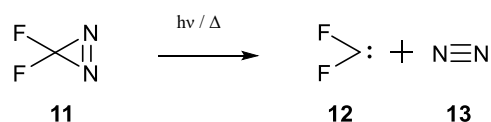
Scheme 1.3   Photolytic or pyrolytic formation of difluorocarbene from difluorodiazirine.

Dialkoxycarbenes were studied in detail in 1988 by Moss *et al*[20]. In contrast to difluorocarbenes, which exhibit ambiphilic and electrophilic characteristics, dialkoxycarbenes **14** exhibit nucleophilic characteristics. As with the difluorocarbenes, these molecules were formed from the relevant dimethoxydiazirine, using photolysis by ultraviolet light. The stabilities of these carbenes, and related compound fluoromethoxycarbene, have been studied in a variety of solvents by laser flash

photolysis[21]. The rate of reaction of dimethoxycarbene with the alcohols spanned from 3.2 x 10^4 s^{-1} (ethanol) to 6.7 x 10^8 s^{-1} (hexafluoroisopropyl alcohol) at room temperature, with solvent effects demonstrating a large influence.

Diaminocarbenes are the most common form of N-heterocyclic carbenes used as metal ligands and catalysts, owing to the stability of the singlet state, with structures employing imidazolium, triazolium and other azolium structures, as well as unconjugated cyclic frames. These diaminocarbenes are typically either imidazolium derived structures **15**, or 1,2,4-triazolium derived structures **16**.
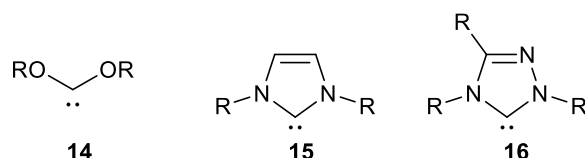
Figure 1.5 Generalised structures of dialkoxycarbenes **14**, imidazole-2-ylidenes **15**, and 1,2,4-triazol-3-ylidenes **16**.

Carbenes with two π-acceptor substituents have predicted singlet multiplicity with linear geometry. Examples of these are di(trifluoromethyl) (**17**), diboroalkanes (**18**), disilanes (**19**) and diphosphenes (**20**).
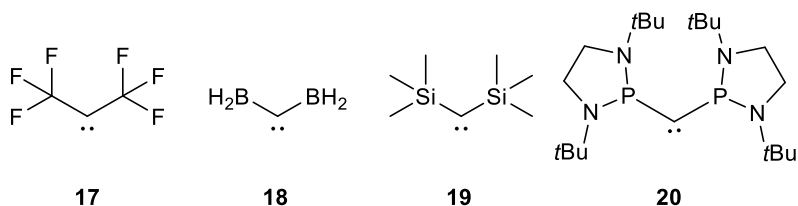
Figure 1.6 Structures for ditrifluoromethylcarbene **17**, diborohydrocarbene **18**, ditrimethylsilylcarbene **19**, and dibis(*tert*butyl)diazophospholidinecarbene **20**.

The symmetric interaction between the empty p orbitals on the α-substituents and the occupied p orbitals at the carbene centre breaks the p orbital degeneracy of linear sp

state carbene systems. This gives the carbene a singlet state with a two-electron, three-centre π-resonance system. Though no carbenes of this family have been isolated, reactivity that supports their existence have been found in some species, namely transient dicarbomethoxycarbenes (**21**)[22,23] and the 'masked' diborylcarbene (**22**)[24] analogues.
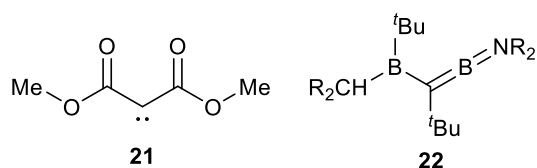
Figure 1.7   Structures of dicarbomethoxycarbene **21** and amino(borylmethylene)borane **22.**

A combination of π-donor and π-acceptor substituents will most typically result in a quasi-linear geometry. Interactions between the filled p orbital on the π-donor substitutent and the p_y orbital on the carbene destabilise the p_y orbital, increasing its energy level. Conversely, interactions between the empty p orbital on the π-acceptor substituent and the p_z orbital stabilise the p_z orbital, decreasing its energy level. The combination of these two effects create an energy gap between p_y and p_z, breaking their degeneracy and creating a system with singlet ground state multiplicity. Examples of these systems include transient halogencarboethoxycarbenes type species **23**[25] and the stable phosphinophosphonio-carbenes, **24**[17], and phosphinosilyl-carbenes **25**[4].
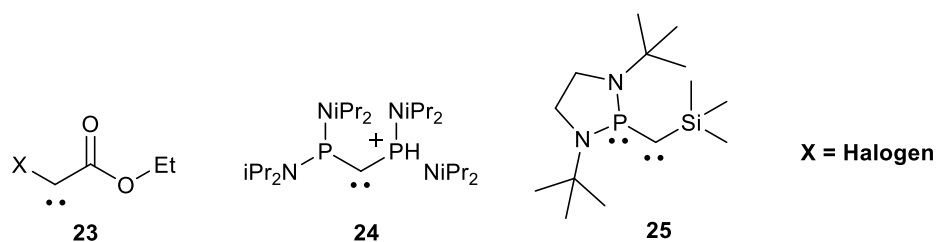
Figure 1.8 Structure of generalised halogencarboethoxycarbene species **23**, phosphinophosphoniocarbene **24** and bis(tertbutyl)diazophosphotrimethylsilylcarbene **25.**

These electronic stabilising effects demonstrate that designing a substitution pattern that stabilises singlet carbenes is a much easier task than one that stabilises triplet carbene systems. Triplet carbene systems are typically stabilised by steric protection, such as with trifluoromethyl groups to kinetically stabilise the molecule.

1.4 Typical pK_a values for N-heterocyclic carbenes

The pK_as of a range of conjugate acids of carbenes have been determined in both D_2O[26,27] (**Figure 1.9**) and DMSO[28,29] (**Figure 1.10**) with the acid base properties of carbenes being well documented[30]. These ranges include the pK_as of a range of triazolium, imidazolium, and thiazolium conjugate acid precursors to triazolyl, imidazolyl and thiazolyl carbenes.

11
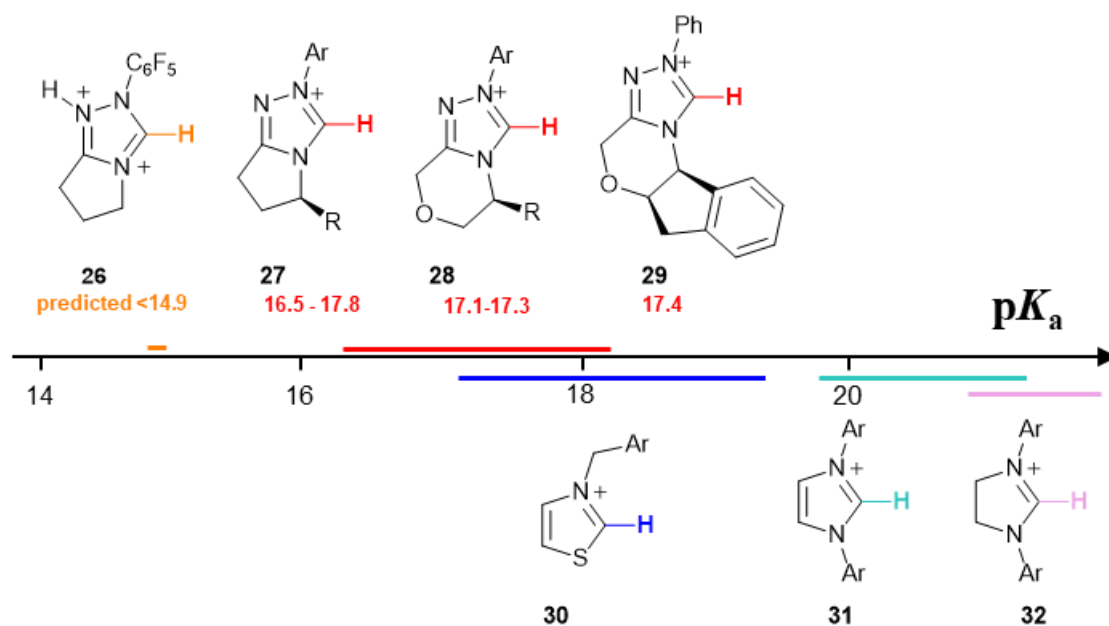
Figure 1.9 pK_a range for a variety of NHC precursors in D_2O[26] adapted from the *Journal of the American Chemistry Society*.

The pK_a of NHCs vary with solvent due to variance in stabilisation for the conjugate base provided by the solvent. The pentafluorophenyl NHC precursor **26** is predictably the most acidic triazolium of the series, because of the inductive electron withdrawing effects of the aryl group on the triazolium ring, which destabilise the cationic conjugate acid relative to the formally neutral carbene. The pentafluorophenyl triazolium **26** has a pK_a of 16.5 in D_2O and 12.1 in DMSO. Triazoliums are typically more acidic than other nitrogen heterocycles with fewer heteroatoms, with a typical acidity range of 16.5-17.8 in D_2O and 13.9-15.5 in DMSO for triazoliums with a 5-membered alkyl chain. Thiazoliums are typically more acidic than imidazoliums, with typical pK_a values of around 18.0 in D_2O and 16.5 in DMSO. Finally imidazoliums are the least acidic group with typical pK_a values of around 20.0 in D_2O and 18.1 to 23.8 in DMSO for aromatic substituents. In DMSO imidazoliums with aliphatic substituents typically have pK_as between 20.3 and 22.8. There is variance in the pK_a values depending on the substituents on the ring for imidazolium type carbenes.
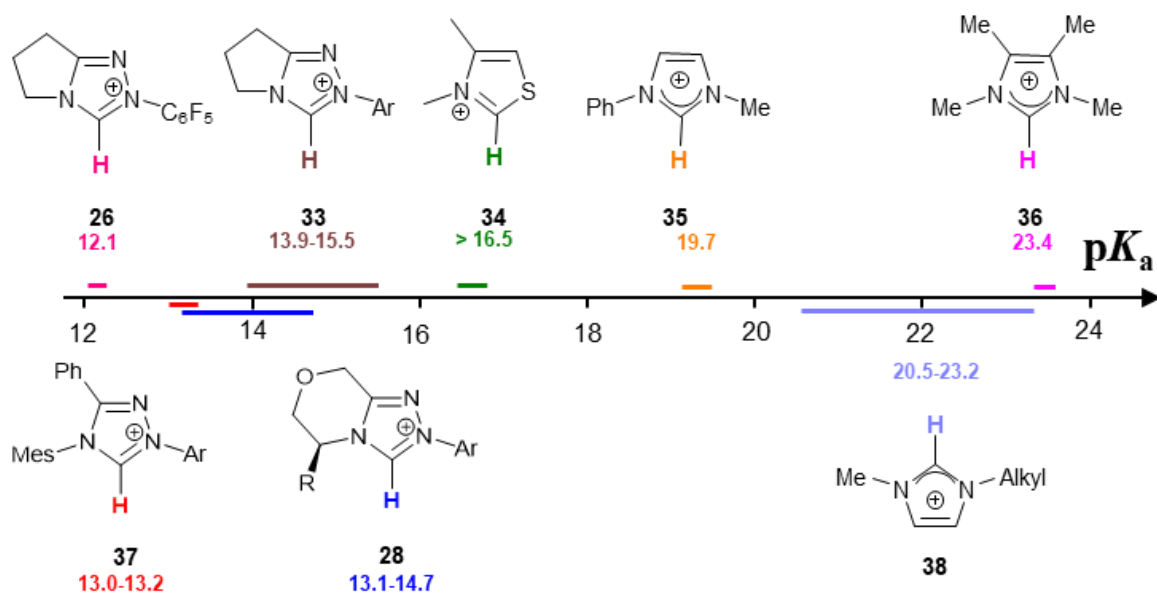
Figure 1.10 pK_a range for a variety of NHC precursors in DMSO[28] adapted from the *Journal of Organic Chemistry*.

Aqueous pK_a values are determined by deuterium exchange analysis, using a buffered solution to determine the rate of hydron transfer at the acidic position. A bracketing indicator method involving the measurement of spectroscopic changes in UV-vis absorption is typically used to access pK_a values in DMSO[28].

1.4.1 Unusual N-*ortho* substituent effects on proton transfer in triazolium-derived carbene systems

Recent studies into the deuterium exchange reactions of *ortho*-disubstituted N-Aryl triazolium salts by Tucker *et al.*[31] have provided additional evidence for the previously hypothesised effects of the N-aryl 2-substituent on pK_a values at N(1).

There is a marked change in the dependence of log k_{ex} values on pD under more acidic conditions for *ortho*-halo substituted N-aryl triazolium salts Figure 1.11[31], and distinct from pD profiles for N-*para*-cyano, mesityl, or phenyl **33** analogues[26].
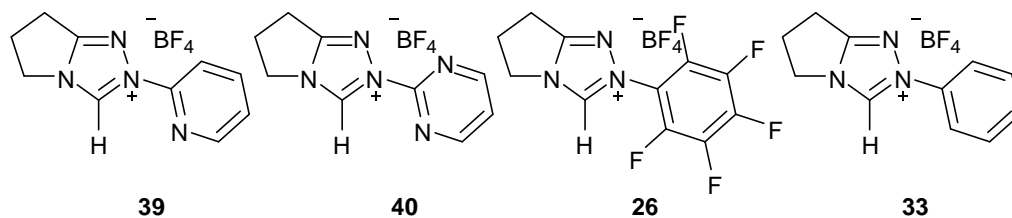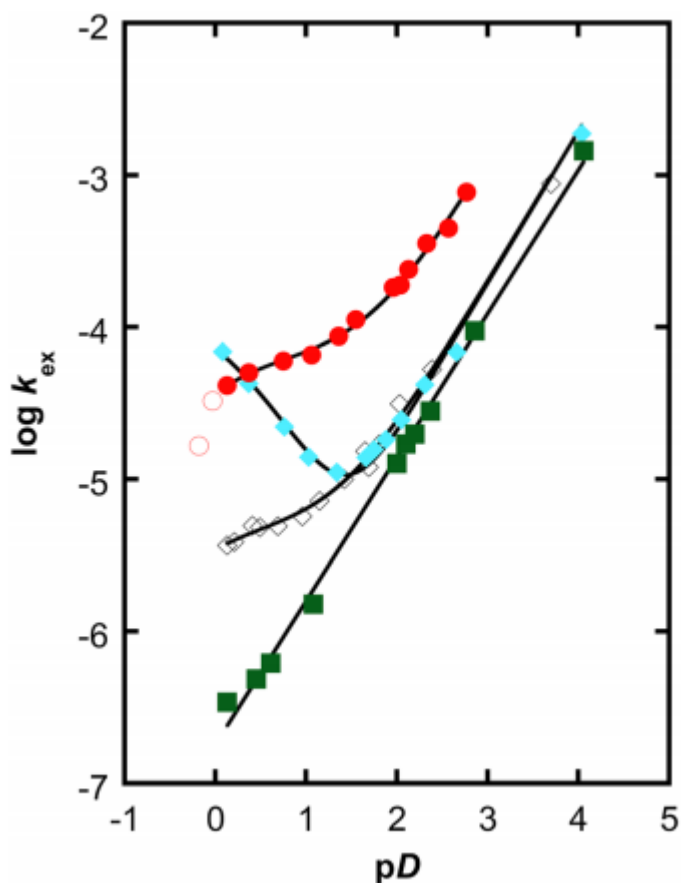
Figure 1.11 p*D* rate profiles for the deuterium exchange reactions of the C(3) proton of triazolium salts **39** (♦), **40** (◊), **26** (●), and **33** (■) in D$_2$O at 25 °C[31] reproduced with permission from the *Journal of Physical Organic Chemistry*.

The p*D* profiles for all the triazolium salts studied are similar, above p*D* 1.5, with k_{DO} values found to be within 10-fold. However under more acidic conditions, there is an altered dependence on p*D* that is more prominent for 2-halo-substituted examples, **Figure 1.11**. The calculated pK_a^N values of the halogens decreases in the order Br>Cl>F, though the difference is small across the series. It is possible that the donor effect on pK_a^N for this

14

series, which favours protonation at N(1), may be to supress any unfavourable electrostatic interactions between N(1) and the spacially proximal N-aryl *ortho*-heteroatoms, though it could also be a result of stabilising though-space N^+-H…*ortho*-X interactions in the N-protonated salt[31].

The study also revealed unique substituent effects for the N-(2-pyridyl)-triazolium system **39**. In this case distinct acid catalysis of deuterium exchange at lower pD values was observed. The proposed explanation involved deprotonation of the C(3) site, in conjunction with protonation of N(1) on the triazolium ring[31] as in **39'** (**Scheme 1.4**) allowing for acid catalysed deprotonation in a way that was unavailable in other triazolium type systems.

39   **39'**
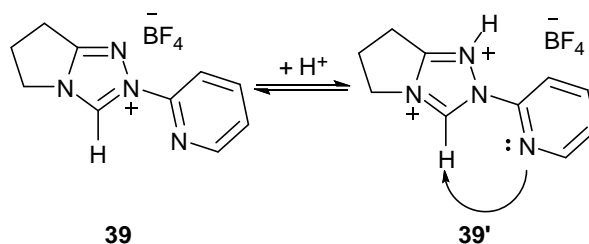
Scheme 1.4 N-Protonation of 6,7-dihydro-2-(2-pyridyl)-5*H*-pyrrolo[2,1-*c*]-1,2,4-triazolium tetrafluoroborate **39** to form **39'** under acidic conditions.

This study also highlighted the need for future work to investigate the additional substitution by both donor and acceptor groups in the 2-pyridyl N-aryl ring. This was required as a means of further exploring the proposed intramolecular proton transfer reaction. Additionally, probing the potential of *ortho*-amino groups of an N-2-anilino substituents as alternative intramolecular general base catalysts was highlighted as a possible avenue of research[31].

Overall, these results highlight the high variability of the roles of the *ortho*-heteroatoms in influencing the chemical proton transfer behaviour of the triazolium salts, and the high propensity of the triazolium scaffold for tuning reactivity to suit a variety of reaction environments.

1.5 The unique 2-substituent effect of aldehydes in the benzoin and Stetter reactions

The reactivity of the NHC-catalysed cross-benzoin reaction has been widely examined synthetically, though until recently the kinetic influence of the aldehyde substrate had not come under close quantitative scrutiny[32]. A more detailed analysis of this reaction is important as benzoin and Stetter transformations are often used to test new NHC scaffolds. It has already been established that reactions involving benzaldehydes with 2-substituents do not typically produce a homo-benzoin product, only a cross-benzoin product. Typically, the favoured product observed results from the formation of the Breslow intermediate from the non-2-substituted benzaldehyde. However, onwards reaction of the Breslow intermediate occurs with the 2-substituted benzaldehyde selectively. This phenomenon was thought to be a result of steric crowding, which prevented either the formation of the hydroxyaryl adduct from the 2-substituted benzaldehyde or the subsequent deprotonation to the Breslow intermediate (**Scheme 1.5**). In a publication by Collett *et al*[32] in 2015, this role of 2-substituents of the condensation of benzaldehyde was probed in detail.
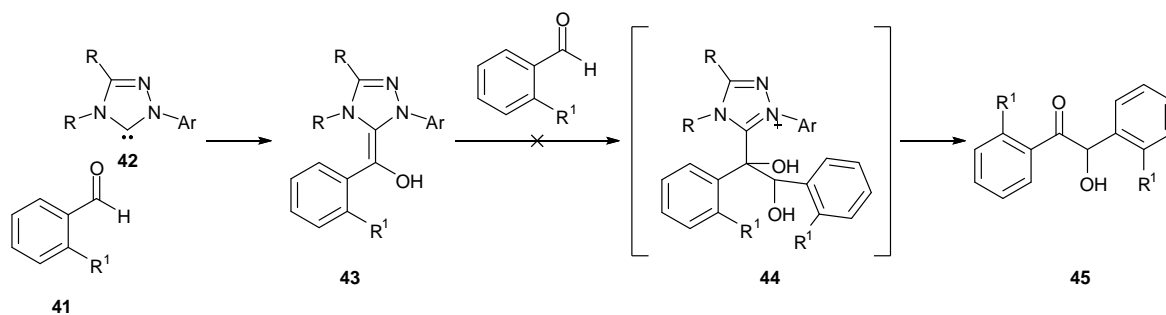
Scheme 1.5 The Breslow intermediate formed from the adduct of a 2-substituted aryl-aldehyde and an NHC **43** is unable to proceed to the benzoin product **45**.

Measurements of equilibrium and rate constants for the reaction of triazolium NHC precatalysts with substituted benzaldehydes to give 3-(hydroxybenzyl)-azolium adducts (**Scheme 1.6**) under both catalytic and stoichiometric conditions have been studied[32]. The results that were obtained from kinetic analysis and fitting data for both the forward and the reverse processes have been used to show that nucleophilic addition into benzaldehydes bearing a 2-heteroatom substituent is particularly fast. In contrast to this, smaller substituent effects were observed on the rate constants of deprotonation of 3-(hydroxybenzyl)-azolium adducts, which fall within the same order of magnitude regardless of aldehyde substitution[32]. The results offer insight into the apparent inconsistency over the second aldehyde addition in cross-benzoin reactions, overturning the assumption that 2-substituted benzaldehydes are less reactive in these reactions in steps up to the formation of the Breslow intermediate based upon steric arguments.
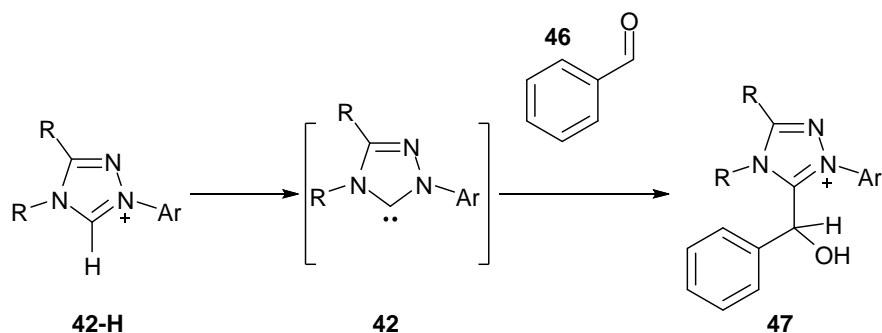
Scheme 1.6 Formation of hydroxylaryl adduct species **47** by the reaction of triazolium derived NHC **42** with aldehyde.

The reaction of the 2-substituted benzaldehydes was examined in detail, probing the kinetics of the forward and reverse reaction. This was aided by isolation of the hydroxyaryl adducts (the 3-(hydroxybenzyl)azolium species) **47**, and kinetic evaluation under identical conditions to those employed for monitoring reactions of aldehyde and triazolium pre-catalysts.

These discoveries provided some insight into the difficulties of the cross-benzoin reaction. This had previously been thought to be a result of steric issues which crowded the nucleophilic addition of the catalyst to the aldehyde. It was also thought that it could be an issue with crowding by the 2-substituents preventing the deprotonation of the hydroxyaryl adduct to form the Breslow intermediate. However in light of the data presented[32] it was apparent that the formation of the hydroxyaryl adduct species **47** was not impeded by the introduction of a 2-substituent to the aldehyde. The visible deuteration of the aldehyde demonstrated there was not an issue with the formation of the Breslow intermediate **43**. The issue was with the addition of a second molecule of the 2-substituted aldehyde to form the transient intermediate state **44** (**Scheme 1.7**). The presence of two 2-substituents, on both the Breslow intermediate and second aldehyde, slow the reaction significantly. Hence the net favoured product overall results from a non-2-substituted Breslow intermediate

reacting with a 2-substitued aldehyde, taking advantage of the acceleratory 2-substituent effect in the second half of the catalytic cycle.
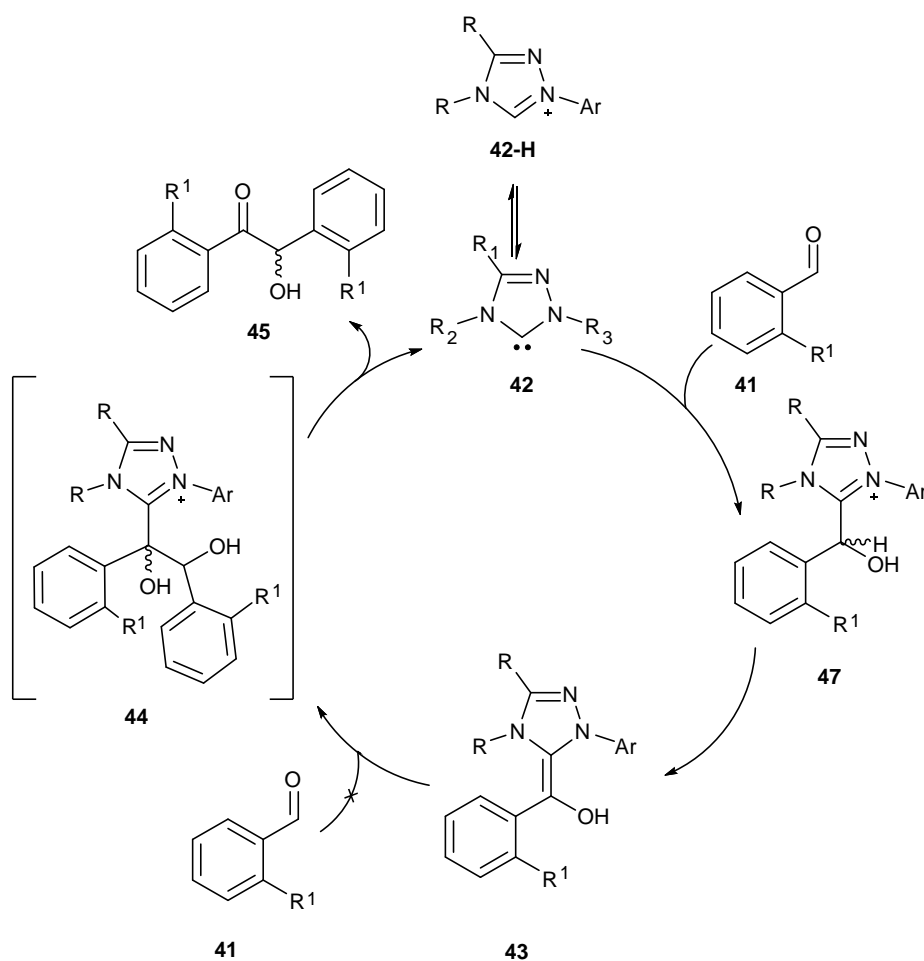
Scheme 1.7 Catalytic cycle for the benzoin condensation with formation of the hydroxyaryl adduct species **47**, formation of the Breslow intermediate **43**, formation of the extended intermediate complex **44**, and the breakdown of this complex to form benzoin, and to reform the starting NHC.

Recent developments in carbene chemistry have also revealed additional examples of the 2-substituent effect, *e.g.* the 2-substituent effect has been exhibited in data for the cross-benzoin condensation of 2-bromobenzaldehyde- derivatives[33].

Though it is clear that the role of 2-substituted aldehydes in the benzoin condensation is different to what had been initially assumed, the origin of the effect is unclear. A possible avenue of research is to control the properties of the 2-substituent of the aldehyde, either by using a substitution with a large steric influence, though isoelectronic with hydrogen, or a substitution with a large electronic influence, though only as hindering as hydrogen. As a 2-benzaldehyde species with a largely influencing electronic species with minimal steric is difficult to produce beyond 2-fluorobenzaldehyde, the most suitable candidate would be a species with large steric influences but minimal electronic influences, such as a 2-silylaldehyde. With this in mind, the intent of this thesis at the outset was to identify the origin of this 2-substituent effect in greater detail, by the use of silylated aldehydic species, as well as to investigate the effects of silyl group induced steric hindrance on other areas of the benzoin condensation.

1.6 Use of silyl substitution in NHC-catalysed transformations

Silicon is an influential member of group 14 as it lies on the dividing line between metals and non-metals. Silicon displays fairly unique properties in the periodicity of groups bonded to it, with the bond length contracting more than would be suggested by arguments based purely on the electronegativity of the elements involved. Elements like oxygen and fluorine bond particularly strongly to silicon as the lone pairs on these elements donate into empty orbitals on the silicon atoms. Fluoride anions are most commonly used to remove silicon groups from organic molecules due to the very strong bond formed between silicon and fluorine, with a bond dissociation energy of 576 ± 17 kJ mol^{-1} in silicon tetrafluoride[34], compared to the bond dissociation energy of a carbon fluorine bond of 513 ± 10 kJ mol^{-1} in carbon tetrafluoride[34]. With silicon bonded to carbon or to silicon, it is difficult to isolate molecules with higher bond orders than one.

The first organic molecule to be isolated with a double bond to a silicon heteroatom was in 1981 by Brook *et al*[35]. This molecule **48** was very sterically hindered, with an adamantyl group and three trimethylsilyl groups to stabilise this highly reactive bond. Though this molecule forms a stable solid at room temperature, when it is exposed to air it reacts exothermically, producing white smoke, melting and partially evaporating. For the formation of stable molecules, the reactivity of higher bond order silicons typically require sterically bulky groups to hinder attack on the reactive bond.

Disilenes **57**, analogues of **48** with a Si=Si bond in place of the C=Si bond, were first discovered in 2001 by Wiberg *et al*[36]. The synthesis of this moiety requires large amounts of steric hindrance as the formation of higher bond order bonds is disfavoured with silicon. Less sterically hindered precursors tend to form cyclotetrasilenes **58**, and bicyclotetrasilanes **59**, with multiple Si-Si single bonds being preferable to higher bond silicon bonds, such as Si=Si or Si≡Si. All of these molecules have bulky supersilyl groups. These groups sterically hinder attack on the highly reactive Si-Si bonds.
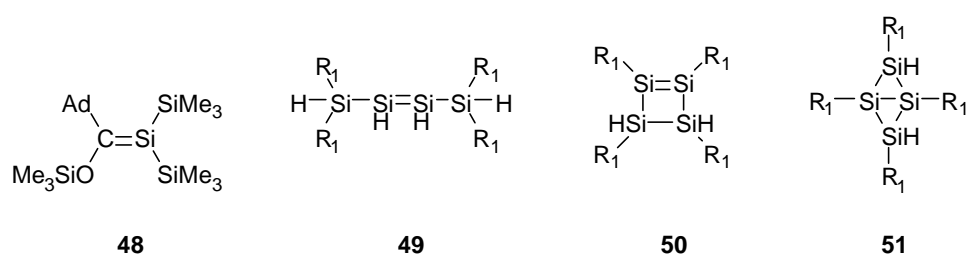
Figure 1.12 Structure of 2-adamantyl-2-trimethylsilyloxy-1,1-bis(bistrimethylsilyl)-1-silaethene **48** and generalised structures of disilenes **49**, cyclotetrasilenes **50**, and bicyclotetrasilanes **51** (R_1 = Si^{t}Bu$_3$).

Other moieties of higher bond order silicon include silaallene type structures, which contain the motif Si=C=X. These silaallene type structures can be further classified into three groups: silaallenes, Si=C=C **52**[37], silaketeneimines, Si=C=N[38] **53**, and silaketenes,

$Si=C=O^{39}$ **54**. Stable silaallenes[37] and silaketeneimines[38] and transient silaketenes[39] have been observed. While having higher order silicon bonds, these molecules can be far more stable compared to silenes and other similar groups.
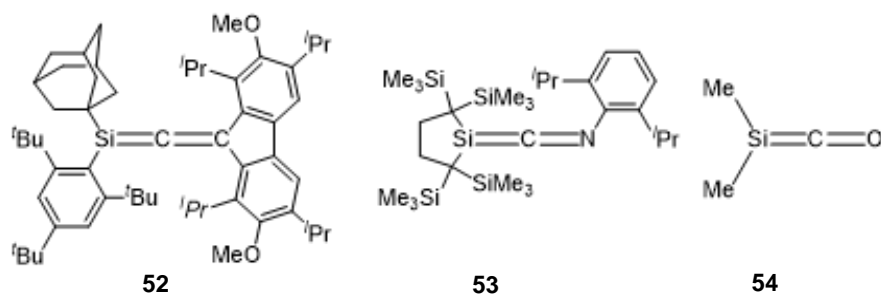
Figure 1.13 Observed stable silaallene **52** and silaketeneimine **53**, and transient silaketene **54** [37–39].

As documented above, the use of azolium type NHCs to promote umpolung reactivity in nucleo philic addition reactions is well documented. Typically d_1 NHC-derived acyl anion is added either to another aldehyde, in the benzoin condensation, or to a Michael acceptor **55**, in the Stetter reaction. Unfortunately, as a result of the high reactivity of the aldehyde moiety, the self-condensation benzoin product is favoured, with the addition to the β-carbon of the conjugate acceptor being disfavoured over direct addition to the carbonyl. Using acylsilanes, such as trimethylsill acylsilanes **64**, instead of aldehydes, it is possible to favour the Stetter product[40].
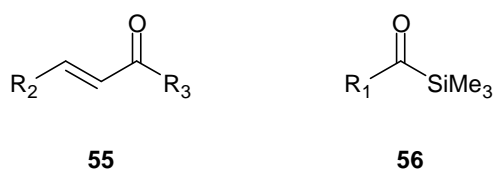
Figure 1.14 Generalised structures of Michael acceptors **55** and trimethlsilyl acylsilanes **56**.

This method provides the desired product, in reaction conditions that are tolerant of both air and water, with yields of up to 72%[41]. The use of milder reaction conditions is favourable as it requires both less stringent control of the reaction environment and less toxic reactants than more conventional uses of acylsilanes as acyl anion precursors. These can require cyanide or fluorine to create the requisite charge density on the oxygen to promote a 1,2 silyl group shift, or Brook rearrangement, to allow the nucleophilic addition of the produced acyl anion to the electrophile[40].

The introduction of the trialkylsilyl groups to the aldehyde allows for the direction of the nucleophilic addition to favour the formation of the Stetter product over the benzoin product, with an adjusted reaction mechanism shown in **Scheme 1.8**[41]. After addition of the carbene **56** to the acylsilane **58**, the silicon shifts onto the oxygen by a Brook rearrangement forming an enaminol **59**, also known as the Breslow intermediate. The silyl ether is then cleaved by addition of a molecule of alcohol present in the reaction mixture to the Breslow intermediate, removing the steric hindrance. This intermediate **60** is unable to react with other molecules of the acylsilane, due to the large steric hindrance of the silyl group, and so must react with the α,β-unsaturated ketone **55**. The formation of the desired Stetter product **62** is enhanced further by the use of thiazolium-derived NHCs, which have a higher proclivity to undergo the Stetter reaction under these conditions[40,41].
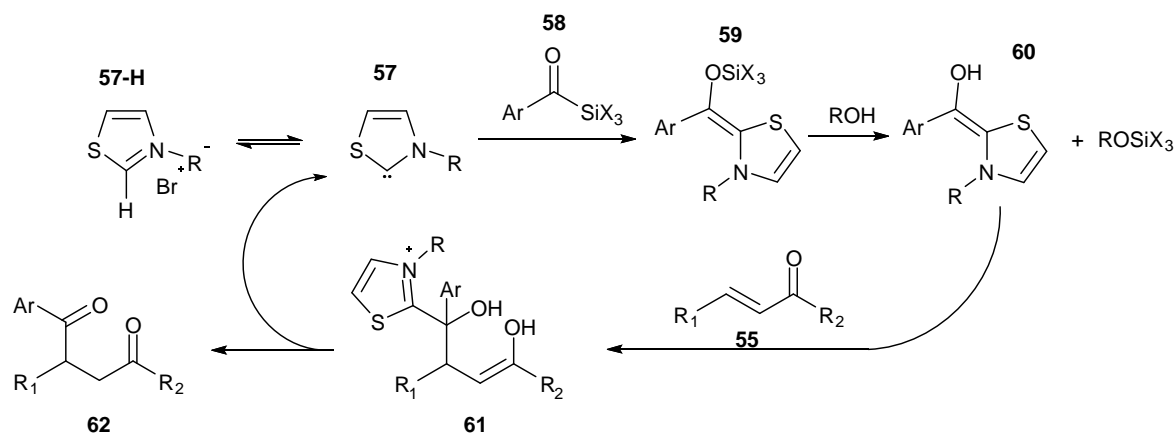
Scheme 1.8 Catalytic cycle for the NHC-catalysed Stetter reaction using acyl silanes.

The sila-Stetter reaction first came under scrutiny in 2004 by Mattson *et al.*[15,16] Initial investigations were followed by a further report into the use of acylsilanes to selectively form the Stetter product. This functionality of acylsilanes allows for elimination of the undesired homo-benzoin product that would otherwise form in these reactions, which is formed when the benzaldehyde derivative is used instead of the acylsilane. This powerful utility of acylsilanes **63** to allow for the selective reaction of the Breslow intermediate has since allowed for the use of the sila-Stetter reaction with acceptor **64** to selectively form precursor structures to bis-spiroacetals, **66**[42,43] (**Scheme 1.9**). The bis-spiroacetals **66** can then be formed through acid catalysed ring closure. The sila-Stetter reaction forms the desired precursor molecule in yield of up to 89% with no identifiable formation of the undesired α-hydroxy ketone product.
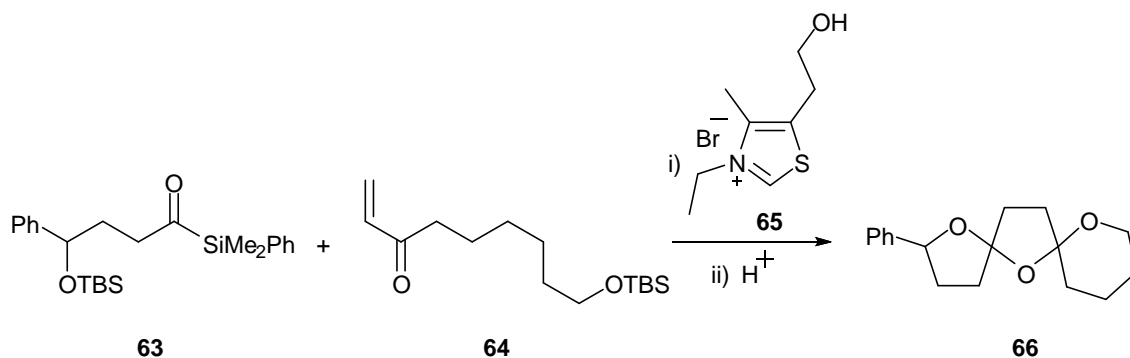
Scheme 1.9 Formation of bis-spiroacetal **66** through an NHC catalysed sila-Stetter reaction between aliphatic acylsilane **63** and vinylketone **64**.

In a combination of silicon chemistry and carbene chemistry, Dhara *et al.*[44] successfully isolated NHC-stabilised 1-hydrosilaimine **67**. When exposed to water, the polarization of the Si=N bond reacts with an O-H bond of water, leading to the formation of silanolate group **68** The use of NHCs to stabilise this normally unstable species also allows for the theoretical possibility of other NHC stabilised silicon species, as well as the interaction of these 1-hydrosilaimine species with other small species with σ-bonds.
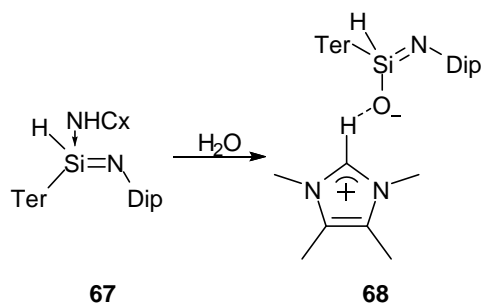
Scheme 1.10 Synthesis of **68** from **67** (Ter = 2,6-Tip$_2$C$_6$H$_3$, Tip = 2,4,6-^{i}Pr$_3$C$_6$H$_2$, Dip = 2,6-^{i}Pr$_2$C$_6$H$_3$, NHCx = 1,3,4,5-tetramethyl imidazole-2-ylidene).
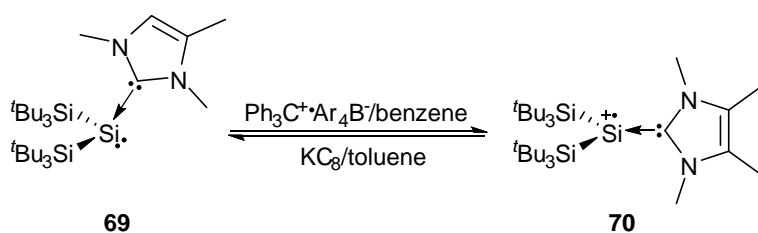
Scheme 1.11 One-electron oxidation of silylene-NHC complex **69** to give NHC-stabilised silylene radical cation **70**.

In a similar way, a neutral silicon (I) species **69** and radical cation silicon (II) species **70** have been trapped as a cation by an NHC by Tanaka *et al*[45]. These two isolated species are sensitive to both moisture and air. The radical cation species has been characterized by X-ray crystallography and electron paramagnetic resonance spectroscopy, showing that this species has a planar structure and π-radical nature. It has mostly sp^2 character, with the positive charge localised predominantly on the central silicon atom. There are other recent examples of silicon (I) radicals stabilised by NHCs in the literature[46]. Recently a disilene species has been trapped as an intermediate species using an NHC[47] which forms after isomerisation of the silicon species, depending on substitution pattern. Silicon radicals have important functionality as intermediates.[48–50] The capture of these reactive species as interacting entities opens opportunities for novel synthetic routes. The use of NHCs to isolate otherwise difficult to obtain species would allow for more facile reaction conditions and avoid more laborious synthetic strategies.

NHC stabilised silicon species have also been used with more exotic heteroatoms: *e.g.* NHC-silicon tellurides **71**[51], NHC-stabilised silylene-nickel formation **72**[52], and in the formation of 2-hydrophosphasilenes **73**[53].
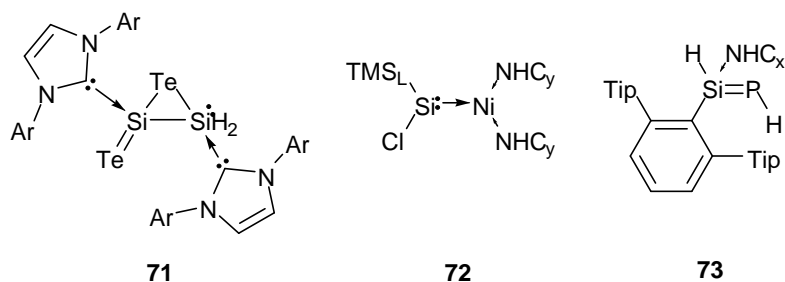
Figure 1.15 NHC-silicon telluride complex **71**, silylene-nickel complex **72**, and hydrophosphasilene **73** (NHC$_y$ = 1,3-diisopropyl-4,5-dimethylimidazol-2-ylidene, TMS$_L$ = N-(2,6-diisopropylphenyl)-trimethylsilylamide, NHC$_x$ = 1,3,4,5-tetramethylimidazol-2-ylidene).

1.7   Use of boron derivatives with NHCs in the formation of boranes

While silicon substitution of NHCs has seen some applications to guide chemoselectivity in the benzoin condensation, there has been significantly more research into other Lewis acidic heteroatoms. A major group that has been studied are NHC-boryl derivatives.

In 2009, Hoveyda *et al.*[54] documented cases of carbon-boron bond formation through the use of imidazole-based carbenes. In these cases β-boron-substituted ketones were formed through the reaction of enones and bis(pinacolato)diboron with imidazole-derived NHCs. During this reaction the free NHC forms a reactive intermediate with the bis(pinacolato)diboron by coordinating to one of the boron atoms to form intermediate species **75**. This activated species is then able to add to the enone via 1,4 addition. The β-boron-substituted ketone product **76** was formed by the conjugate addition of the substrates. The reactive intermediate then proceeds to tautomerise, liberating the carbene from the boron-enolate **77**. This boron-enolate then generates the desired ketone product **78** with an aqueous workup.
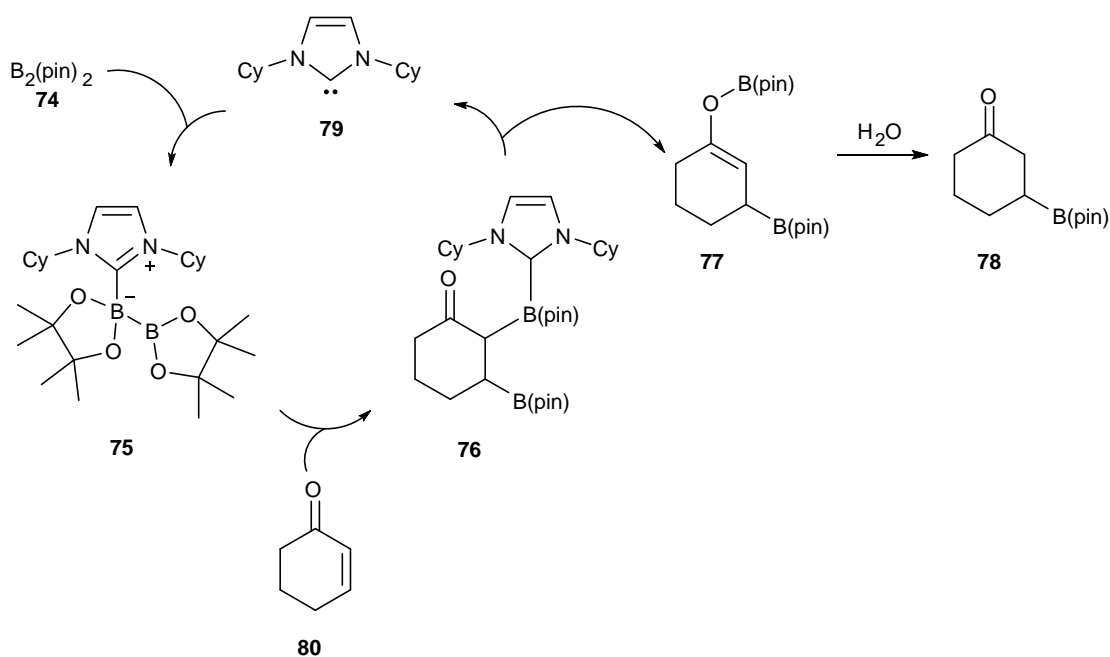
Scheme 1.12 Catalytic cycle for the reaction of 1,3-bis(cyclohexyl)imidazole-2-ylidine with bis(pinacolato)boron, and onwards reaction with 2-cyclohexan-1-one to form 3-(pinacolatoboron)cyclohexanone **78**.

The crystal structure of the intermediate **75,** with the carbene bonded to the bis(pinacolato)diboron was identified by Marder *et al*[55] confirming the physical characteristics of this species. The crystal structure shows a clear boron-NHC interaction, with distorted tetrahedral geometry of the NHC-bound boron atom being clearly visible. There are clear indications of the NHC-bound boron atom undergoing pyramidalisation from sp^2 to sp^3. The distance of the B-B bond has also increased by 0.039 Å relative to the B-B bond length in bis(pinacolato)diboron.
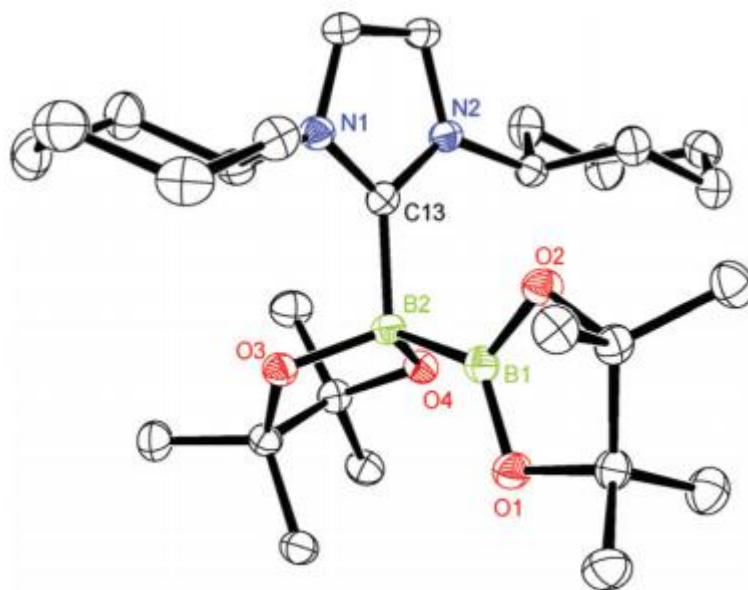
Figure 1.16 X-ray crystallographic structure for the adduct of bis(pinacolato)boron with 1,3-bis(cyclohexyl)imidazole-2-ylidene **75**[55], reproduced with permission from the *Journal of Organic Chemistry*.

These initial reports of Hoveyda *et. al*[54] on the NHC-catalysed boron conjugate addition reactions indicate a tolerance to a variety of Michael acceptors, including cyclic and acyclic ketones, and esters as possible substrates. In the case of β,β-disubstituted Michael acceptors, quaternary carbon centres were formed. Over this variety of Michael acceptors, yields are reasonable to very good, with a range of 44 - >98%, and diastereoselectivity ranges from 1.6 : 1 to 7.2 : 1.
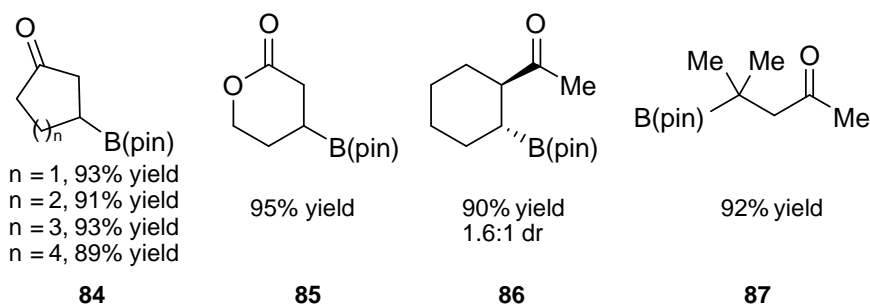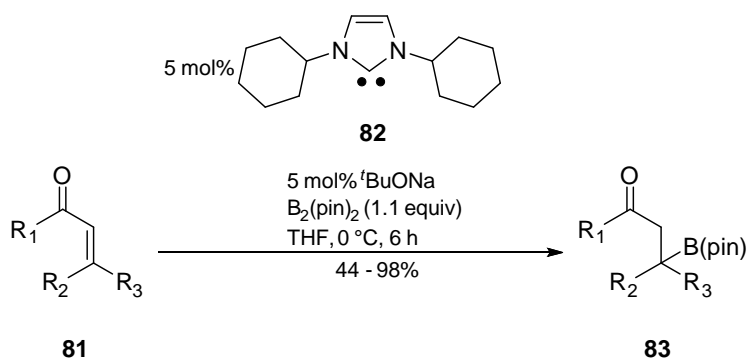
Scheme 1.13 Reaction of Michael acceptors with bis(pinacolator)boron by Marder *et al*. in the presence of an imidazolium derived NHC, and the yields with various ketones[55].

In 2012, Hoveyda *et al*[56] continued to expand upon the NHC-catalysed borylation of Michael acceptors and developed the enantioselective transformation of these species. Unfortunately, initial attempts at an enantioselective reaction pathway were met with limited conversion rates, thought to be chiefly due to steric hindrance. This was due to the use of a sterically demanding NHC **88** coordinating to the bulky bis(pinacolato)diboron **74**. This problem was solved through the use of methanol as an additive to the reaction.

With the introduction of the methanol additive, the reaction proceeded efficiently with a marked improvement to conversion levels **Scheme 1.14**. It was proposed that this was as a result of methanol exchanging with the pinacol of the diboron, causing a reduction of the steric hindrance on the boron, and thus generating a more accessible diboron unit for the sterically demanding NHC.
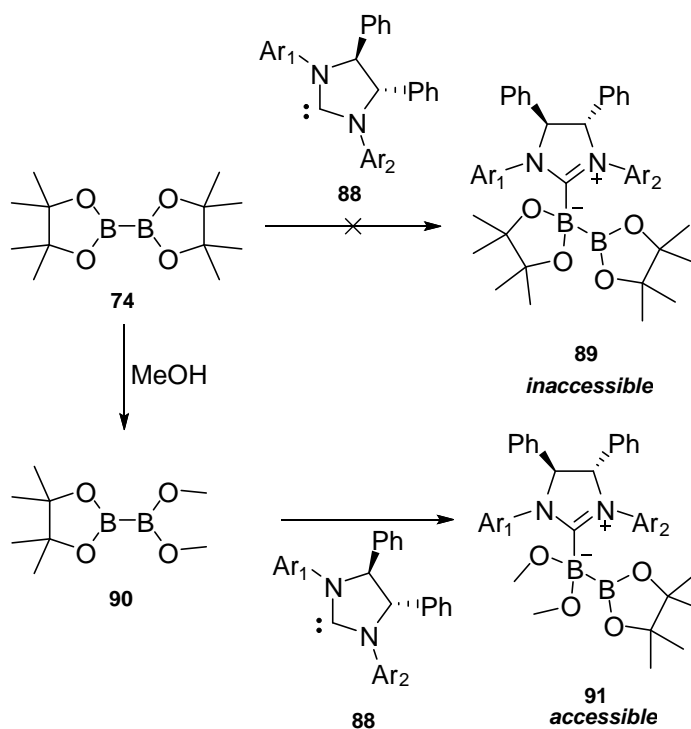
Scheme 1.14 Reducing the steric hindrance of bis(pinacolato)boron **74** with methanol to allow for reaction of boron with an imidazolinium derived carbene **88**.

Under these reaction conditions, a wide variety of Michael acceptors are tolerated, including enones, enals, enoates and α,β-unsaturated amides. The enals are of particular interest in this case, as they have previously been documented to undergo extensive dimerization reactions in the presence of NHCs. Contrary to this, in this reaction scheme the enals produce minimal undesired alternative NHC-catalysed pathways. Within all these groups of Michael acceptors, the yields of the reaction range from 43 – 94%, with enantioselectivity ranging from 42 – 96% *ee*[56].

Scheme for reaction of **81** to **83** with catalyst **91**, DBU, B₂(pin)₂ (1.1 equiv), MeOH (60 equiv), rt - 66 °C, 7 - 36 h, 43 - 94%, catalyst **92**.

Products **93 – 97**:

93 60% yield, 90% ee

94 82% yield, 84% ee

95 60% yield, 90% ee

96 82% yield, 84% ee

97 72% yield, 82% ee
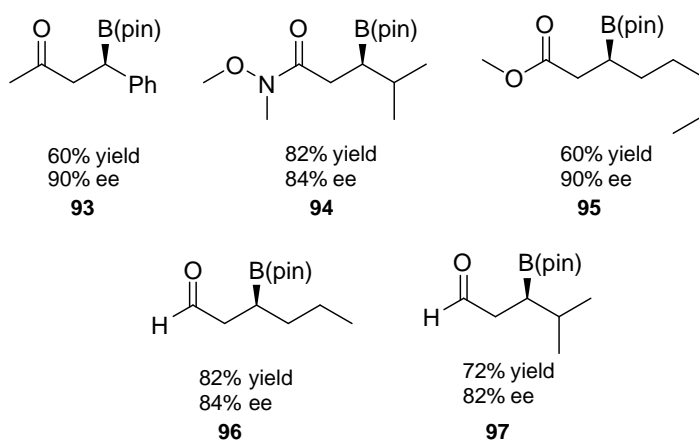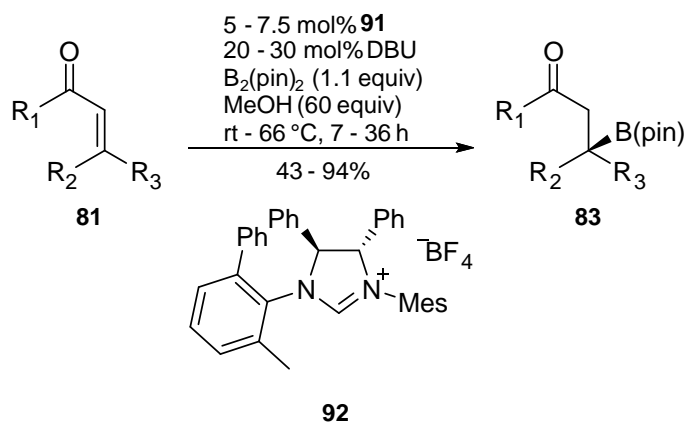
Scheme 1.15 Reaction of bis(pinacolato)boron with Michael acceptors in the presence of **83** with the yields and enantioselectivities of products **93 – 97** shown.

Diboron species have been reported to have other uses in conjunction with NHCs. Marder *et al*. detailed the use of diboron species in the ring expansion of imidazolium-derived NHCs. This process involves an initial attack of the NHC on a boron atom, followed by ring expansion to form a 6 membered heterocycle **100**. This was reported to allow for a facile formation of boron cations[57], which may have further uses in organic synthesis.
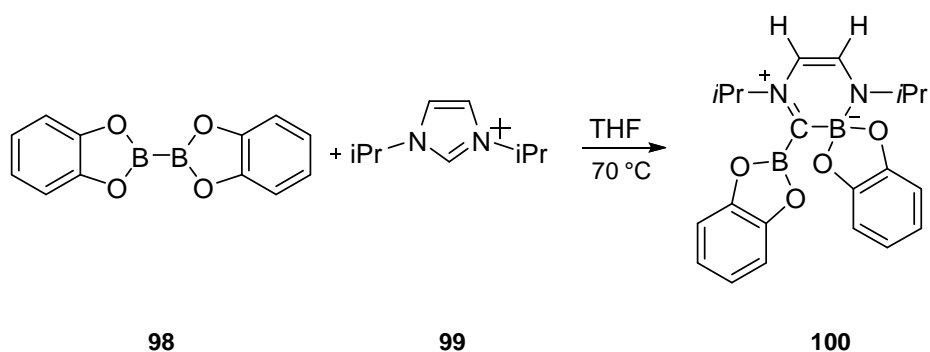
Scheme 1.16 Reaction of bis(catecholato)diboron **98** with 1,3-diisopropyl imidazolium **99** at 70 °C to form ring expanded product **100**.

This ring expansion reaction was found to be applicable to a range of diboron species, including bis(catecholato)diboron, bis(neopentyl glycolato)diboron and bis(ethylene glycolato)diboron, as well as to a range of imidazolium ions[57], allowing for the formation of a variety of different desirable products.

Taniguchi *et al*. documented the use of NHC boranes in a Masume-Bergman-type reaction to form anthracene derivatives, as shown in **Scheme 1.17**. They proposed that the NHC-borane **102** functions as a hydrogen donor to a benzene diyne species **101** to form an intermediate *p*-benzyne species. This then goes on to form the final product **103** and **104**. The results indicate that in non-polar solvents a radical mechanism appears to be preferred, however in polar solvents an ionic mechanism is favoured[58].
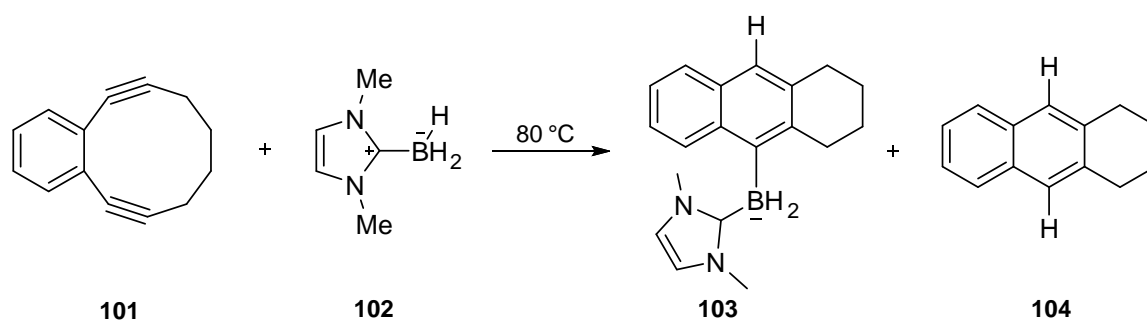
Scheme 1.17 Formation of 1,2,3,4-tetrahydroanthracene **104** by reaction of benzo[3,4]cyclodec-3-ene-1,5,diyne **101** with 1,3-dimethyl imidazolium borane **102**.

1.8 Recent advances for N-heterocyclic carbene applications in organocatalysis

Though previously NHCs have been used in the benzoin condensation and Stetter-type reactions, more recently they have also been shown to function well in the formation of indoles **108** and related compounds through functionalisation of imines **105** by umpolung reactivity[59] **107**, **Scheme 1.18**. NHCs have had functionality identified in annulation[60], the catalytic resolution of amines[61], and acylation[62]. These catalysts are powerful synthetic tools, with diversity in the structures NHCs are capable of accessing. With the functionality to be tuned to a variety of end products, and increasing yields for reactions with recent advances, there is much potential for carbenes to become more prevalent in the field of catalysis as more developments are made.
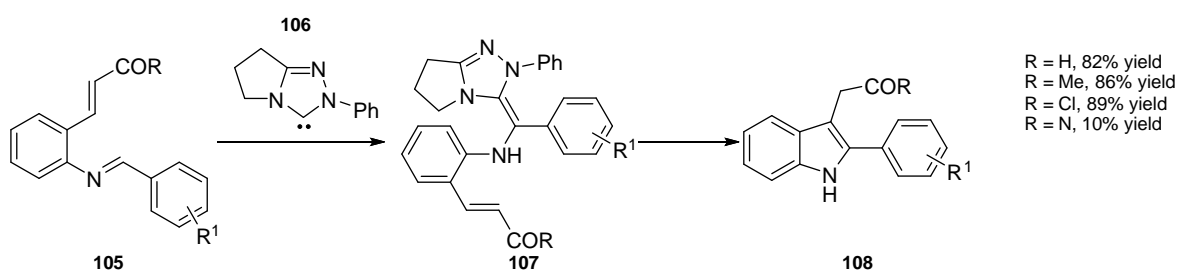
Scheme 1.18 Formation of indole species **108** from imine precursor **105** through NHC-complex enaminol intermediate **107**, including the yields[59].

Recently the intramolecular Stetter reaction has been shown to work in solvent free conditions[63] with up to 98% yield at mild temperatures of 30 °C. There have also been reports of the Stetter reaction being used to create unsubstituted α-pyroles[64], and the synthesis of 4-difluoromethylquinolines.[65] With this wide range of reactivities, NHCs and the Stetter reaction allow for otherwise difficult transformations and so are a powerful tool within the field of organic chemistry. The benzoin condensation has also received attention, with recent developments discovering synthetic pathways for functionalized imidazolidine-2-thiones,[66] site selective cyclization of unsymmetrical dialdoses,[67] as well as the use of solvent free conditions to reduce the catalytic loading in the liquid or semisolid state.[63] With this wide range of developments in both the Stetter and benzoin condensations, the development of catalytic systems without the need for transition metal complexes is well underway, and the potential for NHCs to be used in more carbon-carbon bond forming reactions clearly possible.

1.9   Aims of this Project

The intent of this project is two-fold: first, to further probe the origin of the 2-substituent effect, and second, to probe the influences of steric demand on the N-aryl substituent of pyrrolidine-based triazolium derived NHCs.[68] Silicon was determined as being a viable element to probe the nature of both of these effects, due to the large steric bulk of trialkylsilyl groups and Hammet ρ-value similar to that of hydrogen.
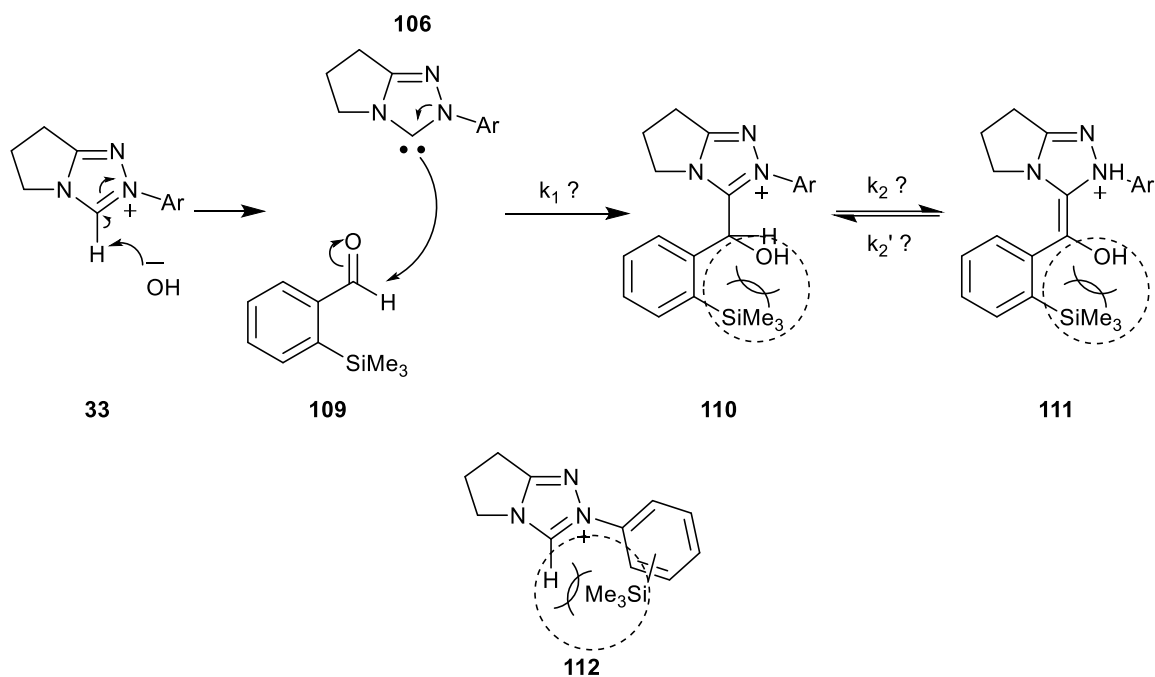
Scheme 1.19 Trimethylsilyl groups in triazolium precursors **112**, in the hydroxyaryl adduct **110** and Breslow intermediate **111** with suspected steric clashes highlighted.

As demonstrated in **Scheme 1.19**, the introduction of the trimethylsilyl group will likely induce torsion of the catalyst, or of the hydroxyaryl adduct, depending on the location of the silane substitution. By examining triazolium substituent effects in proton transfer reactions and benzoin type condensations, we will probe the extent of the effect of the steric hindrance on the acidity of the triazolium NHC precursor, the rate and equilibrium constants for hydroxyaryl adduct formation k_1 and onwards reaction to the Breslow intermediate k_2 and k_2'. It is hoped that this information will allow for a better understanding of the nature of the 2-substituent effect, as well as the effects of sterics on the formation of NHCs. The introduction of Lewis acidic substituents into NHC catalysts is in its infancy, and these proposed structure-activity studies will help predict their influence relative to more commonly used substitution patterns.

To analyse the nature of the 2-substituent effect with silicon, a 2-silyl substituted benzaldehyde is the first synthetic target. There is precedent for this molecule being used

as an intermediate in the formation of porphyrin rings[69]. The preparation of triazolium catalysts with silyl substitution on the N-aryl groups will also be trialled in addition to the synthesis of related N-aryl catalysts with electron withdrawing substituents. Finally, the kinetics and mechanisms of both the proton transfer reactions and benzoin-type condensations of the novel aldehyde and catalysts will be investigated.

2   Results

Results sections **2.1** - **2.5** contain the results obtained while probing the formation of 2-trimethylsilyl benzaldehyde, and the reactions between this aldehydic substrate and triazolium salt derived carbenes. Section **2.4** displays the results obtained for the formation of halogenated triazolium salts, and the onwards reaction of these species in the attempted silylation of the halogen substituent. Section **2.5** displays the incidental findings of the X-ray crystallographic data for 2 trimethylsilyl benzoic acid. Section **2.6** contains the results obtained for the H/D exchange reactions for the halogenated triazolium salts and their calculated k_{DO} and pK_a values.

2.1   Synthesis of 2-trimethylsilyl benzaldehyde

The initial scope of this project was to synthesise 2-trimethylsilyl benzaldehyde, **109** in order to explore the effect of silyl substitution on the benzoin reaction. The synthetic pathway was derived from a literature synthetic route, where 2-trimethylsilyl benzaldehyde had been used in the formation of porphyrin rings[69]. This synthetic pathway used N^1,N^1,N^2-trimethylethylene diamine to direct lithiation to the *ortho*-position by way of reactive intermediate **125**. The reaction was conducted by the addition of butyl lithium to a solution of benzaldehyde and N^1,N^1,N^2-trimethylethylene diamine in dry hexane. In hexane solution, attempts to produce this product resulted in low yield.

0.36 ppm

f1 (ppm)
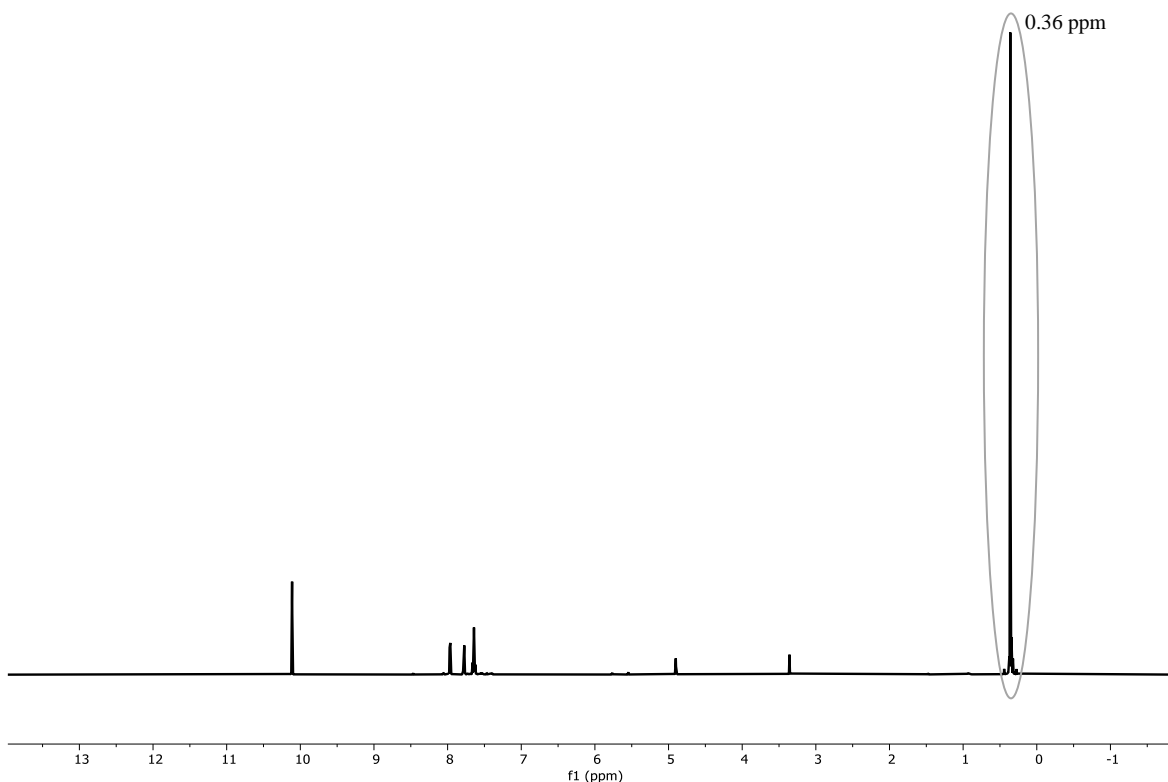
Figure 2.1 ¹H NMR in CDCl₃ of 2-trimethylsilyl benzaldehyde **109**, showing the distinctive trimethylsilyl peak at 0.36 ppm, circled in grey.

Optimisation work was carried out to increase yield. Reaction times of 16 h, 20 h, 24 h and 26 h were attempted. The alternative use of THF as a solvent led to much improved conversions and product formation. A 24-hour reaction time was required for optimal lithiation results. Longer reaction times of 24 hours gave higher conversions than shorter times of 16 to 20 hours. The progress of the reaction was followed by ¹H NMR spectroscopy, monitoring the peak at 0.36 ppm with deuterated chloroform as the solvent **Figure 2.1**. After addition of the silyl electrophile, the onwards reaction proceeded quickly, with complete conversion within 1 hour (**Scheme 2.1**). When the reaction with the electrophile was complete, it was quenched with dilute acid (HCl, 0.1 M).

39
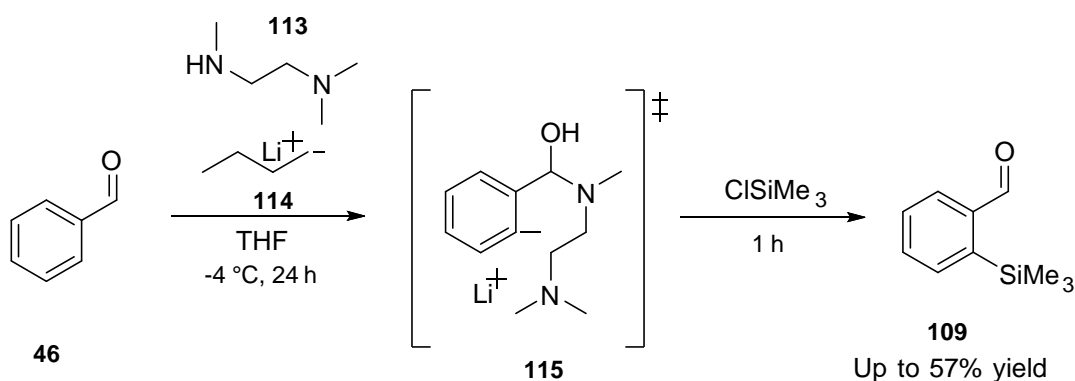
Scheme 2.1 Formation of 2-trimethylsilyl benzaldehyde **109** through lithiation of benzaldehyde **46**, followed by reaction of trimethylsilyl chloride as an electrophile with intermediate **125**, to give a yield of 57%.

The yield of the desired product was improved, from 0% to 57%, with changes to the purification method. Initially, the presence of 2-trimethlsilyl benzaldehyde was inferred by a peak at 0.36 ppm using ^{1}H NMR with deuterated chloroform **Figure 2.1**, and an ion of weight 164 by mass spectroscopy with the correct ion profile, though it was difficult to obtain a product at reasonable purity in useful quantities. The elution solvent and the length of the column, were both important in obtaining good yields of product. The solvent mix that was identified as most useful for the purification of the silyl product from unreacted benzaldehyde was a hexane and ethyl acetate mixture (2 : 1).

It was further speculated that the unexpectedly low yield of the product (**Table 2.1**) was due to side reactions between the silyl group and the surface of the column so efforts were made to minimise the residence time of the product on the column. For the column, a ratio of 25 : 1 silica : reaction mixture by weight was found to be optimal. With these refinements to both the synthetic method (**Table 2.1**), and the purification, the final yield of the desired product was 57%, with good purity. Attempts were also made to use acetic

acid in the place of HCl as the quenching agent. Acetic acid was ineffective for the reaction and no isolated yield was obtained in this case (entry 5 of **Table 2.1**).

Solvent	Quenching agent	Column conditions (hexane : ethyl acetate)	Butyl lithium equivalents	Isolated yield (%)
Hexane	HCl	3 : 1	3.0	0
Hexane	HCl	4 : 1	2.5	0
Hexane	HCl	9 : 1	2.5	11
THF	HCl	9 : 1	2.5	57
THF	Acetic acid	9 : 1	2.5	0

Table 2.1   Changes in the yield of the formation of 2-trimethylsilyl benzaldehyde, dependent upon column conditions, butyl lithium equivalents, reaction solvents and quenching agents.

A second reaction pathway was attempted, using 2-bromobenzaldehyde ethylene acetal **126** to forgo the use of N^1,N^1,N^2-trimethylethylene diamine, as shown in **Figure 2.2**. The end product of this reaction would be 2-trimethylsilyl benzaldehyde ethylene acetal **128**. After the completion of this reaction, a further step would be used to convert **128** to 2-trimethylsilyl benzaldehyde **109**.
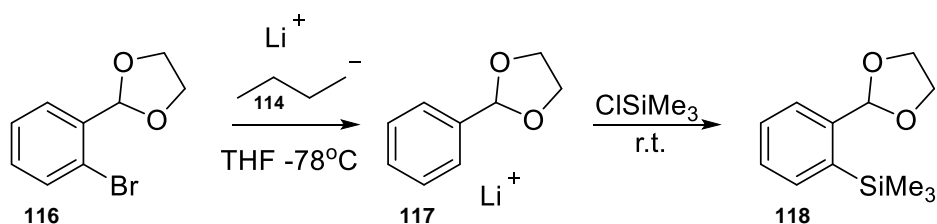
Figure 2.2   Attempted formation of 2-trimethylsilyl benzaldehyde ethylene acetal **128**.

The reaction was progress of the reaction was monitored by tlc. With the initial difficulties in optimising the reaction first reaction, it was hoped a different reaction pathway may result in higher yields. After initial attempts at this reaction, the desired product of 2-

trimethylsilyl benzaldehyde **109** was not obtained and attempts to optimise this reaction pathway were discontinued.

2.1.1 Desilylation of 2-Trimethylsilyl Benzaldehyde
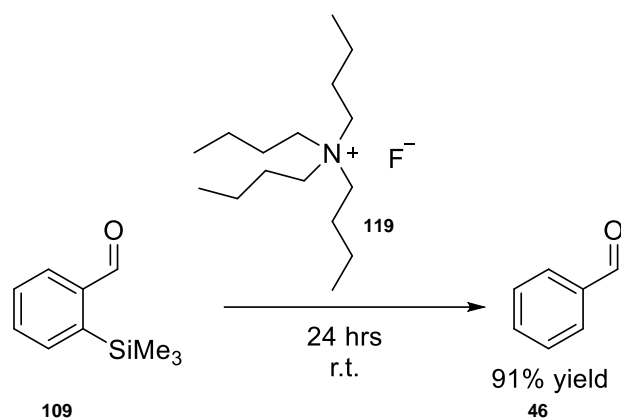
Figure 2.3 attempted removal of the silyl group of the 2-trimethylsilyl benzaldehyde using tetrabutylammonium fluoride **129**, using THF as a solvent

Attempts were made to remove the silyl group of the 2-trimethylsilyl benzaldehyde **109** using tetrabutylammonium fluoride **129** and THF as a solvent. The reaction was allowed to progress for 24 hours at room temperature, after which the solvent was remove. The remaining oil was dissolved in DCM, washed with water, and dried. The desilylation of 2-triemthylsilyl benzaldeyde happened without difficulty, and ^{1}H NMR identified the product as benzaldehyde **46**. The reaction produced a 91% yield.

2.1.2 Crystal structure of 2-trimethylsilylbenzoic acid

During the experimentation of the reaction of 2-trimethylsilyl benzaldehyde with various triazolium salts, some unused sample was allowed to oxidise to the benzoic acid form **61**. A crystal structure of this was then identified using X-ray crystallography, with full X-ray data shown in **Appendix 1**. The silyl group induces some steric congestion into the aryl

ring, which was not present with the silyl group removed; some strain was identified using the full X-ray crystallographic data for this molecule. Bond lengths between C1 and C2, and C2 and C3 in **Figure 2.4** are lengthened in comparison to bond lengths between C4 and C5, and C5 and C6. This would indicate some disturbed aromaticity possibly due to the steric congestion of the trimethylsilyl group and the carboxylic acid group. Although an X-ray structure of 2-trimethylsilyl banzaldehyde **109** was not obtained, the structure of **130** provides additional evidence of successful 2-silylation.
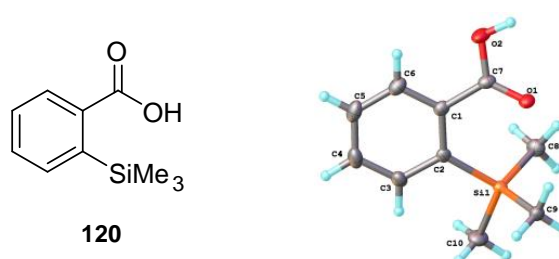
Figure 2.4   Image of 2-trimethylsilyl benzoic acid **130** produced using X-ray crystallography.

2.2   Reactions of 2-trimethylsilyl benzaldehyde with a selection of catalysts in the homo- and cross-benzoin reactions

The 2-trimethylsilyl benzaldehyde that was prepared was used as a substrate to probe the 2-substituent effect in the benzoin condensation. This was done by utilising typical benzoin conditions using N-pentafluorophenyl **26**, N-phenyl **33**, N-mesityl **131**, and N-parafluorophenyl **132** (**Figure 2.5**) triazolium salt pre-catalysts in d_4-methanol with a triethylamine buffer at 25 °C. For the homo-benzoin studies, catalysts **26**, **131**, and **132** were used in ratios of 1 : 1.2, 1 : 1.5, 1 : 1.7 and 1 : 2 respectively for benzaldehyde : catalyst. The reaction progress was monitored by ^{1}H NMR spectroscopy.
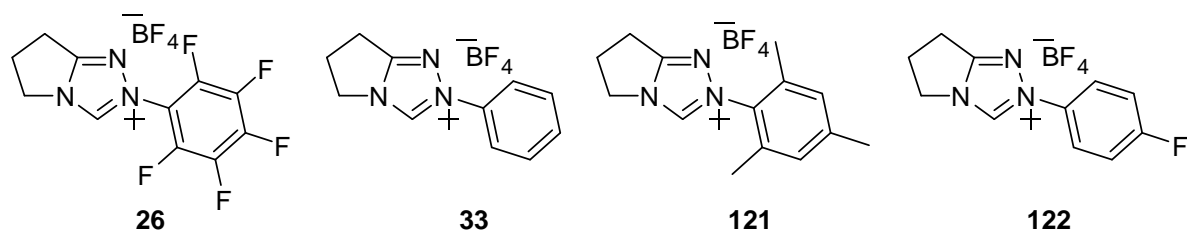
Figure 2.5 Four triazolium salts used to probe the nature of the 2-trimethylsilylbenzaldehyde benzoin and cross-benzoin reactions.

The desired homo-benzoin transformation was not observed and no isolated silylated homo-benzoin product **123** was obtained (**Scheme 2.2**). For the reaction in the presence of the N-phenyl catalyst **33**, several small peaks were observed in the silyl region by ^{1}H NMR spectroscopy during the reaction. No clear isolable product, such as the homo-benzoin derivative **123**, was observed by LC-MS and ^{1}H NMR spectroscopy on completion of the reaction, suggesting that the transformation in **Scheme 2.2** is not the favoured product under these conditions, and may not be formed. Peaks observed at 6.25 ppm, **Figure 2.6**, are potentially consistent with the initial hydroxyaryl adduct formed upon addition of NHC to 2-trimethylsilyl benzaldehyde **109**, however, there are clearly multiple by-products. Test homo-benzoin studies of 2-trimethylsilyl benzaldehyde **109** were also conducted using the N-mesityl **131** and N-parafluorophenyl **132** triazolium catalyst, and similar behaviours were observed. Again, no benzoin product was identifiable. Peaks potentially consistent with a hydroxyaryl adduct species are again observed, and generally fewer peaks are visible in the spectra of experiments with the latter two catalysts.
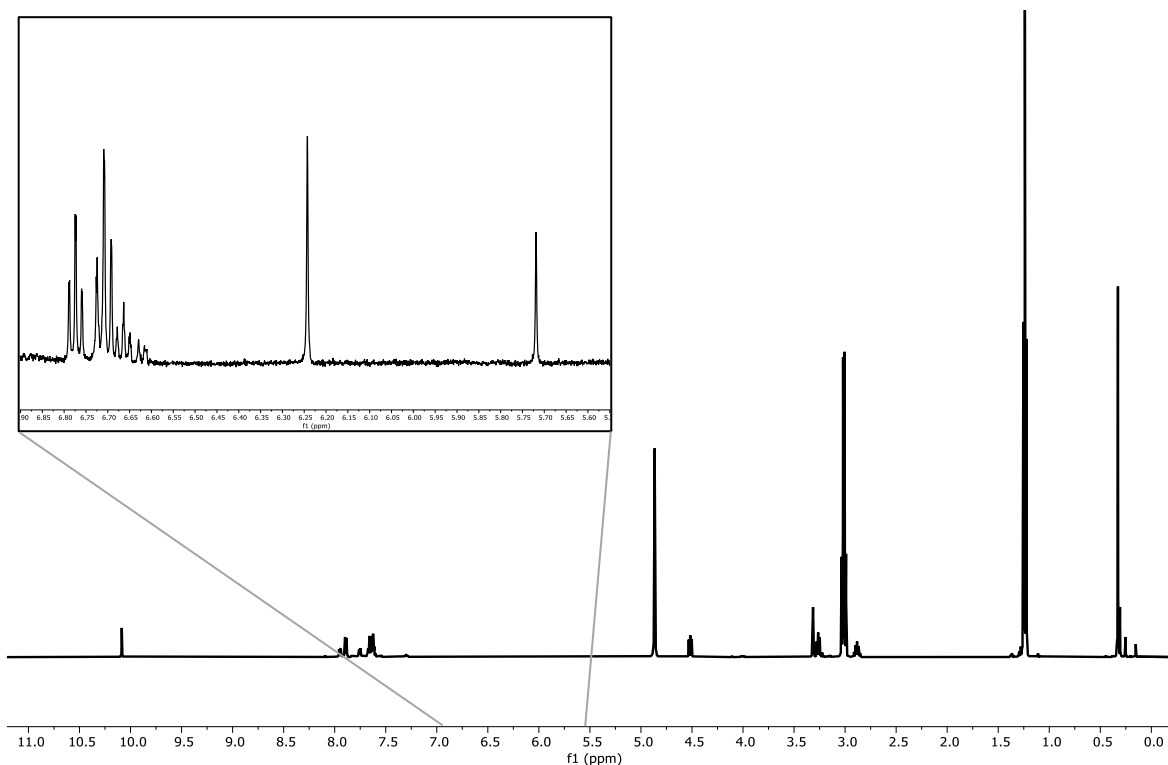
Figure 2.6 ^{1}H NMR in CDCl$_3$ of the reaction between the N-phenyl triazolium salt **33** and 2-trimethylsilyl benzaldehyde **109**. The insert shows the region between 6.90 and 5.55 ppm showing small quantities of the suspected hydroxyaryl adduct product at 6.25 ppm.
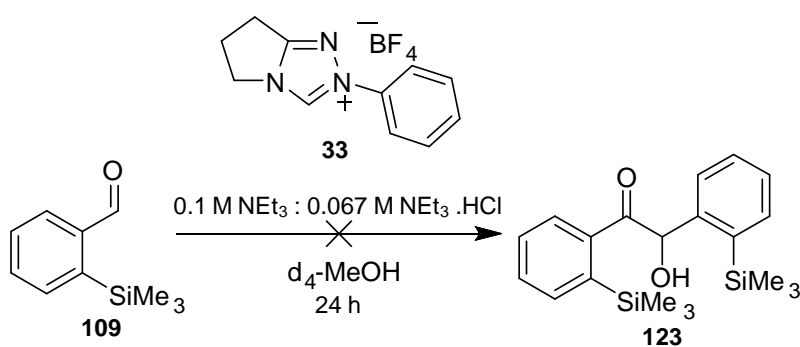
Scheme 2.2 Unobserved transformation of 2-trimethylsilyl benzaldehyde **109** to a homo-benzoin derivative catalysed by N-phenyl triazolium salt **33** with a 0.167 M buffer of triethylamine and triethylamine hydrochloride in d$_4$-methanol.

45

The next step was to determine whether the 2-trimethylsilyl benzaldehyde would out-compete the known homo-benzoin reaction of benzaldehyde (**Scheme 2.3**). Given the behaviour observed for other 2-substituted aldehydes[31], it is possible that the 2-trimethylsilyl benzaldehyde would react preferably with the Breslow intermediate derived from non-2-substituted benzaldehyde in a cross-benzoin reaction rather than the onward benzaldehyde homo-benzoin reaction. With this, it would be possible to determine whether the modified substrate could be used for cross-benzoin reactions. As 2-heteroatom and 2-alkyl benzaldehyde derivatives generally outcompete benzaldehyde derivatives with no 2-substitution in coupling with the Breslow intermediate[32], 2-trimethylsilyl benzaldehyde could be used to access the normally inaccessible benzoin derivative. With the removal of the silyl group, this could give access to the normal minor cross-product.

Shown in **Figure 2.7** is an ^{1}H NMR spectral overlay for the reaction of the N-pentafluorophenyl catalyst in the attempted cross-benzoin reaction of 2-trimethylsilylbenzaldehyde with benzaldehyde. In all cross-benzoin test reactions, equimolar amounts of the aldehydes were used, and a ratio of 1 : 1 : 2 was used for benzaldehyde : 2-trimethylsilyl benzaldehyde : catalyst.
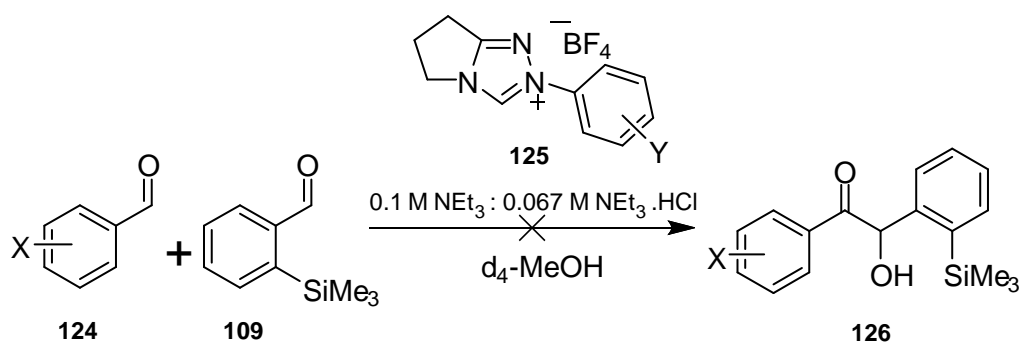
Scheme 2.3 Unobserved cross-benzoin condensation reaction between 2-trimethylsilyl benzaldehyde **109** and a variety of substituted aldehydes **124** with a 0.167 M buffer of

46

triethylamine and triethylamine hydrochloride in the presence of N-aryl triazolium salts **125**.
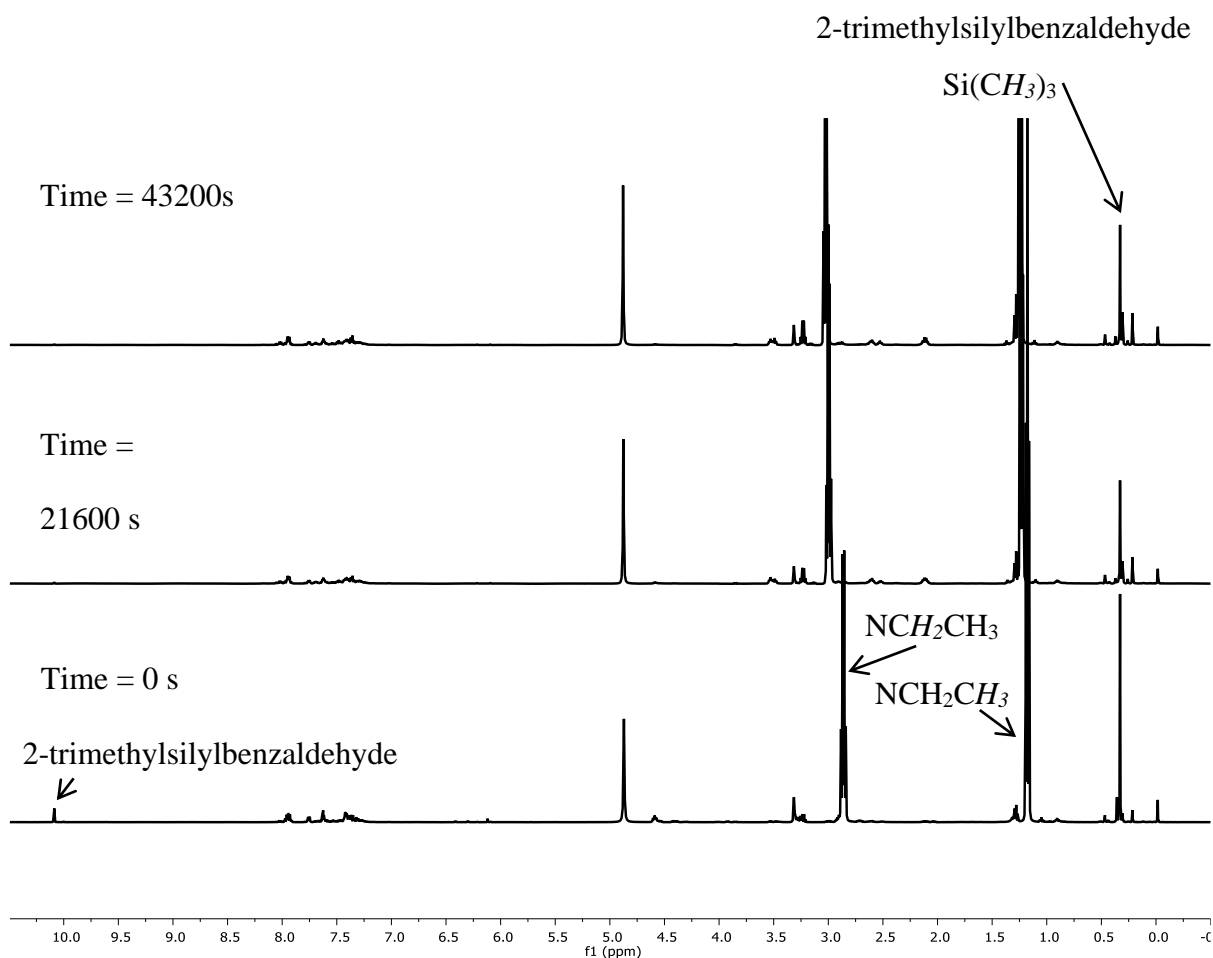
Figure 2.7 ^{1}H NMR spectra in d_4-methanol showing the progress of the reaction of benzaldehyde and 2-trimethylsilyl benzaldehyde in the presence of N-pentafluorophenyl triazolium salt **17**, buffered with 0.167 M triethylamine and triethylamine hydrochloride.

From the work of Jiayun Zhu in the O'Donoghue group, it has been observed that d_1-deuteration of aldehydes by the N-pentafluorophenyl catalyst is relatively rapid, **Scheme 2.3**, where X = H, and this would likely be true by the same mechanism where X = SiMe$_3$[70]. As a result of this, products of the benzoin condensation of d_1-deuterated aldehydes may be unobservable in the region of 5.5-6.5 ppm that would normally be used to look for protons indicative of benzoin formation[67].
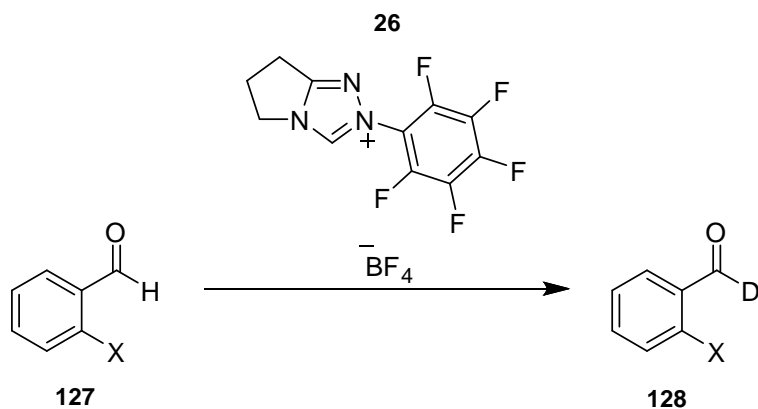
Figure 2.8   Deuteration of aldehydic protons by the N-pentafluorophenyl catalyst **26**, observed to occur rapidly.

Of the catalysts that were used, the N-pentafluorophenyl substituted triazolium salt derived NHC **26** produced the most diverse range of peaks on the ^{1}H NMR spectrum, with multiple peaks appearing in the aryl regions and the alkyl regions (**Figure 2.7**). The aldehydic peak at ~10 ppm is much decreased for benzaldehyde at t = 0. The integral of the peak for the aldehydic proton of 2-trimethylsilyl benzaldehyde at 10.09 ppm reduced to 15% of its initial value over the course of 7 hours and 15 minutes. Over the course of this reaction the integral area of the corresponding singlet owing to the Si(CH_3)$_3$ at 0.33 ppm reduced to 85% of its initial value. This indicates both significant deuteration of the aldehydic proton, and also a breakdown of the 2-trimethylsilyl benzaldehyde. While there are multiple small peaks in the silyl region, it was not clear whether these correspond to the formation of a desired benzoin product under these conditions. **Scheme 2.4**.
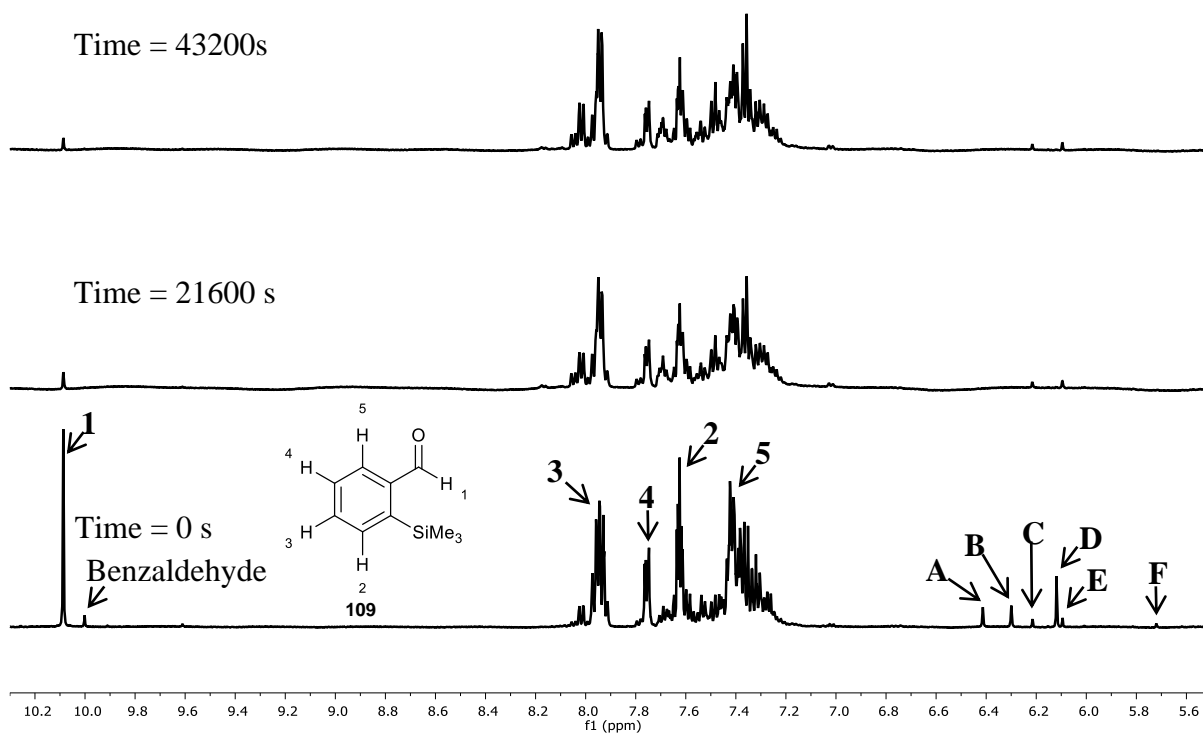
Figure 2.9   Expansion from 10.2 ppm to 3.8 ppm to show peaks in the aromatic and aliphatic regions of **Figure 2.7**.

There are 6 aliphatic peaks between 6.5 ppm and 6.0 ppm in **Figure 2.9**, labelled **A**, **B**, **C**, **D**, **E**, and **F**. Peaks **A**, **B** and **D** had reached an initial maximum value by the completion of the first spectrum, and decayed to where the integral area could not be determined over background levels over the first 1 hour and 25 minutes.
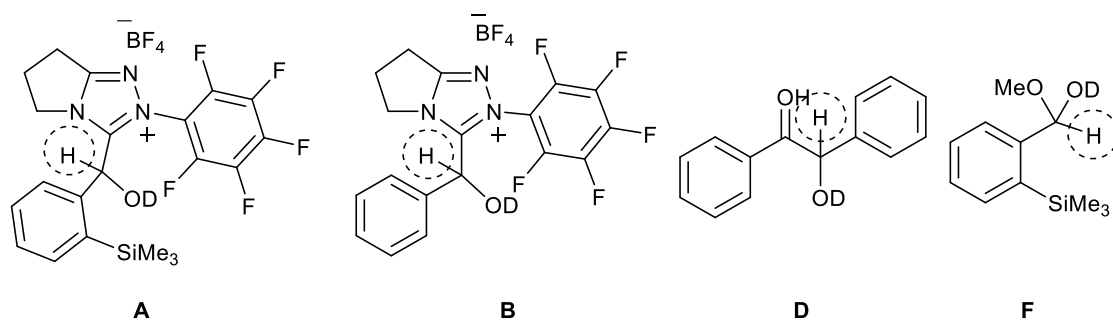
Figure 2.10 Molecules corresponding to peaks B, D, and F, and proposed molecule corresponding to A in **Figure 2.9**.

As there is no significant change in **C** and **E** over the course of the reaction in relation to the baseline noise levels, these peaks are likely due to impurities or by-products. The peak at 6.12 ppm is consistent with the homo-benzoin product of benzaldehyde **D** (**Figure 2.10**), as has been previously identified by Jiayun Zhu of the O'Donoghue group[70]. Peak **B**, at 6.30 ppm, corresponds to identified values for the hydroxyaryl adduct intermediate species of benzaldehyde and the N-pentafluorophenyl catalyst **26**[70]. The peak at 5.72 ppm, labelled **F**, is due to formation of the hemiacetal of the silyl aldehyde, **Scheme 2.4**. This is formed from the addition of the methanol solvent to 2-trimethylsilylbenzaldehyde, and is in equilibrium with the free aldehyde. The remaining peak at 6.41 ppm, **A**, remains unidentified, though could either be the hydroxyaryl adduct of the pentafluorophenyl catalyst **26** and 2-trimethylsilylbenzaldehyde, **Figure 2.10**, or could be an alternative benzoin product.
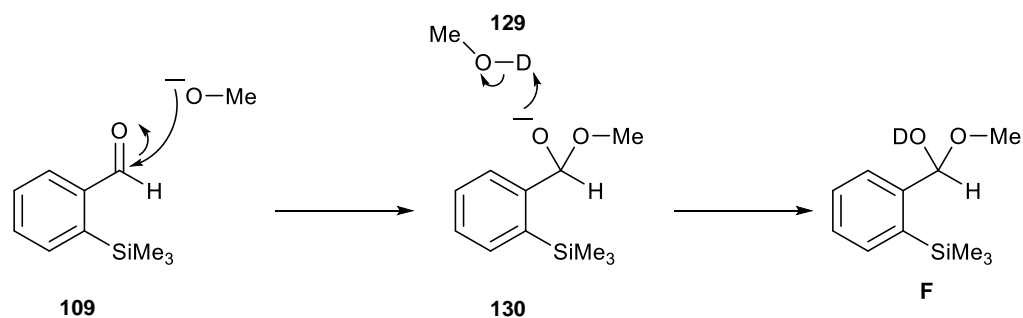
Scheme 2.4 Formation of the hemiacetal of trimethylsilyl benzaldehyde **F** from trimethylsilyl benzaldehyde **109** and deuterated methanol **129**.

A decrease in peaks **2**, **3**, **4**, and **5** was also observed, corresponding to the aryl protons of 2-trimethylsilyl benzaldehyde. The combination of the change of these sets of peaks suggests that there is possibly some formation of the hydroxyaryl adduct species, and a further benzoin product, however additional peaks show other reactions are also occurring in the reaction mixture.

Time =

43200s

Time =

21600 s

Time = 0 s

←Si(CH₃)₃

109

0.95 0.90 0.85 0.80 0.75 0.70 0.65 0.60 0.55 0.50 0.45 0.40 0.35 0.30 0.25 0.20 0.15 0.10 0.05 0.00 -0.05 -0.10 -0.15 -0.20
f1 (ppm)
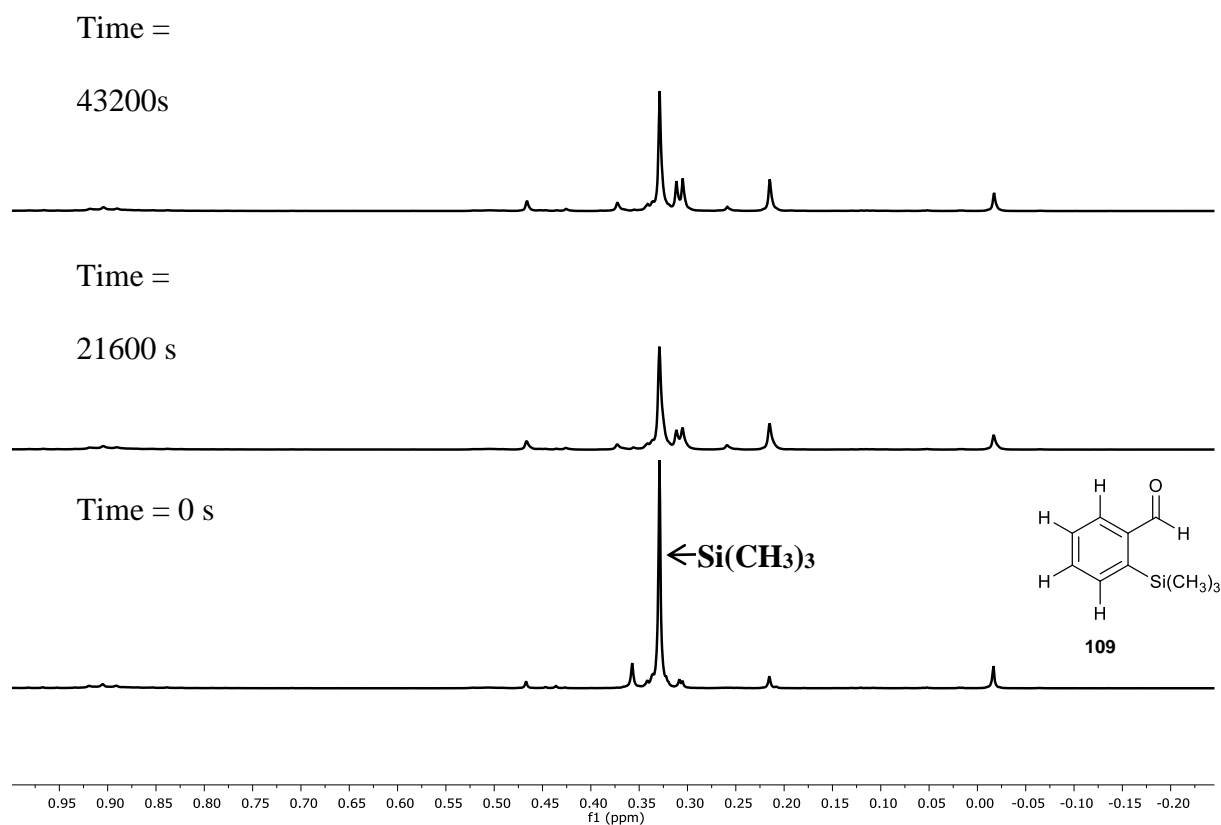
Figure 2.11   Expansion of 1.00 ppm to 0.25 ppm of **Figure 2.7** of the ^{1}H NMR spectrum in d₄-methanol of the reaction between benzaldehyde and 2-trimethylsilyl benzaldehyde in the presence of the N-pentafluorophenyl triazolium salt **26**, buffered with 0.167 M triethylamine and triethylamine hydroxchloride, giving more detail of the silyl region of the ^{1}H NMR spectra.

The NMR spectrum in **Figure 2.11** shows the silyl region of **Figure 2.7**. The singlet peak at 0.33 ppm corresponds to the SiMe₃ group of 2-trimethylsilyl benzaldehyde **109**. Other peaks in the silyl region form during the course of the reaction time; however none of the changes in intensity of these peaks appears to correspond to peaks **A**, **B**, **C D**, or **E** in **Figure 2.9**. However, as there is likely deuteration of protons with peaks in the benzoin region, formation of a benzoin product cannot be ruled out on this basis. Due to the complexity of peaks in this region, coupled with the complexity of the peaks in the

aromatic regions in **Figure 2.9**, it is difficult to find definitive evidence for formation of a distinct benzoin product. Attempts to observe the desired product by LC-MS did not give evidence of the formation of the desired product. It is likely that silyl migration occurs, giving rise to the large number of peaks in the silyl region. A representative scheme for a covalent mechanism for this migration has been presented in **Scheme 2.5**, though a more complex radical mechanism may also be possible.
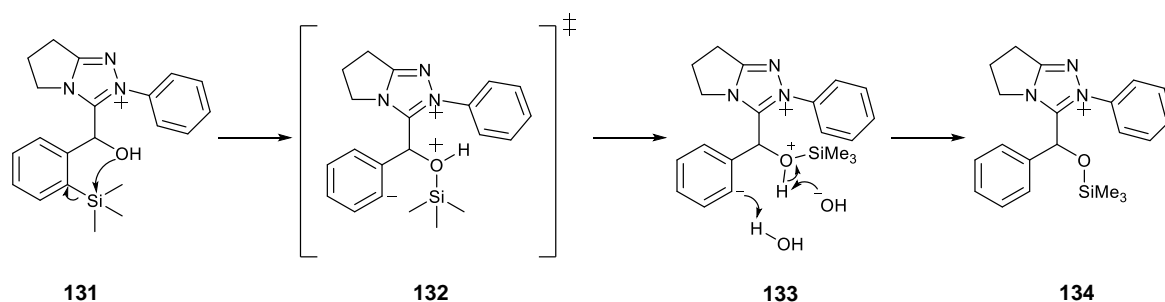
Scheme 2.5   Representative scheme for suspected silyl migration from the aromatic ring to the hydroxyl group.

The N-*para*-fluorophenyl substituted triazolium salt derived catalyst **122** also produced unidentifiable products, though at a slower rate. It was speculated that the reason for this slower rate of reaction was a result of a reduced electronic impact of the NHC N-aryl substituent in the second case, and potentially less silyl group migration. With the N-*para*-fluoro catalyst, **Figure 2.12**, the integral area of the peak corresponding to the silyl aldehydic proton reduced to 84% intensity over 16 hours. The integral area of the peak corresponding to the trimethylsilyl group reduced to 95% intensity during this time. Though there are some unwanted reactions, these are reduced in incidence in comparison to what was observed with the penta-fluoro catalyst **26**. There is a lower incidence of deuteration in comparison to similar timepoints in **Figure 2.7** The aldehydic peaks in **Figure 2.12** and **Figure 2.13** appear to have decreased by more than 5-15% upon glancing

at the spectra, however, there is spectral broadening so the true decrease is much lower after integration.

2-trimethylsilylbenzaldehyde silyl group

Time = 57600s

2-trimethylsilylbenzaldehyde

Time = 2880 s

Time = 0 s
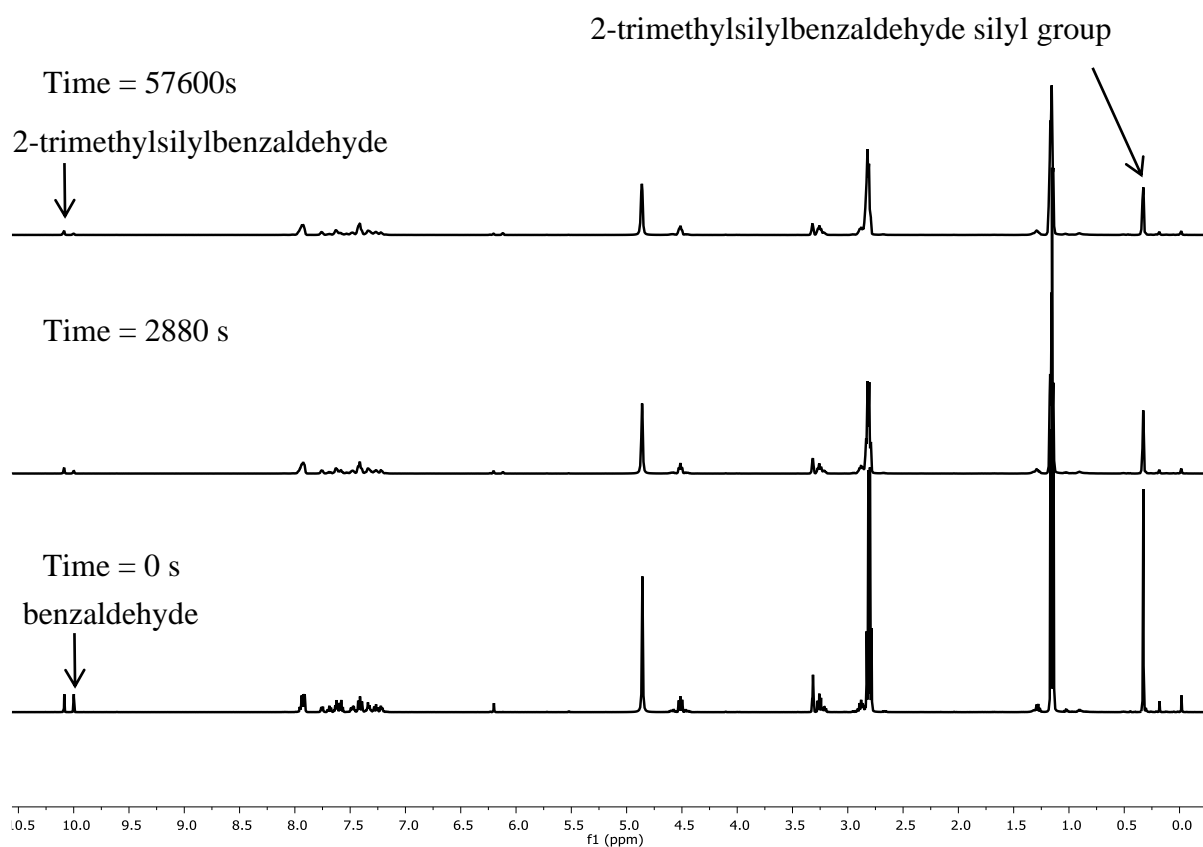
benzaldehyde

Figure 2.12 ^{1}H NMR spectral overlay of the attempted benzoin condensation between 2-trimethylsilyl benzaldehyde and benzaldehyde in d$_4$-methanol in the presence of the N-*para*-fluorophenyl triazolium salt **122**, buffered with 0.067 M : 0.1 M NEt$_3$·HCl : NEt$_3$.
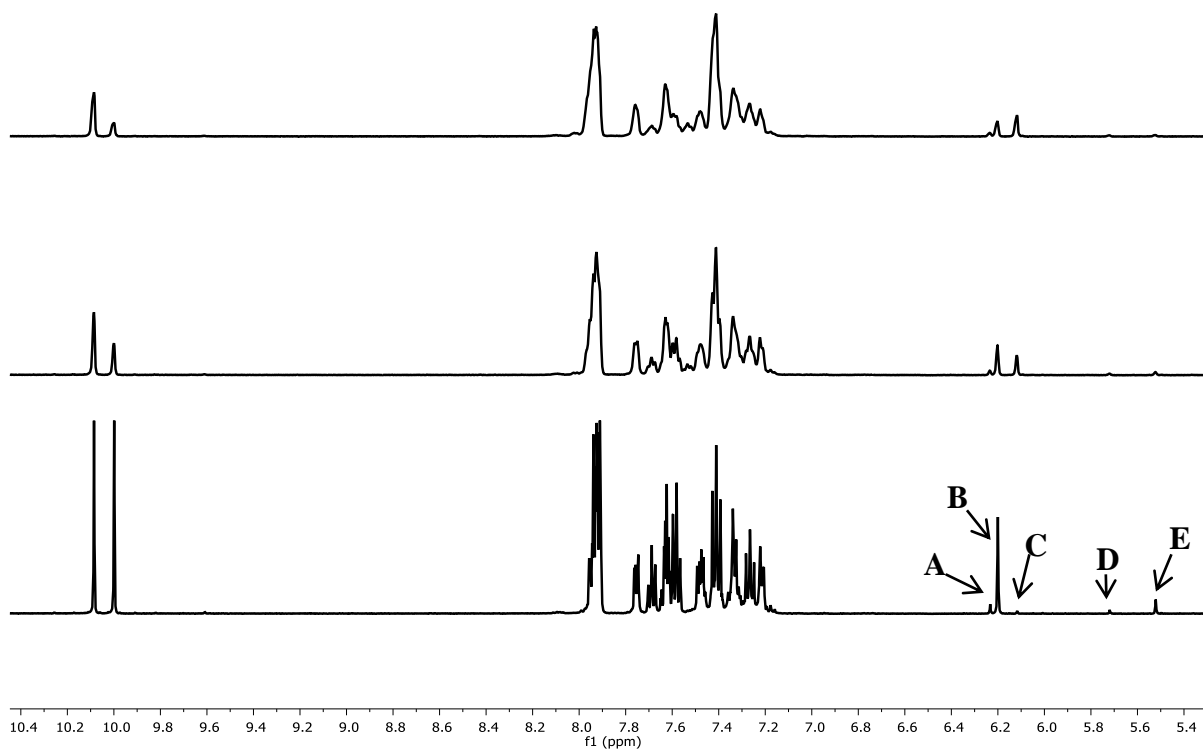
Figure 2.13 Expansion of the 10.4 ppm to 5.3 ppm region of the ^{1}H NMR spectrum **Figure 2.12** giving more detail of the aromatic and benzylic proton regions in the attempted benzoin condensation between 2-trimethylsilyl benzaldehyde and benzaldehyde in d$_4$-methanol in the presence of the N-*para*-fluorophenyl triazolium salt **122**, buffered with 0.067 M : 0.1 M NEt$_3$·HCl : NEt$_3$.

There are peaks at 0.0 ppm and 0.3 ppm in **Figure 2.12**. It is unclear what these peaks could correspond to, with possibilities being small concentrations of NHC-silylaldehyde adducts, or of liberated trimethylsilyl groups from proto desilylation. In **Figure 2.13** there are peaks at 6.23 ppm, 6.20 ppm, 6.12 ppm, 5.72 ppm and 5.52 ppm, labelled **A**, **B**, **C**, **D** and **E** respectively.

55
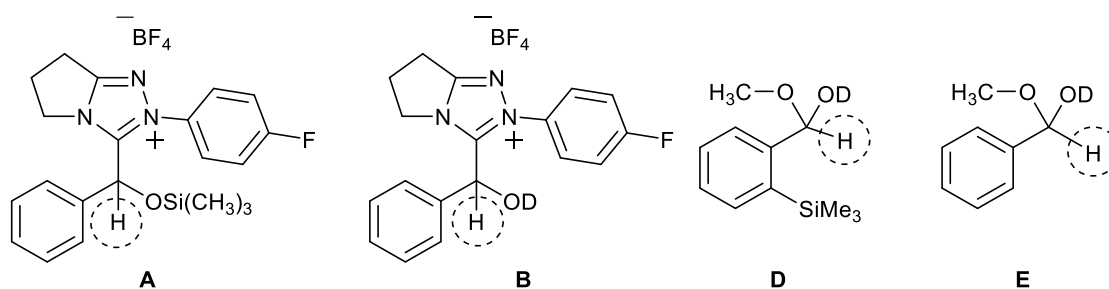
Figure 2.14 Molecules corresponding to peaks **B**, **D**, **E**, and the potential adduct corresponding to **A** of **Figure 2.13** with the protons corresponding to these peaks circled.

Peak **E**, at 5.52 ppm, corresponds to the formation of the hemiacetal of benzaldehyde with methanol, and Peak **D**, at 5.72, corresponds to the hemiacetal of 2-trimethylsilyl benzaldehyde with methanol, as seen in **Figure 2.9**. The largest peak, **B** at 6.20 ppm, is the hydroxyaryl-NHC adduct between the N-*para*-fluorophenyl catalyst **122** and benzaldehyde, as identified by Jiayun Zhu of the O'Donoghue group. Peak **A**, at 6.23 ppm, has previously been observed in the homo-benzoin study of 2-trimethylbenzaldehyde with the N-*para*-fluorophenyl catalyst **122**, and so is most likely the adduct between these two species. However, it is unclear where the trimethylsilyl group is bonded within this species as there may have been silyl migration from carbon to oxygen. Additional NMR experiments, such as Nuclear Overhauser effect (NOE) studies could identify this in future. Peak **C** is minor and does not change substantially, this could be due to a minor by-product of the reaction mixture.
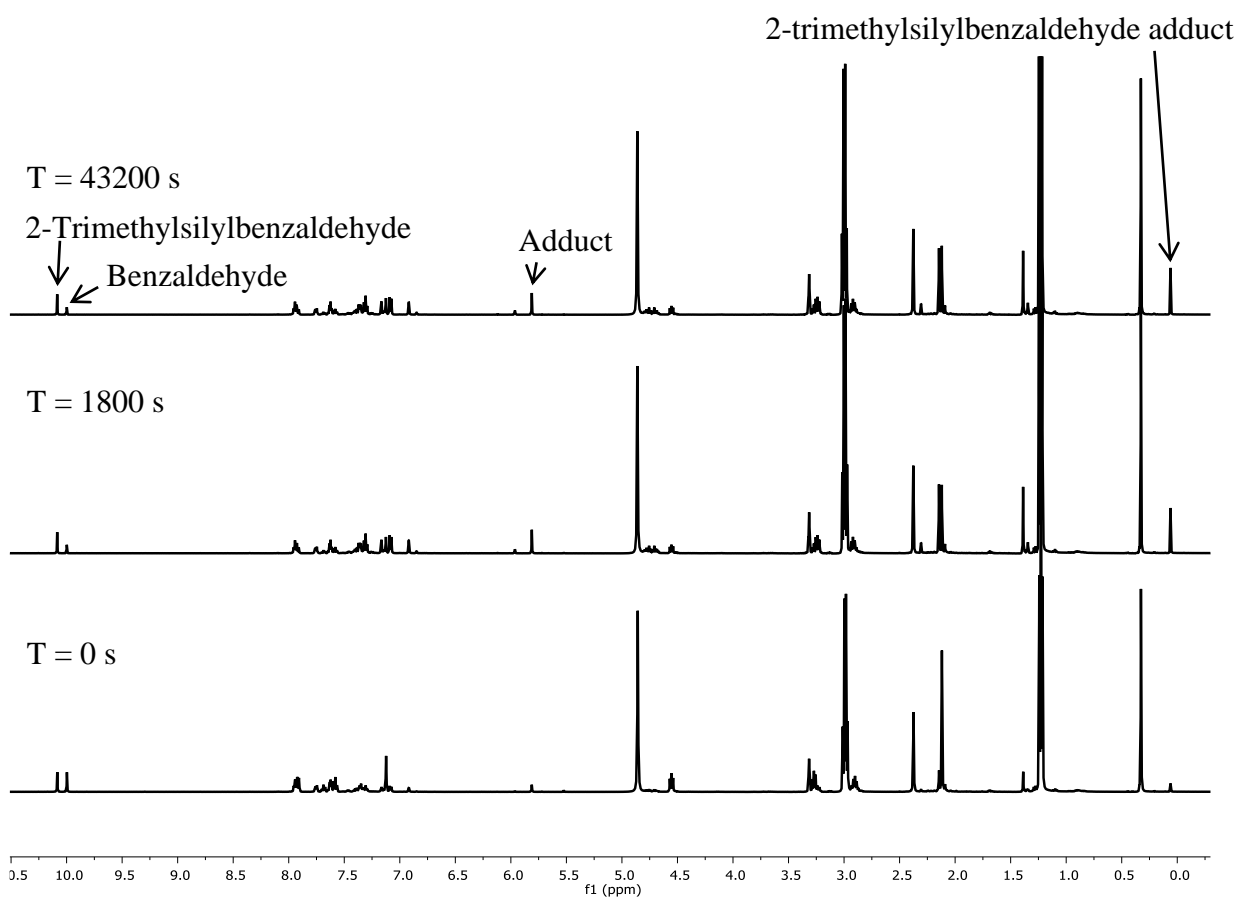
Figure 2.15 ^{1}H NMR spectra for the cross-benzoin reaction between benzaldehyde **46** and 2-trimethylsilylbenzaldehyde **109** in d$_4$-methanol using the N-mesityl triazolium salt **121** derived NHC over the course of a 12 hour period, buffered with 0.067 M : 0.1 M NEt$_3$·HCl : NEt$_3$.

In **Figure 2.15** and the expansion, **Figure 2.16**, representative spectra are shown for the progression of the reaction of the attempted cross-benzoin condensation of benzaldehyde **46** and 2-trimethylsilyl benzaldehyde **109** catalysed by the N-mesityl triazolium salt **121**. At T = 0, initial peaks can be observed for the aldehydic protons of benzaldehyde and 2-trimethylsilyl benzaldehyde at 10.00 ppm and 10.08 ppm respectively. The peak at 0.33 ppm corresponds to the trimethylsilyl group of the 2-trimethylsilyl benzaldehyde. There are peaks at 4.55 ppm, 3.28 ppm and 2.90 ppm which correspond to the CH$_2$ groups of the fused aliphatic ring of the N-mesityl catalyst. As the chemical shift

of the aldehydic proton in d_1-chloroform of 2-trimethylsilyl benzaldehyde is 10.17 ppm, and the chemical shift of the aldehydic proton of benzaldehyde is 10.01 ppm, it can be inferred that the peaks at 10.0 ppm and 10.08 ppm in d_4-methanol correspond to benzaldehyde and 2-trimethysilylbenzaldehyde respectively. This is supported by observations during the homo-benzoin studies.
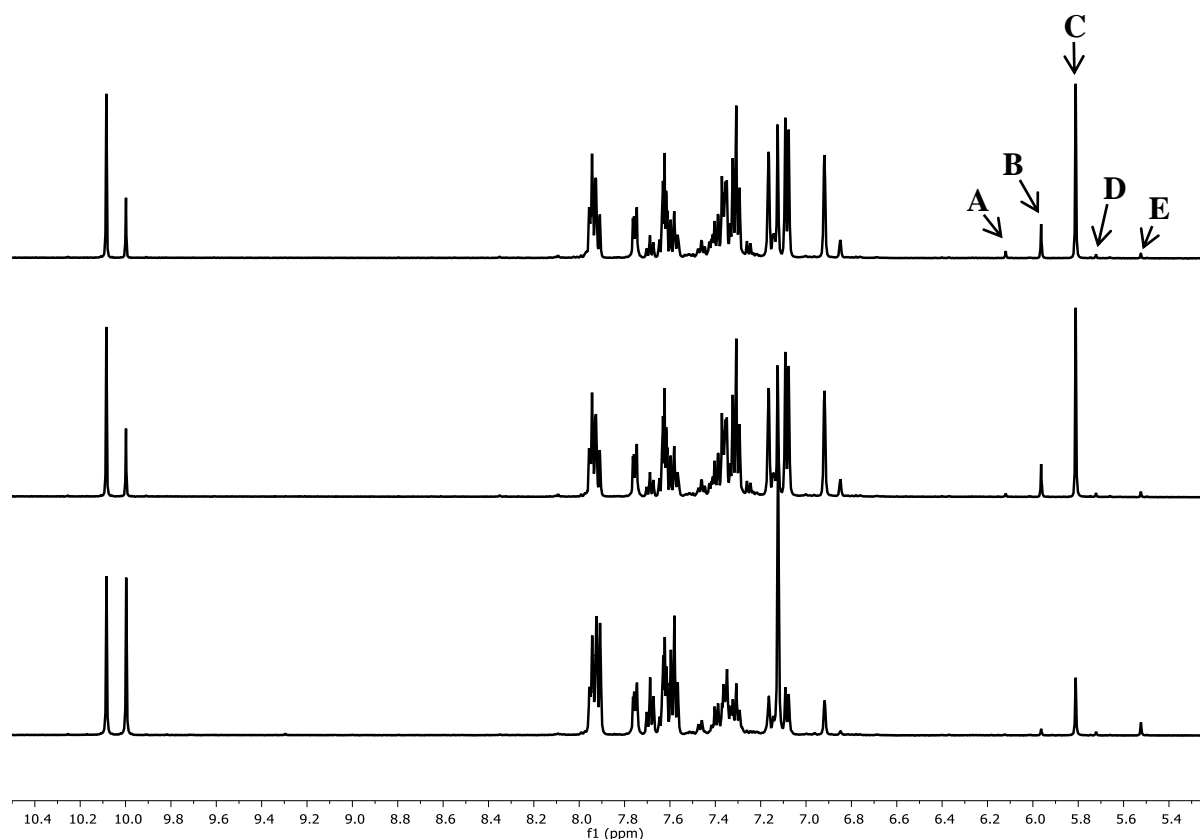
Figure 2.16   Expansion from 10.5 ppm to 5.2 ppm of the ^{1}H NMR spectra in **Figure 2.15** of the reaction between benzaldehyde and 2-trimethlsilyl benzaldehyde **109** in d_4-methanol catalysed by the N-mesityl triazolium salt **121** derived NHC over the course a 12 hour period, showing the aromatic region and the benzylic proton region.

In **Figure 2.16** the peaks observed over the course of the reaction at 6.12 ppm, 5.96 ppm, 5.81 ppm, 5.72 ppm and 5.52 ppm, are labelled **A**, **B**, **C**, **D**, and **E** respectively. Peak **B**, at 5.96 ppm, started at a minimum value, and increased to a maximum value over 14

hours. The integral area of peaks **D** and **E**, at 5.72 ppm and 5.52 ppm, remained constant over the course of the reaction. The integral area of the peak **A**, at 6.12 ppm, increased at a constant rate over the course of the reaction. From the work of Jiayun Zhu of the O'Donoghue group[70], we know that peak **C**, at 5.81 ppm, corresponds to the hydroxyaryl adduct between the N-mesityl catalyst and benzaldehyde, whereas peak **A**, at 6.12 ppm, corresponds to the homo-benzoin product of benzaldehyde. Peaks **D** and **E**, at 5.72 ppm and 5.52 ppm respectively, correspond to the hemiacetal product of benzaldehyde and methanol, and the hemiacetal of 2-trimethylsilylbenzaldehyde and methanol respectively. By a process of elimination, peak **B**, at 5.96 ppm, likely corresponds the hydroxyaryl adduct species between the N-mesityl catalyst **121** and 2-trimethylsilylbenzaldehyde, similar to peak **A** in **Figure 2.13** for catalyst **122**. As before, additional ^{1}H NMR experiments such as NOE studies would be required to identify whether silyl migration, particularly in an intramolecular manner from carbon to oxygen, had occurred.
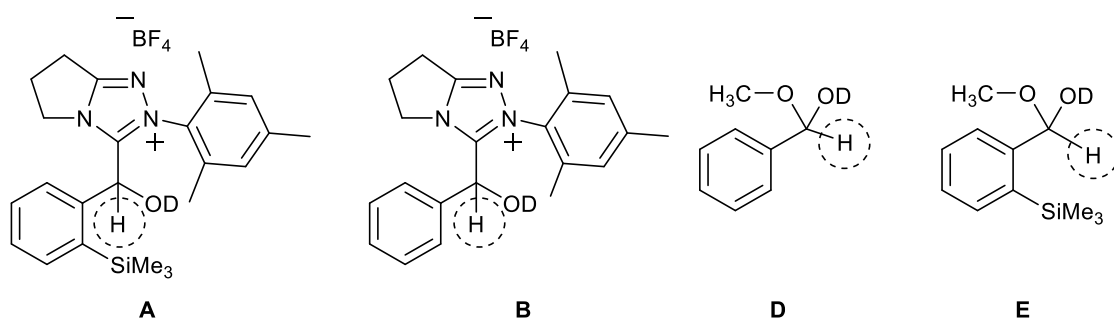
Figure 2.17 Molecules potentially corresponding to peaks **A**, **B**, **D**, and **E** of **Figure 2.16**, with protons corresponding to these peaks circled.

Over the course of the 14 hours of reaction time, the integral area of the silyl aldehydic peak at 10.08 decreased to 89% of the initial value at T = 0. The integral area of the benzaldehydic peak at 10.00 decreased to 33% of the initial value. The integral area of the peak at 0.33 ppm decreased to 89% of the initial value, which is consistent with the change in the area of the peak at 10.08. The integral area of the peak at 5.96 ppm increased to ~20% of the initial integral area of the peak at 10.08. The integral area of the peak at 5.81 increased to 108% of the initial integral area of the peak at 10.00. The integral area of the peak at 0.06 ppm increased to 18% of the initial integral area of the peak at 0.33 ppm. New peaks appear at 3.25 ppm and 2.91 ppm, though changes in integral areas of these peaks cannot be resolved due to the peaks at 3.25 ppm and 2.90 ppm respectively. These integral changes are consistent with the formation of adducts of the mesityl catalyst with both 2-trimethylsilyl benzaldehyde and benzaldehyde. There also appears to be the formation of benzoin, with no evidence for formation of cross-benzoin observed in the silyl region of the spectrum. Small discrepancies in the integral areas relative to each other are likely due to error.
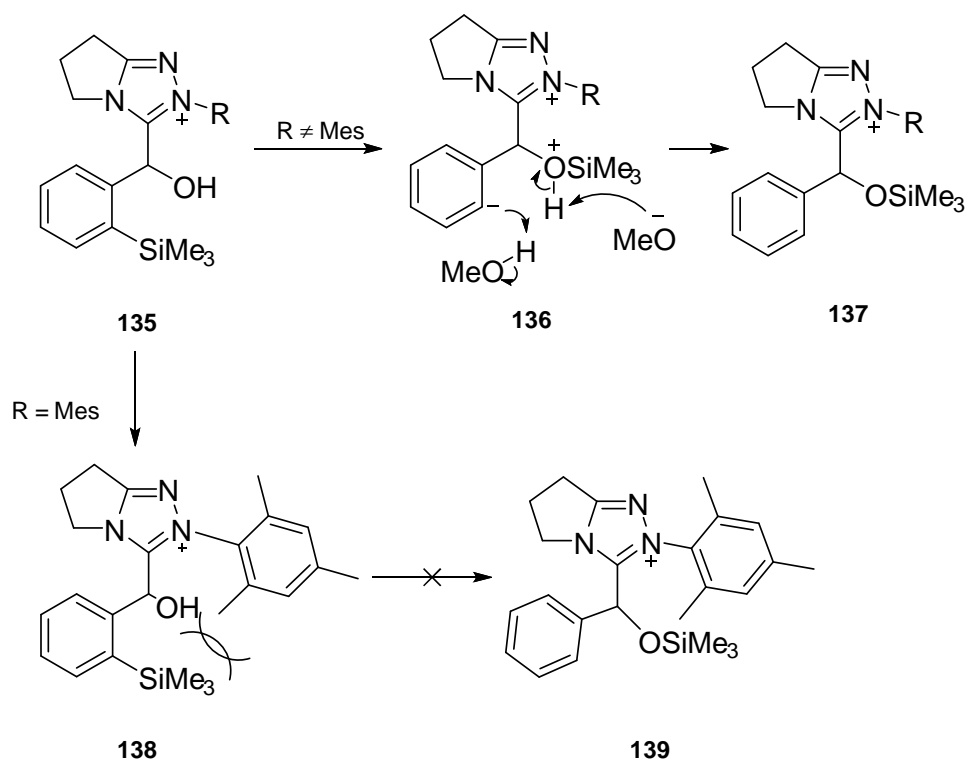
Scheme 2.6   Migration of the trimethylsilyl group onto the oxygen may be inhibited by the steric hindrance of the mesityl N-aryl group on the trimethylsilyl group and the hydroxyl group.

In the case of the mesityl catalyst **121**, the reaction appeared to proceed to the expected trimethylsilyl hydroxylaryladduct intermediate with no additional species observed. It was thought that the success of this reaction was as a direct result of steric hindrance of the hydroxyl group and on the trimethylsilyl group by the methyl groups on the mesityl N-aryl substituent, shown in **Scheme 2.6**, allowing the hydroxyaryl adduct to maintain its core skeletal structure without unwanted side reactions such as silyl migration. The peak at 5.96 ppm integrates with the new peak in the silyl region at 0.06 ppm, inferring that these are both as a result of the formation of the trimethylsilyl hydroxyaryl adduct species.

In summary, reactions of 2-trimethylsilyl benzaldehyde with three different catalysts in cross-benzoin reactions with benzaldehyde were monitored by ^{1}H NMR spectroscopy over the course of the reaction. It appeared that the benzaldehyde homo-benzoin reaction outcompeted the cross-reaction with 2-trimethylsilyl benzaldehyde, producing the undesired homo-benzoin product. As there is evidence for formation of the first hydroxyaryl adduct, this may indicate that either the formation of the Breslow intermediate from a silylaldehyde-derived adduct or the onward Breslow intermediate reaction with 2-trimethylsilyl benzaldehyde is slow.

2.3   Further cross-benzoin kinetic studies using 2-trimethylsilyl benzaldehyde

One of our aims for studying the cross-benzoin reactions with silylated aldehyde, was to potentially manipulate the observed 2-substituent effect to produce molecules such as **140**. This silyl group of this product could then be abstracted with desilylating agents such as TBAF **119** to produce molecules such as **141**; which are more difficult to produce through other methods, **Scheme 2.6**.
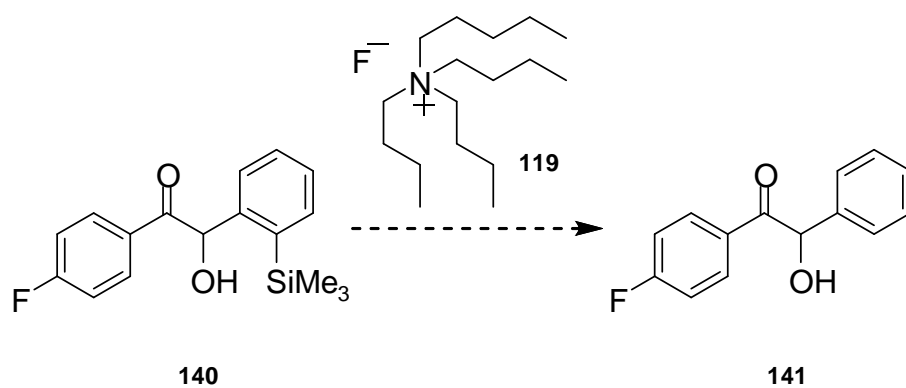
Scheme 2.7   Potential route for the formation of 2-hydroxy-1-(4-fluorophenyl)-2-phenylethan-1-one **141** from 2-hydroxy-1-(4-fluorophenyl)-2-2-trimethylsilylphenylethan-1-one **140** using tetrabutylammonium fluoride **119**.

Further studies into competition reactions of the benzoin condensation between 2-trimethylsilyl benzaldehyde **109** were also conducted with 4-fluorobenzaldehyde. ^{1}H NMR spectra obtained in these studies were substantially more difficult to analyse in comparison to spectra of the benzaldehyde and 2-trimethylsilyl benzaldehyde cross-benzoin studies and future work should employ 2D NMR to help with assignments.

As mentioned in the previous section, the benzaldehyde homo-benzoin reaction completely outcompeted any reaction with 2-trimethylsilyl benzaldehyde, **Figure 2.15**. The only product species produced was the undesired benzaldehyde-derived homo-benzoin product, although there was good evidence for the formation of the NHC-2-silylaldehyde adduct.

Attempts were also made to isolate the hydroxyaryl adduct species of 2-trimethylsilyl benzaldehyde with NHC derivatives of triazolium salts **26**, **33** and **121**, **Scheme 2.3**, though these did not appear to form a single distinct silylated product. The reaction to form these products was done in the presence of a triethylamine buffer with acetonitrile as the solvent, and was monitored by NMR spectroscopy until the signal of the aldehydic proton was unobservable and reaction was considered complete. Although initially observable by LC—MS, at the end of the reaction, it appeared that there was some degradation of the desired final product, the hydroxyaryl adduct. It was unclear whether this was a side reaction pathway, or an onwards inter- or intra-molecular reaction of an unstable hydroxyaryl adduct species under these conditions.

Efforts were then made to discern the origin of the degradation of any intermediates formed. Initial attempts were made to analyse the reaction mixture of the cross-benzoin reactions by liquid chromatography coupled with mass spectrometry. The spectra obtained from the initial probes into the outcome of the reaction were indistinct with large numbers

of products making the origin of the degradation difficult to evaluate. Origins of this degradation were thought to be through transfer of the silyl group, as in **Scheme 2.5**, particularly to the hydroxyl group of the hydroxyaryl adduct. Efforts were made to isolate the products associated with larger peaks on the liquid chromatography trace; though it was found that exposure of these molecules to water greatly accelerated the rate of degradation. All purified fractions obtained from high performance liquid chromatography degraded to several products that could not be resolved by both NMR and LC-MS spectrometry.
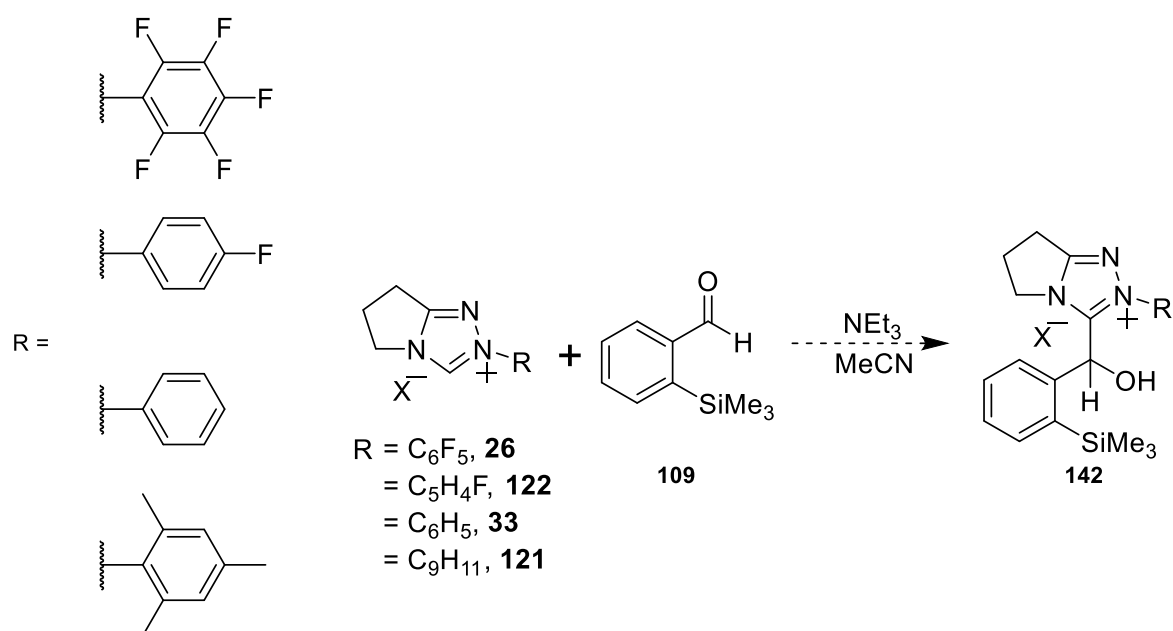
Scheme 2.8   General reaction scheme for the attempted synthetic formation of the hydroxyaryl adduct species from a triazolium salt and 2-trimethylsilyl benzaldehyde.

2.4 Towards the synthesis of silylated triazolium salts

After the difficulties in pursuing the reactions of 2-trimethylsilylbenzaldehyde, the effects of large, sterically-hindering silyl groups as part of the NHC triazolium salt structure became the next avenue of exploration.
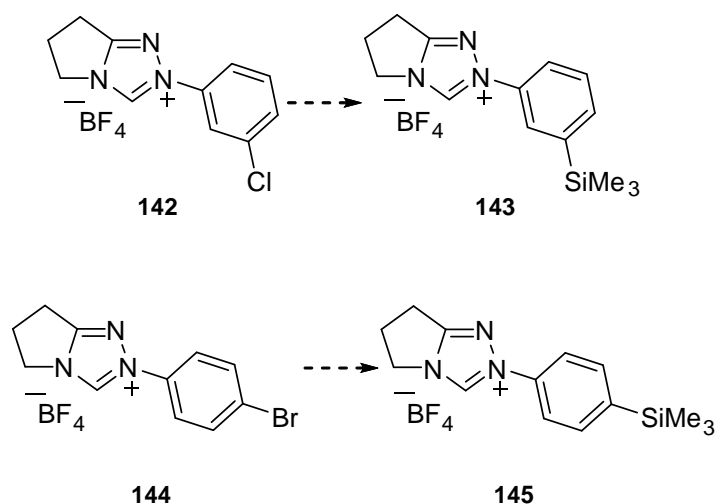
Figure 2.18 Planned transformations to produce silylated triazolium salts **143** and **145** from triazolium salts **142** and **144**.

Two triazolium salts **142** and **144** were prepared, with *meta*-chloro and *para*-bromo N-aryl substituents, respectively. The intent was to use the halogen synthetic handles in these salts to incorporate silyl substituents on the N-aryl groups. The silyl groups would be added to regions which were removed from the catalytic site of the molecule. This was done to examine the effects of the introduction of a silyl group, without direct interference closer to the reactive site. It was postulated that the silyl group may induce a change in the planarity of the N-aryl group in relation to the triazolium ring. The effect of this altered conformation could then be examined on the rate of reaction of the benzoin condensation. These catalysts were targeted, as the relevant N-aryl hydrazine precursors required for the synthetic procedures were readily available commercially.
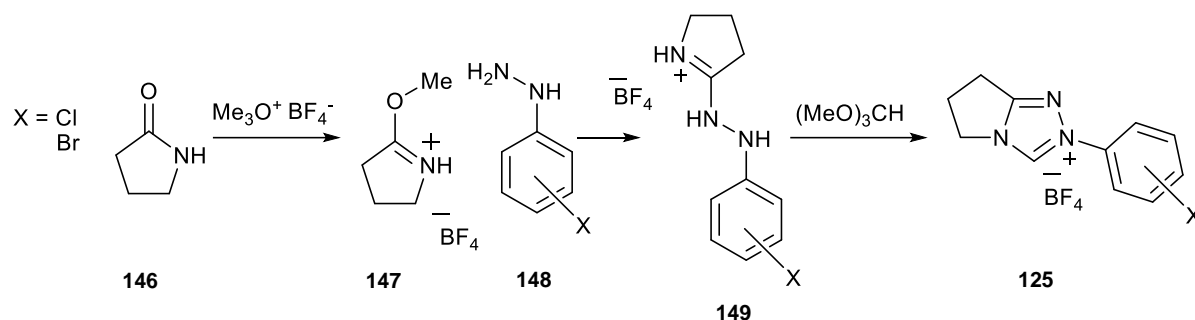
Scheme 2.9 Reaction scheme for the formation of halogenated triazolium salts using the reaction path described by Rovis *et al.*[68]

Triazolium catalyst **142** is not reported in the literature, however, triazolium catalyst **144** was reported in 2017[28]. Initial work into the synthetic procedure towards the *meta*-chloro catalytic system utilised previous synthetic routes to related N-aryl triazolium salts developed in the group based on modifications of that published by Rovis, **Scheme 2.9**[68,71]. Good isolated yields (83%) of this catalyst were obtained with excellent purity. In contrast to this, the *para*-bromo analogue **144** proved more difficult to prepare and isolate.

The reaction procedure used to produce the *para*-bromocatalyst was attempted first. The amidrazone **149** (X=4-Br), was produced in yields of 76%, in the first step. This was determined by terminating the reaction at this stage and analysing the reaction mixture by ^{1}H NMR. The ring closure of the amidrazone **149** with trimethylorthoformate was less successful, with a failure to produce much of the desired product. Catalytic quantities of hydrochloric acid were added to promote this final step, which resulted in a reasonable isolated yield (57%) of the desired product.
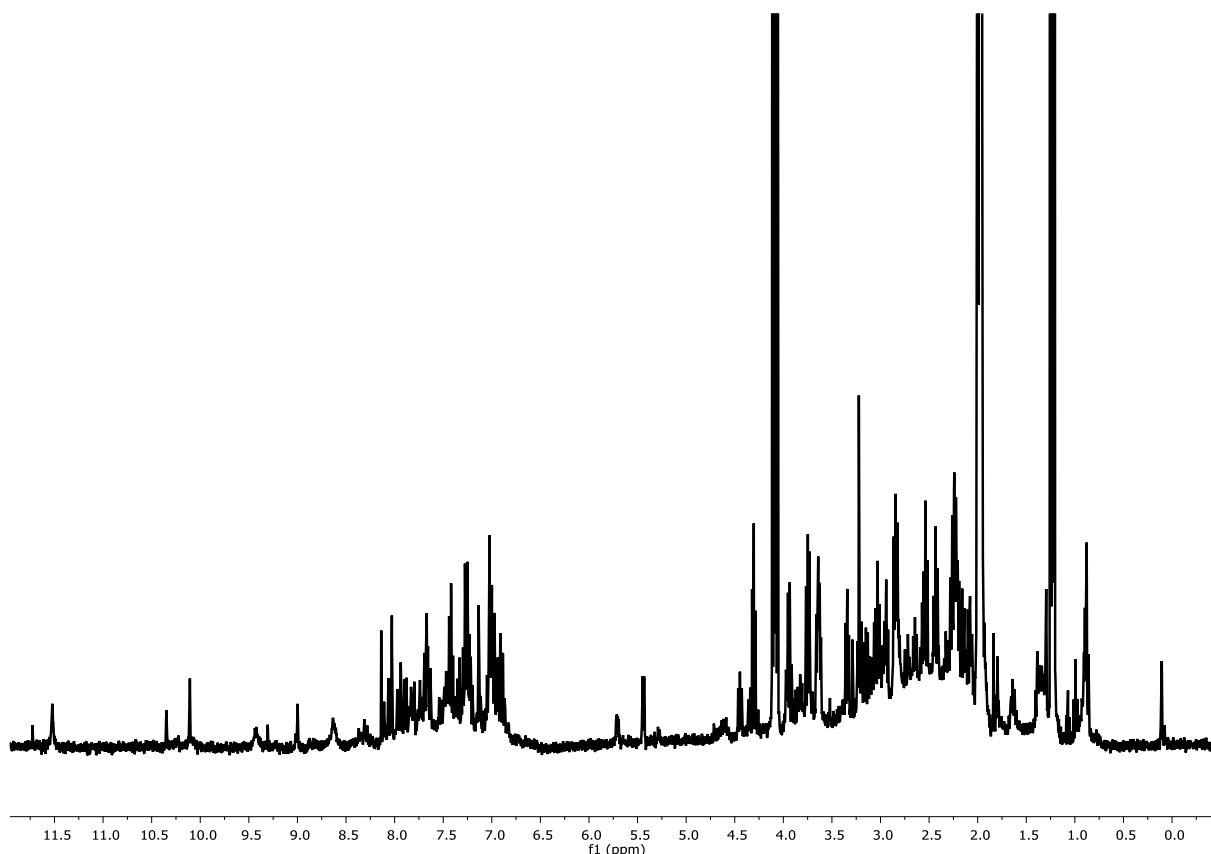
Figure 2.19 ^{1}H NMR spectrum in d$_3$-acetonitrile of the reaction mixture of the *meta*-chloro triazolium salt **142** after lithiation and silylation, showing the large number of unidentifiable peaks.

The *meta*-chloro triazolium salt **142** was a desirable starting point for organolithiation. The objective was to abstract the chlorine with butyl lithium, followed by the addition of trimethylsilylchloride as an electrophile. Previously, in more simple cases in the literature, this was a potential route for silylation. The addition of a butyl lithium solution to the triazolium salt **142** in dry THF caused decomposition, **Figure 2.19**, with many unidentifiable peaks. There is also the potential of nucleophilic addition of the butyl anion, promoting the opening of the triazolium ring.

With the introduction of tetramethylethylene diamine (TMEDA), the amount of side reactions were reduced, though no single distinct product was formed in this case

either, **Figure 2.20**. There is a corresponding increase in the integral area of the remaining peaks between 4.5 and 0.0 ppm. It was thought that during the organolithiation process with the *meta*-chloro triazolium salt, the catalyst had instead been deprotonated at C(3) of the central triazole ring by the butyl lithium reagent, though it was not possible to identify a product of this clearly by NMR spectrometry, **Figure 2.20**. The addition of tetramethylethylenediamine appeared to reduce the peaks owing to unidentified products.
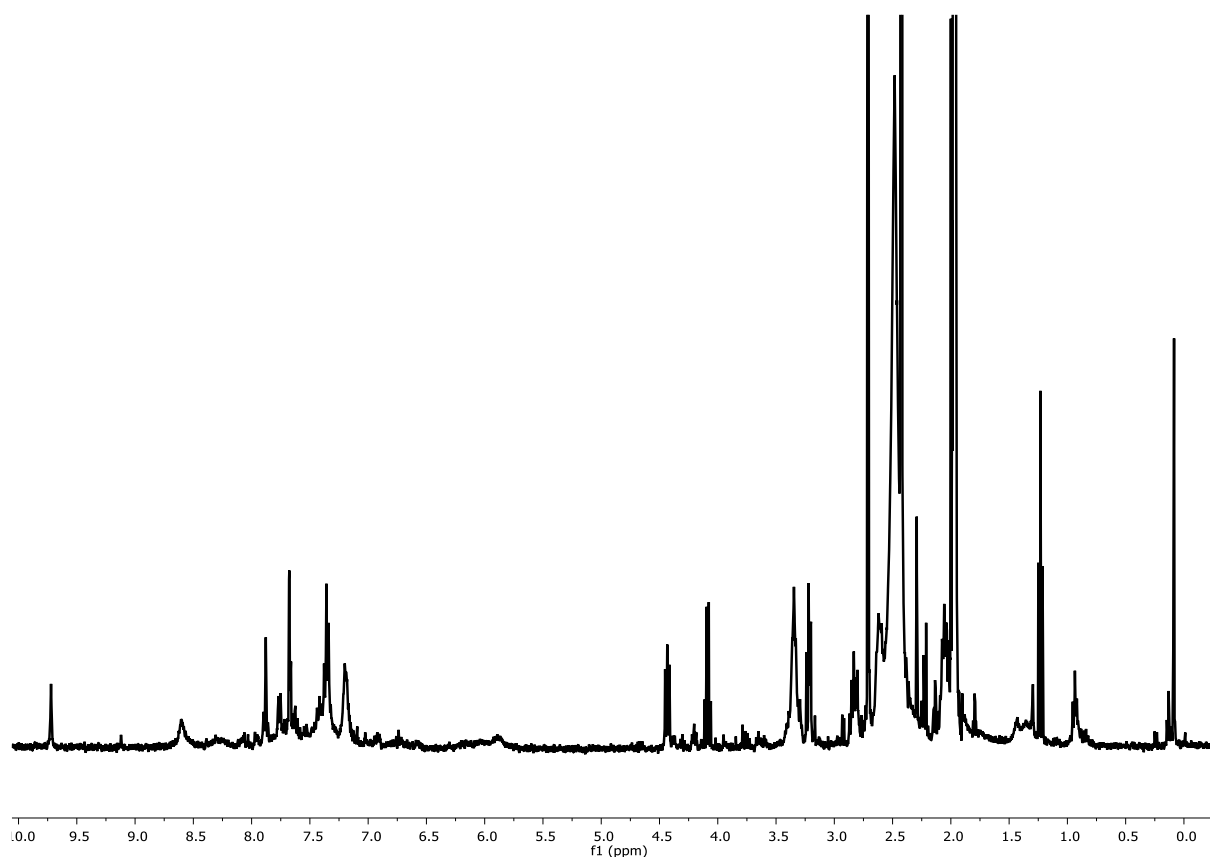
Figure 2.20 ^{1}H NMR spectrum in d$_3$-acetonitrile of the reaction mixture of the *meta*-chloro triazolium salt **142** after lithiation and silylation, with TMEDA added during lithiation.

X = Cl, H

150
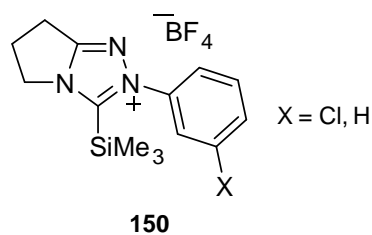
Figure 2.21 Potential products of the silylation experiments in which the C(3) position is silylated and the triazolium structure has remained intact.

By contrast the *para*-bromo triazolium salt **144** was identified as a good candidate for a Grignard style reaction. Grignard reagents had previously been used in silylation, so it was hoped that this would be a potential route for silylation of a triazolium salt. After formation of the organo-magnesium-bromide, trimethylsilylchloride would be added directly as an electrophile to trap the carbanion intermediate.

Investigations into the Grignard type reaction did not yield the desired product. Upon addition of the magnesium and iodine to the reaction mixture, the reaction changed colour, suggesting the success of the initiation. Upon the addition of the electrophile to the reaction, it appeared that the desired product had not been formed, as shown in **Figure 2.22**, as there are no defining peaks expected of the product. After the Grignard reaction had been completed, the solvent was removed under reduced pressure to give a black residue. The residue was exposed to THF, and the organic components that dissolved were examined by ^{1}H NMR spectroscopy. The results of this are shown in **Figure 2.22** and **Figure 2.23**. There is no clear correlation between peaks in the silyl region and peaks in other regions. There was significant conversion of the initial triazolium salt, though there is no clear product. Similar to the organolithiation experiments, it is possible that the reactive carbene centre had ligated onto the magnesium as a result of deprotonation at C(3) of the central triazole. Under the harsher conditions of the reaction, this may have allowed for the

69

ring opening of the triazolium structure. There is also the possibility that the magnesium

has not reacted solely with the bromine of the N-aryl ring, and that the Grignard reagent

has not reacted solely with the C(3) carbon of the triazole, leading to greater complexity of

the spectrum. It is difficult to resolve the formation of any products, such as the N-phenyl

triazolium, that might be observable were these reaction pathways to happen.
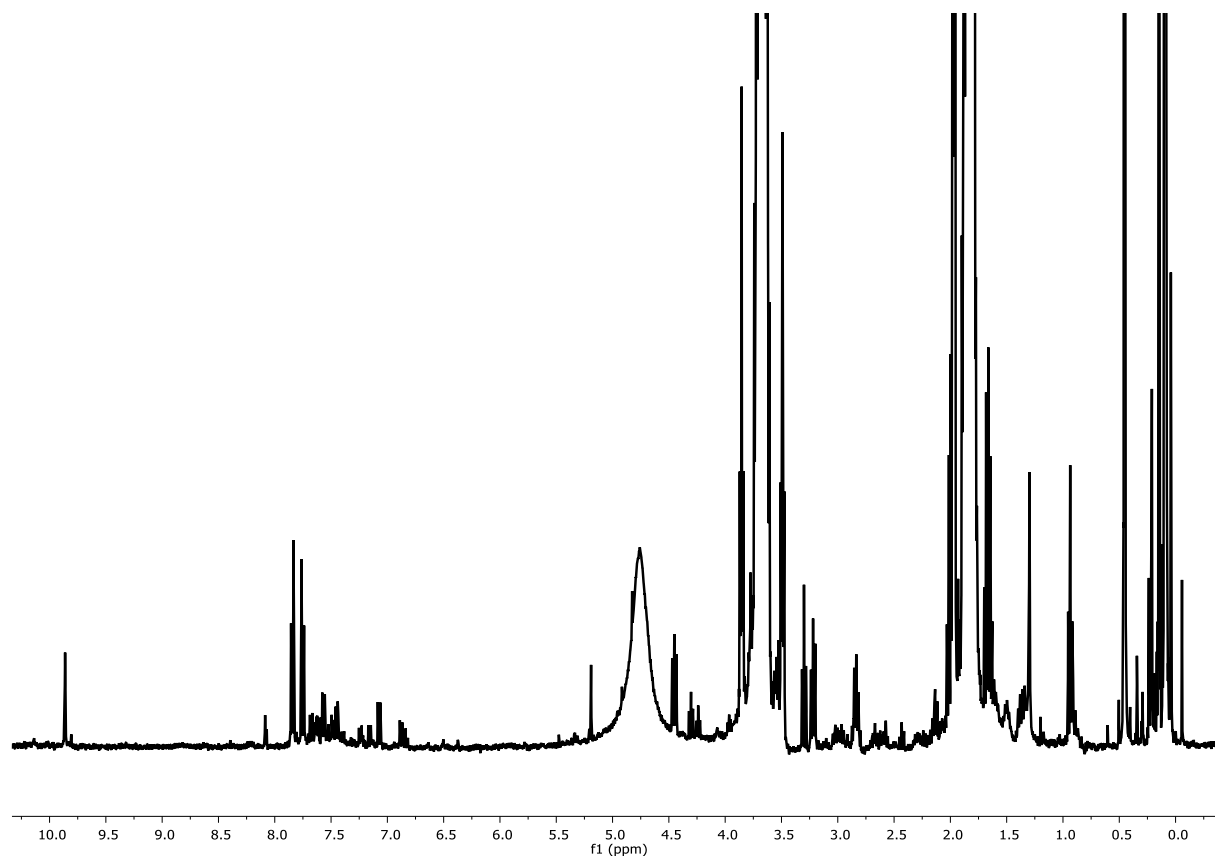
Figure 2.22 ^{1}H NMR spectrum in d4-methanol for the product of the attempted silylation

of the aryl ring of the *para*-bromo triazolium salt **144** under Grignard conditions.

70
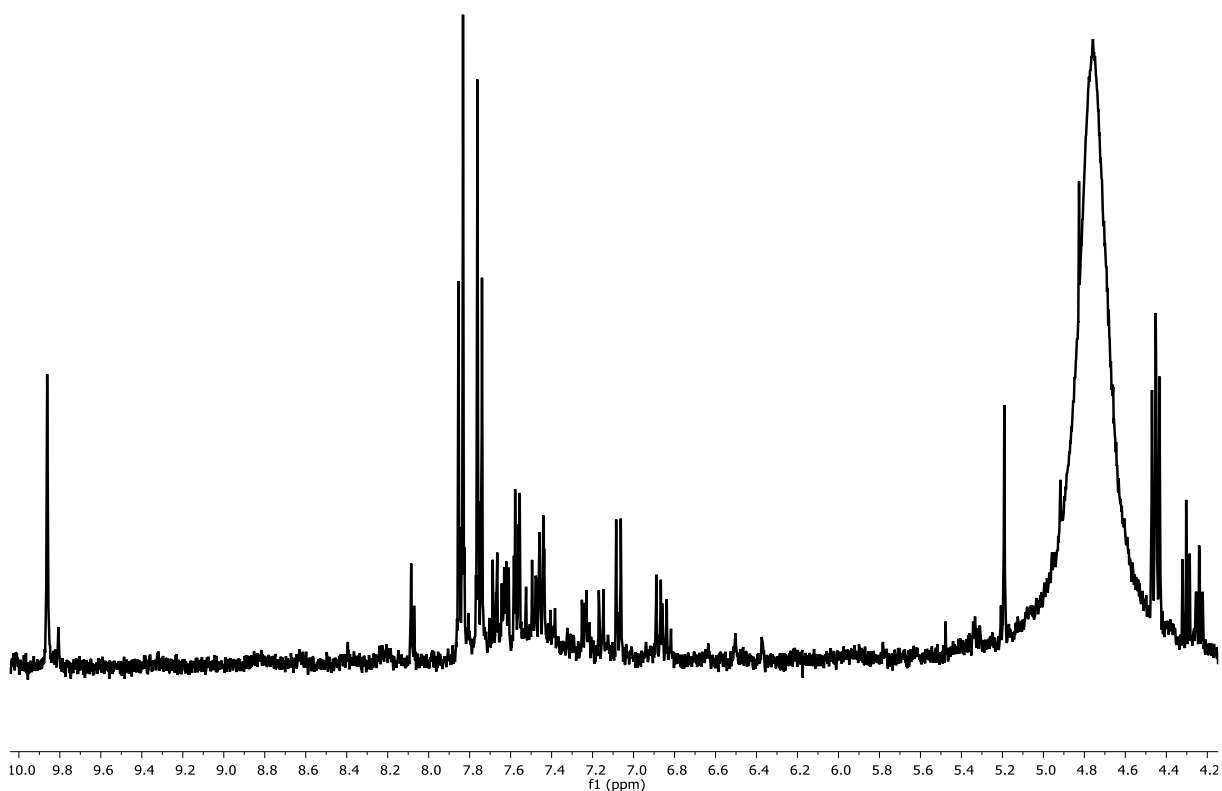
Figure 2.23 Expansion of the ^{1}H NMR spectrum in d$_4$-methanol of compound **144** in the region from 10.0 ppm to 4.2 ppm of **Figure 2.22** in d$_4$-methanol.

151   **152**   **153**
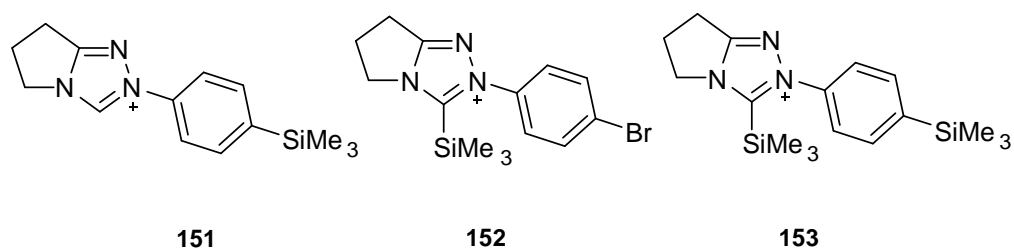
Figure 2.24 Potential products from the silylation reaction of *para*-bromo phenyl triazolium salt **144**.

The crude unidentified products of the Grignard-type reaction were isolated both under normal atmospheric pressure and under vacuum. The products were stable for a few days under vacuum and though unstable upon exposure to air as was noted by ^{1}H NMR spectra obtained for the reaction mixture. While peaks could not be resolved on these

spectra, the number and complexity of peaks increased with exposure to air. Possible problems that may have arisen from these reactions were identified, though the data acquired from the reactions proved inconclusive to determine the reason with complete certainty. It was unclear what the major product was, though it appeared to be sensitive to water. LC-MS and NMR suggest that the products of the reaction were limited to a few major possible products, **Figure 2.24**, though further efforts to identify these products were unsuccessful.

There is also the possibility of attack on the triazolium ring by iodine, the radical initiator for the reaction, resulting in degradation. Unfortunately, while interactions between Lewis bases and 1,2,4-triazolium salts have been investigated[56,72], there have been no publications into the interactions between Lewis acids and 1,2,4-triazolium salts.

During the writing of this thesis, Jiayun Zhu in the O'Donoghue group recrystallized both the *m*-chloro and *p*-bromo triazolium salts prepared in this thesis and collected X-ray crystallographic data on these, with resulting images shown in **Figure 2.25** and **Figure 2.26**. For full data on these molecules, see **Appendix 2**.
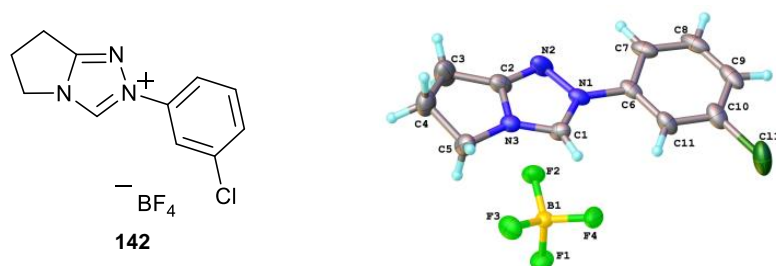
Figure 2.25 Image produced by X-ray crystallography data of the *m*-chloro phenyl triazolium salt **142**.
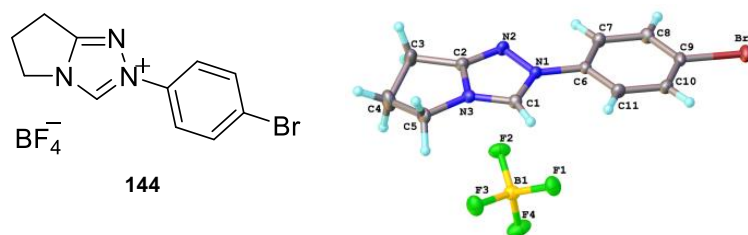
Figure 2.26   Image produced by X-ray crystallography data of the *p*-bromo phenyl triazolium salt **144**.

2.5   Deuterium exchange reactions of 1,2,4-triazolium ions followed by ^{1}H NMR spectroscopy

To identify the acid dissociation constant, pK_a, of the two triazoliums synthesised during this project, **142** and **144**, deuterium exchange experiments were carried out in accordance with previous studies into triazolium salt **33** within the research group[31]. Deuterium exchange reactions for 1,2,4-triazolium ions **33**, **142**, and **144** (10 mM) in D_2O at 25 °C at constant ionic strength $I = 1.0$ (KCl) were carried out at a range of p*D* values[*]. The exchange of the C(3)-H proton for deuterium was followed by ^{1}H NMR spectroscopy (400 and 500 MHz), resulting in the disappearance of the C(3)-H singlet signal. From these data, first-order rate constants for the deuteroxide ion-catalysed exchange, k_{ex} (s^{-1}), were determined, with the intent to estimate carbon acid pK_a values.

---

[*] The data presented for triazolium salts **142** and **144** is newly reported here. The data for triazolium salt **33** is used to determine the accuracy of the results given, relative to previously observed experimental data for the acidity of triazolium salts
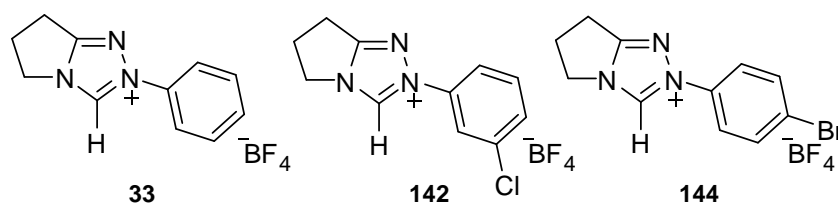
Figure 2.27   Three triazolium salts used in the determination of pK_as of salts **142** and **144**.

2.5.1   Determination of first-order rate constants for exchange k_{ex}

Deuterium exchange reactions were carried out in D_2O solutions of DCl, phosphoric acid buffer, or formic acid buffer in the pD range 0.69 - 3.25 at 25 ˚C and I = 1.0 (KCl). Reactions were typically initiated by the addition of buffer (1 mL) containing internal standard, tetramethylammonium deuteriosulphate (~1 mM), to the substrate (2 mg). Of the resulting solution, 0.8 mL was placed in a capped NMR tube. These samples were stored between NMR analysis in a water bath thermostated at 25 ˚C. At regular intervals, the samples were analysed by ^{1}H NMR spectroscopy.

In cases where the half-life exhibited was shorter than 1 h, the reactions were thermostatted at 25 ˚C directly in the 500 MHz NMR instrument. Over the course of the reaction, the samples were analysed at regular intervals by ^{1}H NMR spectroscopy. Measurement times, t, were calculated from the time at the midpoint of the NMR experiment.

The progress of the deuteration reactions were followed by observing the decrease of the peak at approximately 10 ppm, corresponding to the integral area of the C(3)-H peak of the triazolium ion relative to the integral area of the fixed peak at 3.02 ppm. This corresponded to the non-exchangeable methyl-hydrogens of the internal standard tetramethylammonium deuteriosulphate. The fraction of the remaining, undeuterated triazolium ion, f(s), was

determined using **Equation 2.1**. The pseudo-first-order rate constants, k_{ex}, were determined from semilogarithmic plots of f(s) against time, as shown in **Equation 2.2**. These plots were linear for the observed time frame of the reaction, typically three half-lives.

$$f(s) = \frac{(A_{C(3)H}/A_{std})_t}{(A_{C(3)H}/A_{std})_{t=0}}$$

Equation 2.1

$$\ln f(s) = -k_{ex}t$$

Equation 2.2

2.5.1.a 2-(3-Chlorophenyl)-6,7-dihydro-5*H*-pyrrolo[2,1-c][1,2,4]triazol-2-ium tetrafluoroborate

142   **142-D**
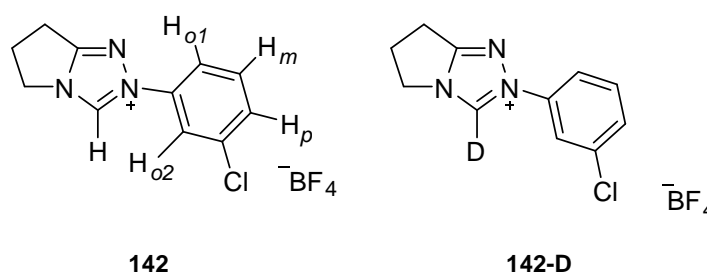
Figure 2.28   Triazolium salt **142** and deuterated form **142-D.**

Pseudo-first-order rate constants for the deuteroxide ion-catalysed exchange of the C(3)-H of triazolium salt **142** to form the corresponding deuterated triazolium salt **142-D** in solutions of DCl were determined by ^{1}H HMR spectroscopy (400 MHz).

A representative set of spectra taken at three time points during the observed H/D exchange reaction at p*D* 0.70 (0.4 M DCl) are shown in **Figure 2.29**. Deuterium exchange at the C(3)-H position resulted in the disappearance of the C(3)-H singlet at 10.00 ppm over the course of the reaction. The extent of exchange was measured relative to the 12 equivalent non-exchangeable protons of the internal standard at 3.02 ppm. In **Figure 2.28**, on the aryl substituent, the *ortho* hydrogen atoms have been labelled H$_{o1}$ and H$_{o2}$, the *meta*

hydrogen has been labelled H$_m$ and the *para* hydrogen has been labelled H$_p$. The signal for H$_{o2}$ appears at 7.74 ppm, the signal for H$_p$ appears at 7.53 ppm and the signals for H$_{o1}$ and H$_m$ appear at 7.45 as a multiplet Signals corresponding to the three CH$_2$ groups on the five-membered ring appear as two sets of triplets at 4.35 and 3.10 ppm and a pentet at 2.70 ppm. No change was observed in the integrated area of any other peak relative to the internal standard, indicating that deuterium exchange does not occur at any position other than at C(3)-H under these conditions.

Figure 2.29 Representative ^{1}H NMR spectra at 400 MHz of triazolium salt **142** (10 mM, pD 0.70) obtained during exchange of the C(3)-H (s, 10.00 ppm) for deuterium in D$_2$O at 25 ˚C and I = 1.0 (KCl) [internal standard, tetramethylammonium deuteriosulphate (s, 3.02 ppm)]

Experimentally-observed first-order rate constants for exchange, k_{ex} (s^{-1}), were determined

from the slopes of semilogarithmic plots of f(s) against time at each pD. Reaction data and

values of k_{ex} are presented in

Table 2.2.

The concentration of deuteroxide ion is given by **Equation 2.3**, where K_W is the value for

the ion product of D$_2$O at 25 °C and is equal to $10^{-14.87}$ M^2. A value for the apparent activity

coefficient of deuteroxide ion $\gamma_{DO} = 0.73$ at $I = 1.0$ (KCl).

$$[DO^-] = \frac{10^{(pD - pK_W)}}{\gamma_{DO}}$$

Equation 2.3

Table 2.2: **Reaction data and first-order rate constants for exchange of the C(3)-H of triazolium salt 142 for deuterium in solutions of DCl in D$_2$O at 25°C and $I = 1.0$ (KCl)**

[DCl], M	[DO]$^-$, M^a	time, s	f(s)^b	ln f(s)	k_{ex}, s^{-1c}
		4620	1.000	0.000	
		27840	0.956	-0.045	
		92400	0.851	-0.161	
	9.26 x 10^{-15}	114240	0.807	-0.215	
0.4					1.96 x 10^{-6}
	(pD = 0.70)	193260	0.705	-0.349	
		282420	0.575	-0.553	
		354180	0.500	-0.693	
		440580	0.414	-0.881	

77

		522060	0.363	-1.014	
		691680	0.261	-1.342	
		806820	0.212	-1.549	
		1120920	0.111	-2.200	
		2100	1.000	0.000	
		25380	0.937	-0.065	
		85440	0.771	-0.259	
		114000	0.684	-0.380	
		172020	0.564	-0.573	
0.2	1.89×10^{-14} (pD = 1.01)	200640	0.529	-0.637	3.19×10^{-6}
		273540	0.413	-0.884	
		356400	0.310	-1.170	
		374820	0.303	-1.192	
		527400	0.181	-1.708	
		684360	0.116	-2.151	
		1440	1.000	0.000	
		21480	0.934	-0.069	
		85080	0.688	-0.374	
		106380	0.643	-0.442	
0.1	2.80×10^{-14} (pD = 1.18)	174480	0.482	-0.731	4.29×10^{-6}
		192180	0.443	-0.815	
		255120	0.331	-1.107	
		262320	0.318	-1.146	
		340500	0.233	-1.456	

		426840	0.158	-1.843	
		537660	0.103	-2.269	
		780	1.000	0.000	
		13500	0.822	-0.195	
		28080	0.665	-0.408	
		75000	0.415	-0.880	
0.04	7.70×10^{-14}	85380	0.353	-1.041	1.15×10^{-5}
	(pD = 1.62)	99840	0.314	-1.157	
		114180	0.257	-1.358	
		158340	0.158	-1.847	
		186180	0.120	-2.120	
		200640	0.090	-2.409	
		720	1.000	0.000	
		7500	0.787	-0.240	
		14700	0.610	-0.495	
	1.89×10^{-13}	22320	0.468	-0.760	
0.01					3.35×10^{-5}
	(pD = 2.01)	29040	0.379	-0.970	
		36240	0.299	-1.208	
		43560	0.234	-1.451	
		91800	0.047	-3.066	

(a) Concentration of deuteroxide ion calculated using **Equation 2.3**. (b) Fraction of substrate remaining, $f(s)$, calculated using **Equation 2.3**. (c) Pseudo-first-order rate constant for exchange, k_{ex} (s^{-1}), obtained from the slope of the plot of $\ln f(s)$ against time in **Figure 2.30** and **Figure 2.31**.

Figure 2.30 Semilogarithmic plots of the fraction of unexchanged substrate against time for the deuterium exchange reactions of **142** in solutions of DCl in D_2O at 25 ˚C and $I = 1.0$ (KCl).

Figure 2.31 Semilogarithmic plots of the fraction of unexchanged substrate against time for the deuterium exchange reactions of **142** in solutions of DCl in D$_2$O at 25 ˚C and I = 1.0 (KCl).

2.5.1.b 2-(4-Bromophenyl)-6,7-dihydro-5*H*-pyrrolo[2,1-c][1,2,4]triazol-2-ium

   tetrafluoroborate
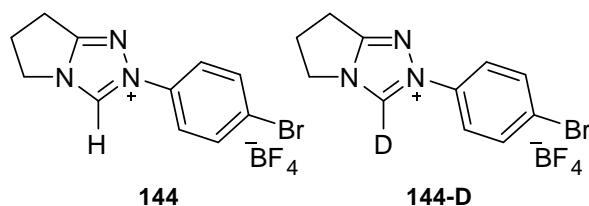
Figure 2.32   Triazolium salt **144** and deuterated form **144-D.**

Pseudo-first-order rate constants for the deuteroxide ion-catalysed exchange of the C(3)-H of triazolium ion **144** to form the corresponding deuterated triazolium ion **144-D** in solutions of DCl were determined by ^{1}H HMR spectroscopy (400 MHz).

A representative set of spectra taken at three time points during the observed H/D exchange reaction at p*D* 0.69 (0.4 M DCl) is shown in **Figure 2.33**. Deuterium exchange at the C(3)-H position resulted in the disappearance of the C(3)-H singlet at 9.99 ppm over the course of the reaction. The extent of exchange was measured relative to the 12 equivalent non-exchangeable protons of the internal standard at 3.02 ppm. Signals corresponding to the *ortho*-CH and *meta*-CH hydrogens on the aryl substituent appear at 7.66, and 7.55 ppm respectively. Signals corresponding to the three CH_2 groups on the five-membered ring appear as two sets of triplets at 4.35 and 3.09 ppm and a pentet at 2.70 ppm. No change was observed in the integrated area of any other peak relative to the internal standard, indicating that deuterium exchange does not occur at any position other than at C(3)-H under these conditions.
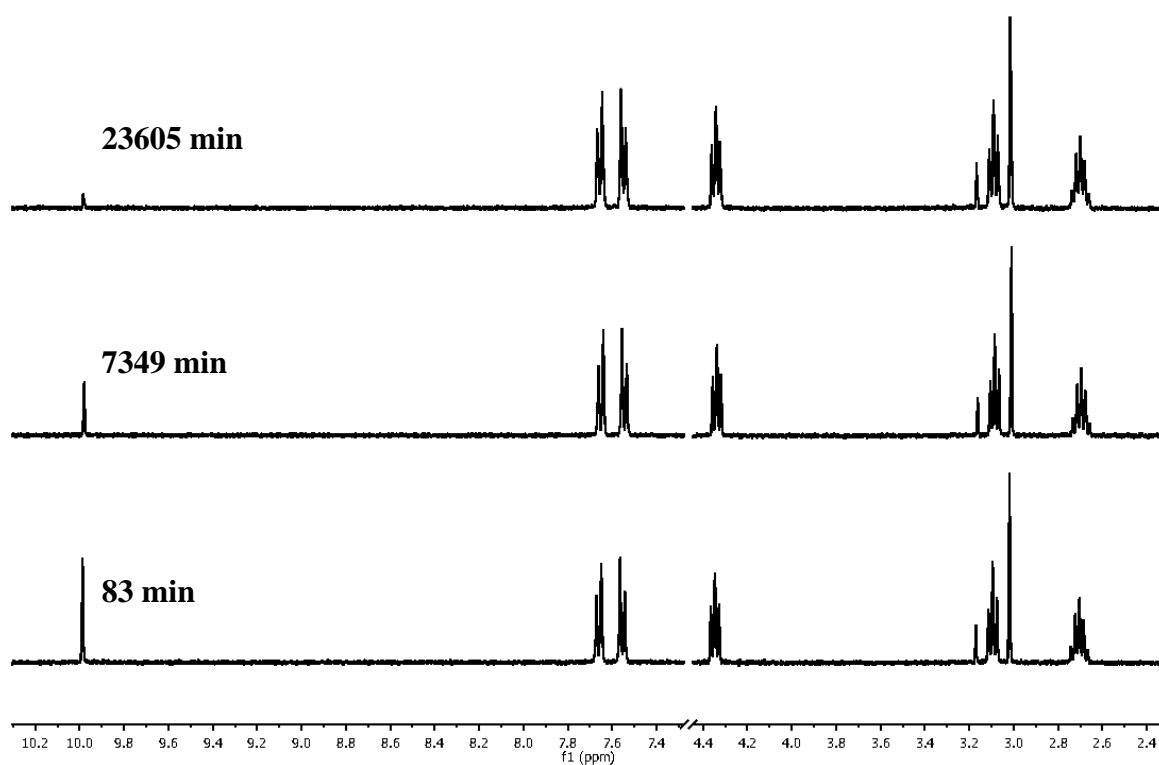
Figure 2.33 Representative ^{1}H NMR spectra at 400 MHz of triazolium salt 80 (10 mM, pD 0.69) obtained during exchange of the C(3)-H (s, 9.99 ppm) for deuterium in D$_2$O at 25 °C and I = 1.0 (KCl) [internal standard, tetramethylammonium deuteriosulphate (s, 3.02 ppm)].

Experimentally observed first-order rate constants for exchange, k_{ex} (s^{-1}), were determined from the slopes of semilogarithmic plots of f(s) against time at each pD. Reaction data and values of k_{ex} are presented in **Table 2.3**.

Table 2.3: Reaction data and first-order rate constants for exchange of the C(3)-H of triazolium salt 144 for deuterium in solutions of DCl in D_2O at 25°C and $I = 1.0$ (KCl)

[DCl]	[DO]⁻	time, s	$f(s)$	ln $f(s)$	k_{ex}, s⁻¹
		4980	1.000	0.000	
		92760	0.870	-0.139	
		114600	0.837	-0.178	
		193560	0.736	-0.306	
		259440	0.680	-0.386	
	9.05×10^{-15}	354420	0.580	-0.544	
0.4					1.49×10^{-6}
	(pD = 0.69)	440940	0.519	-0.655	
		522420	0.461	-0.775	
		691920	0.366	-1.006	
		873240	0.269	-1.313	
		1074060	0.202	-1.600	
		1416300	0.121	-2.109	
		2400	1.000	0.000	
		25680	0.921	-0.083	
	1.89×10^{-14}	85680	0.784	-0.243	
0.2		114240	0.721	-0.328	2.68×10^{-6}
	(pD = 1.01)	172260	0.611	-0.492	
		200820	0.585	-0.536	
		273780	0.478	-0.738	

		288660	0.463	-0.771	
		375060	0.351	-1.047	
		466800	0.275	-1.290	
		601500	0.199	-1.612	
		786720	0.122	-2.107	
		1920	1.000	0.000	
		21900	0.935	-0.067	
		85380	0.734	-0.309	
		106740	0.708	-0.345	
		174840	0.545	-0.607	
0.1	2.80×10^{-14} (pD = 1.18)	192540	0.527	-0.641	3.49×10^{-6}
		255600	0.414	-0.881	
		340800	0.305	-1.188	
		381480	0.265	-1.329	
		457380	0.212	-1.551	
		617400	0.114	-2.168	
		1140	1.000	0.000	
		13920	0.901	-0.104	
		28320	0.778	-0.251	
0.04	8.07×10^{-14} (pD = 1.64)	75360	0.524	-0.645	9.49×10^{-6}
		100020	0.411	-0.890	
		114420	0.355	-1.036	
		158580	0.236	-1.445	
		171960	0.204	-1.591	

		200880	0.151	-1.893	
		248520	0.096	-2.345	
		1140	1.000	0.000	
		7860	0.827	-0.190	
		15120	0.653	-0.426	
0.01	1.85×10^{-13}	22560	0.521	-0.651	2.94×10^{-5}
	$(pD = 2.00)$	29280	0.439	-0.824	
		36720	0.347	-1.059	
		43800	0.283	-1.262	
		93420	0.066	-2.721	
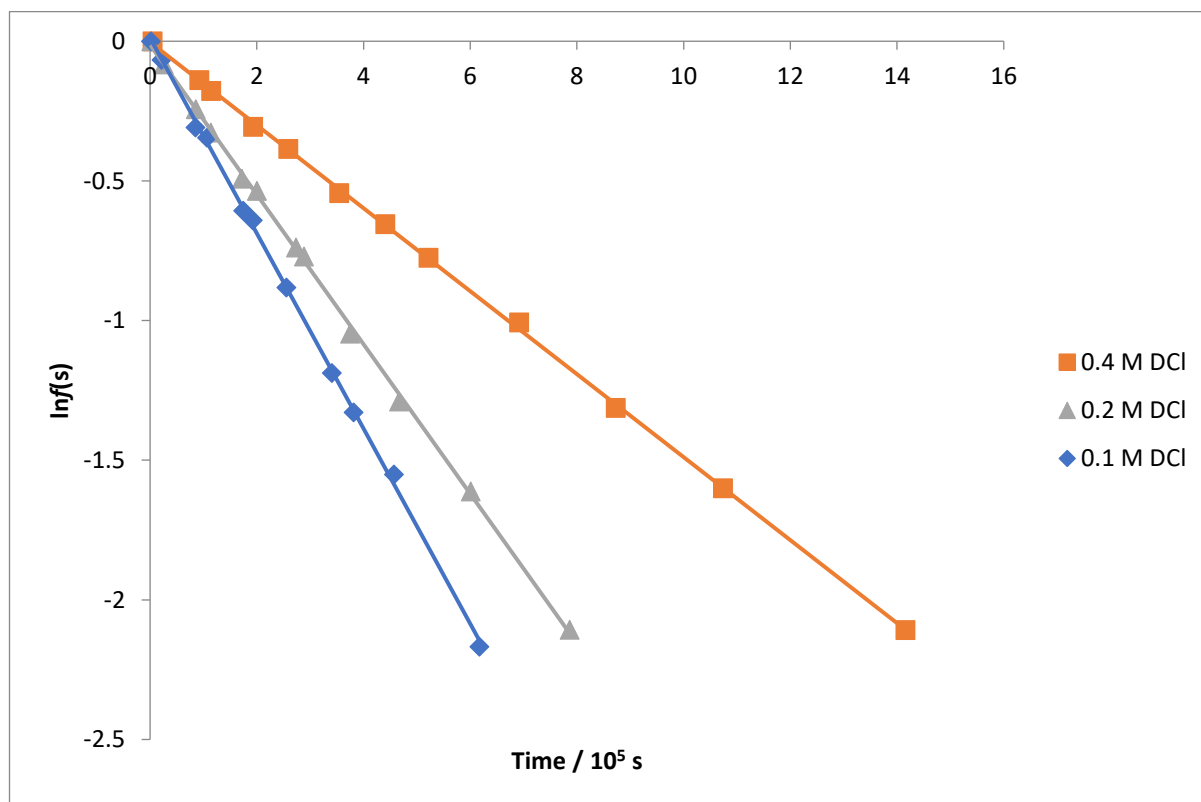
Figure 2.34 Semilogarithmic plots of the fraction of unexchanged substrate against time for the deuterium exchange reactions of **144** in solutions of DCl in D_2O at 25 ˚C and $I = 1.0$ (KCl).
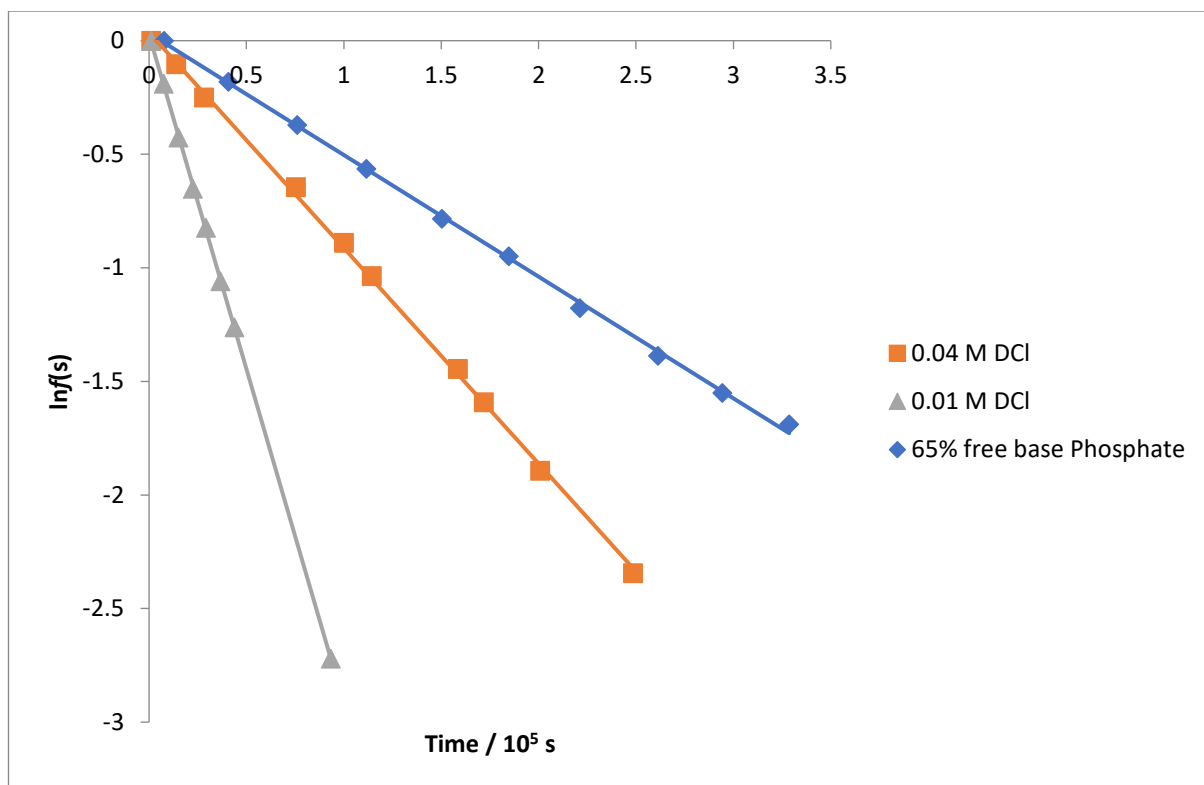
Figure 2.35 Semilogarithmic plots of the fraction of unexchanged substrate against time for the deuterium exchange reactions of **144** in solutions of DCl in D_2O at 25 ˚C and I = 1.0 (KCl).

### 2.5.1.c 2-Phenyl-6,7-dihydro-5*H*-pyrrolo[2,1-c][1,2,4]triazol-2-ium tetrafluoroborate
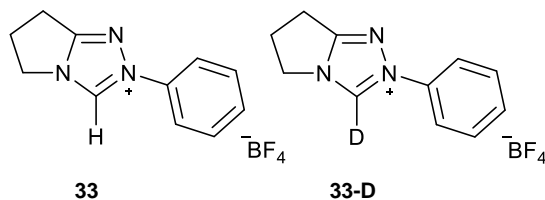
Figure 2.36 Triazolium salt **33** and deuterated form **33-D**.

Pseudo-first-order rate constants for the deuteroxide ion-catalysed exchange of the C(3)-H of triazolium ion **33** to form the corresponding deuterated triazolium ion **33-D** in solutions of DCl were determined by ^{1}H HMR spectroscopy (400 MHz).

A representative set of spectra taken at three time points during the observed H/D exchange reaction at p*D* 0.69 (0.4 M DCl) is shown in **Figure 2.37**. Deuterium exchange at the C(3)-H position resulted in the disappearance of the C(3)-H singlet at 10.00 ppm over the course of the reaction. The extent of exchange was measured relative to the 12 equivalent non-exchangeable protons of the internal standard at 3.02 ppm. Signals corresponding to the *ortho*-CH, *meta*-CH and *para*-CH groups on the aryl substituent appear as two multiplets from 7.44 - 7.65 ppm. Signals corresponding to the three CH_2 groups on the five-membered ring appear as two sets of triplets at 4.34 and 3.09 ppm and a pentet at 2.70 ppm. No change was observed in the integrated area of any other peak relative to the internal standard, indicating that deuterium exchange does not occur at any position other than at C(3)-H under these conditions.
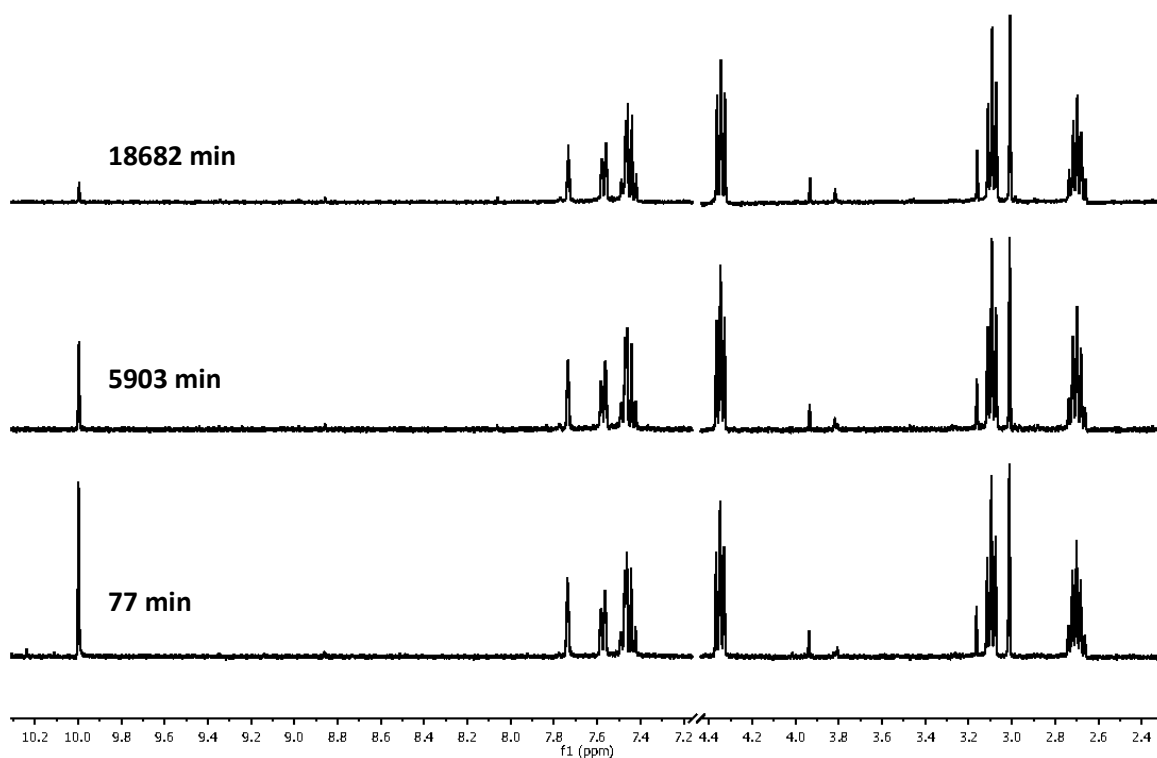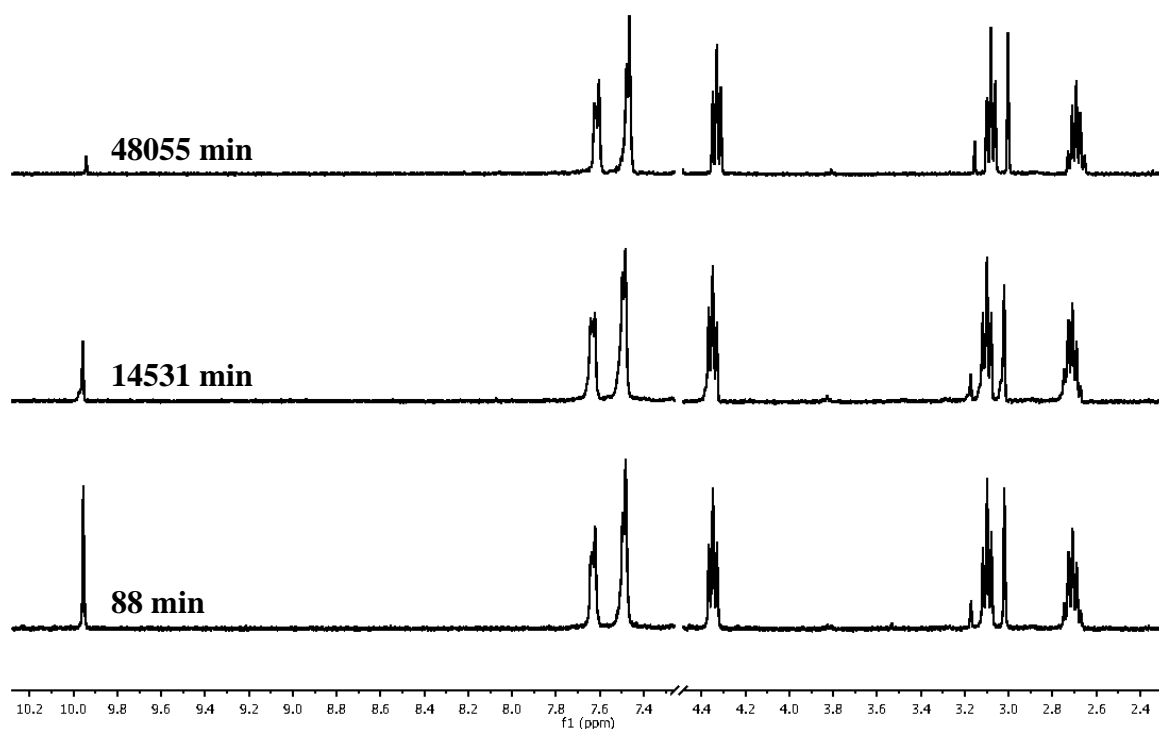
Figure 2.37 Representative ^{1}H NMR spectra at 400 MHz of triazolium salt 18 (10 mM, pD 0.69) obtained during exchange of the C(3)-H (s, 9.99 ppm) for deuterium in D$_2$O at 25 ˚C and I = 1.0 (KCl) [internal standard, tetramethylammonium deuteriosulphate (s, 3.02 ppm)].

Experimentally observed first-order rate constants for exchange, k_{ex} (s^{-1}), were determined from the slopes of semilogarithmic plots of f(s) against time at each pD. Reaction data and values of k_{ex} are presented in **Table 2.4**.

Table 2.4: Reaction data and first-order rate constants for exchange of the C(3)-H of triazolium salt **33** for deuterium in solutions of DCl in D_2O at 25°C and I = 1.0 (KCl)

[DCl]	[DO]⁻	time, s	$f(s)$	ln $f(s)$	k_{ex}, s⁻¹
		5260	1.000	0.000	
		93292	0.930	-0.073	
		290035	0.817	-0.203	
		366431	0.758	-0.278	
		517188	0.671	-0.399	
		699344	0.596	-0.518	
0.4	4.90 x 10⁻¹⁴ (pD = 0.69)	871831	0.504	-0.685	7.27 x 10⁻⁷
		1128554	0.428	-0.848	
		1382617	0.377	-0.976	
		1736899	0.268	-1.316	
		2629623	0.150	-1.900	
		2883288	0.122	-2.106	
		2693	1.000	0.000	
		85868	0.905	-0.100	
		114427	0.873	-0.136	
0.2	1.02 x 10⁻¹³ (pD = 1.01)	201015	0.772	-0.259	1.43 x 10⁻⁶
		288849	0.675	-0.392	
		375239	0.589	-0.529	
		466995	0.519	-0.655	

90

		601671	0.430	-0.844	
		786905	0.329	-1.111	
		862946	0.300	-1.203	
		3362	1.000	0.000	
		24954	0.962	-0.039	
		91592	0.832	-0.184	
		172251	0.720	-0.329	
		212913	0.671	-0.399	
		258587	0.614	-0.487	
0.1	1.51×10^{-13} (pD = 1.18)	353493	0.521	-0.651	1.87×10^{-6}
		456099	0.427	-0.851	
		608307	0.321	-1.135	
		717668	0.277	-1.285	
		891804	0.184	-1.691	
		1153187	0.114	-2.170	
		1466	1.000	0.000	
		14352	0.940	-0.062	
		28521	0.859	-0.152	
		75556	0.677	-0.390	
0.04	3.89×10^{-13} (pD = 1.59)	100236	0.598	-0.515	5.32×10^{-6}
		114606	0.562	-0.577	
		158792	0.431	-0.841	
		201040	0.360	-1.022	
		259530	0.273	-1.299	

91

		336951	0.172	-1.758	
		422476	0.102	-2.287	
		1508	1.000	0.000	
		8237	0.868	-0.141	
		15513	0.759	-0.275	
		23368	0.665	-0.408	
0.01	1.00×10^{-12} (pD = 2.00)	29512	0.583	-0.539	1.95×10^{-5}
		37053	0.499	-0.695	
		44007	0.456	-0.785	
		93626	0.164	-1.811	
		116377	0.107	-2.236	
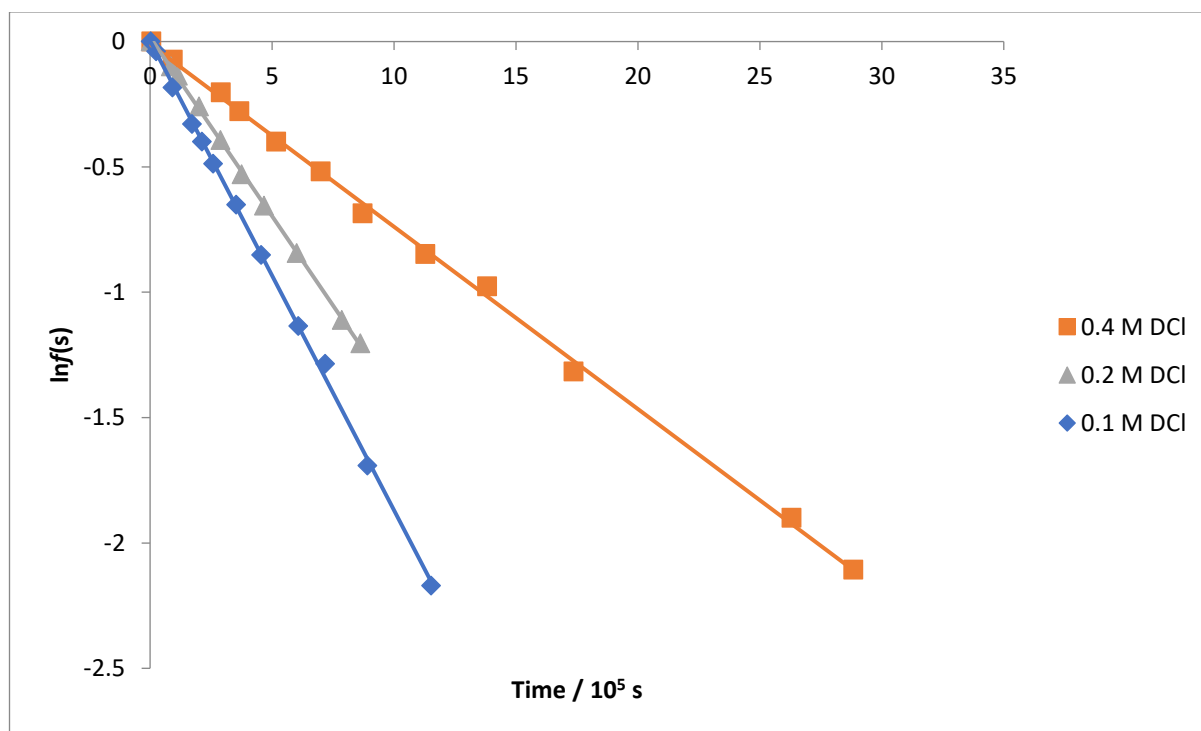
Figure 2.38 Semilogarithmic plots of the fraction of unexchanged substrate against time for the deuterium exchange reactions of 18 in solutions of DCl in D_2O at 25 ˚C and I = 1.0
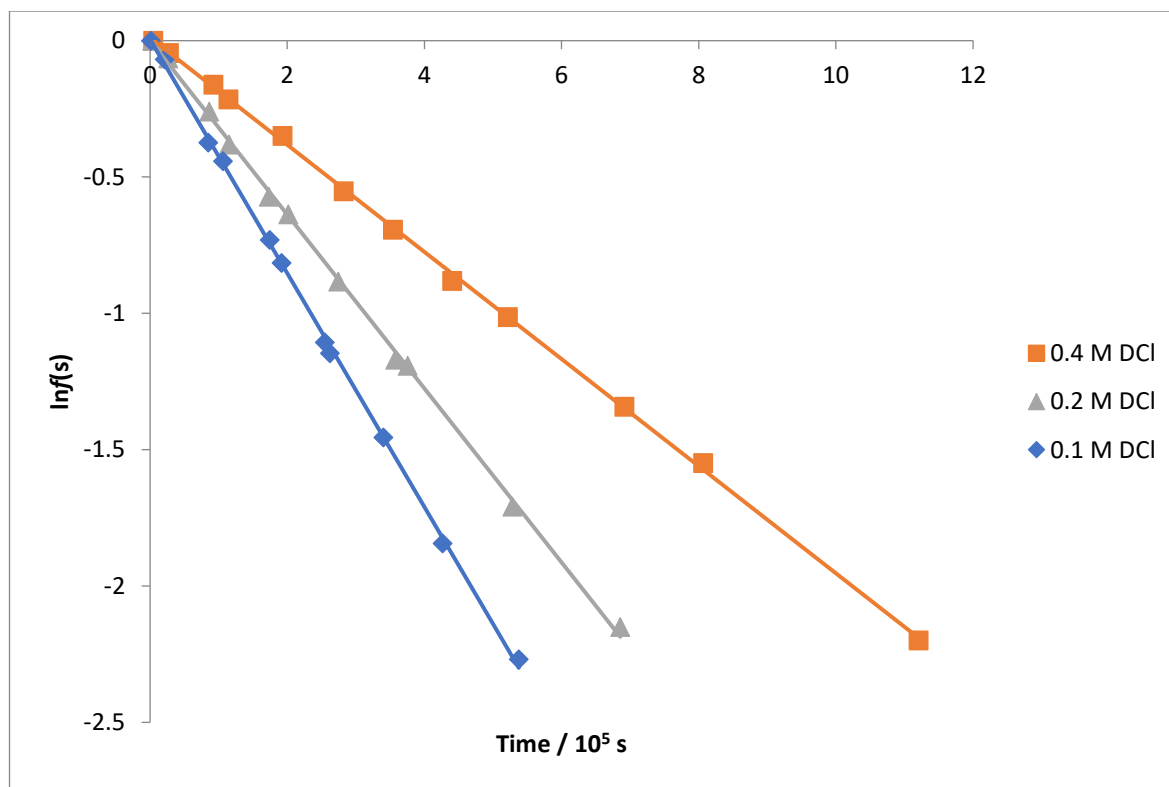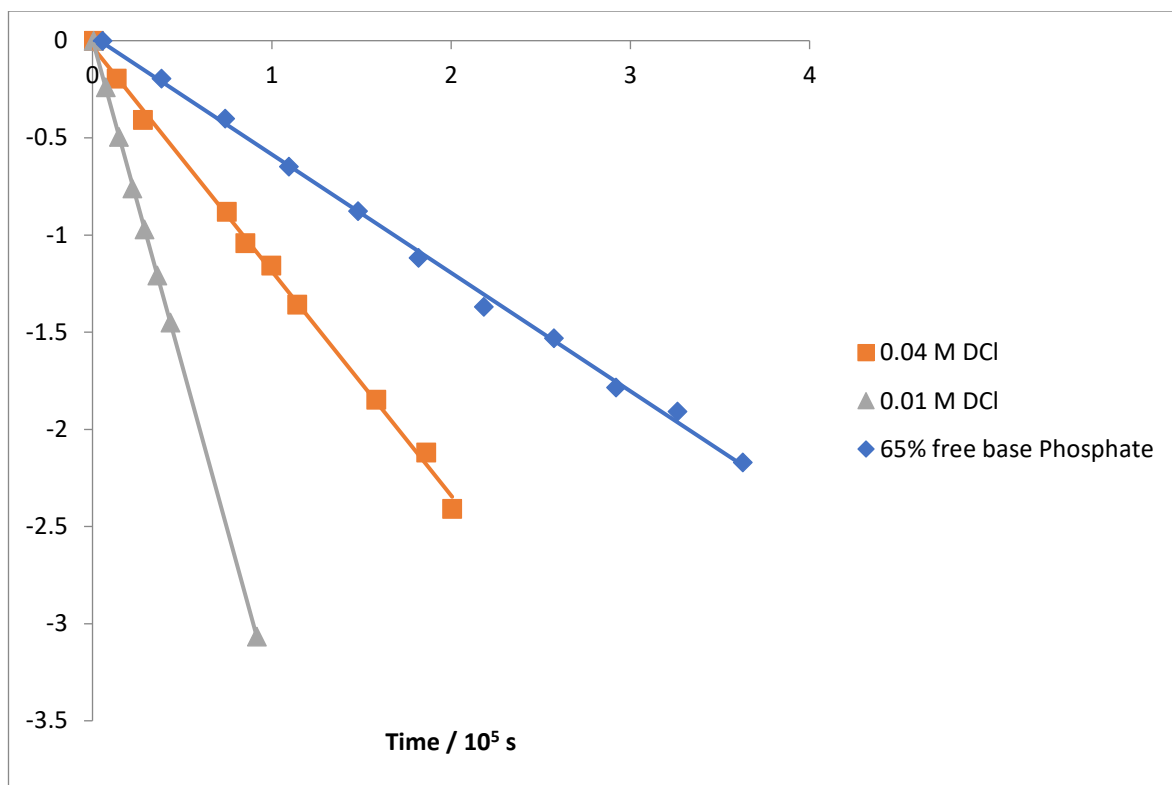
(KCl).
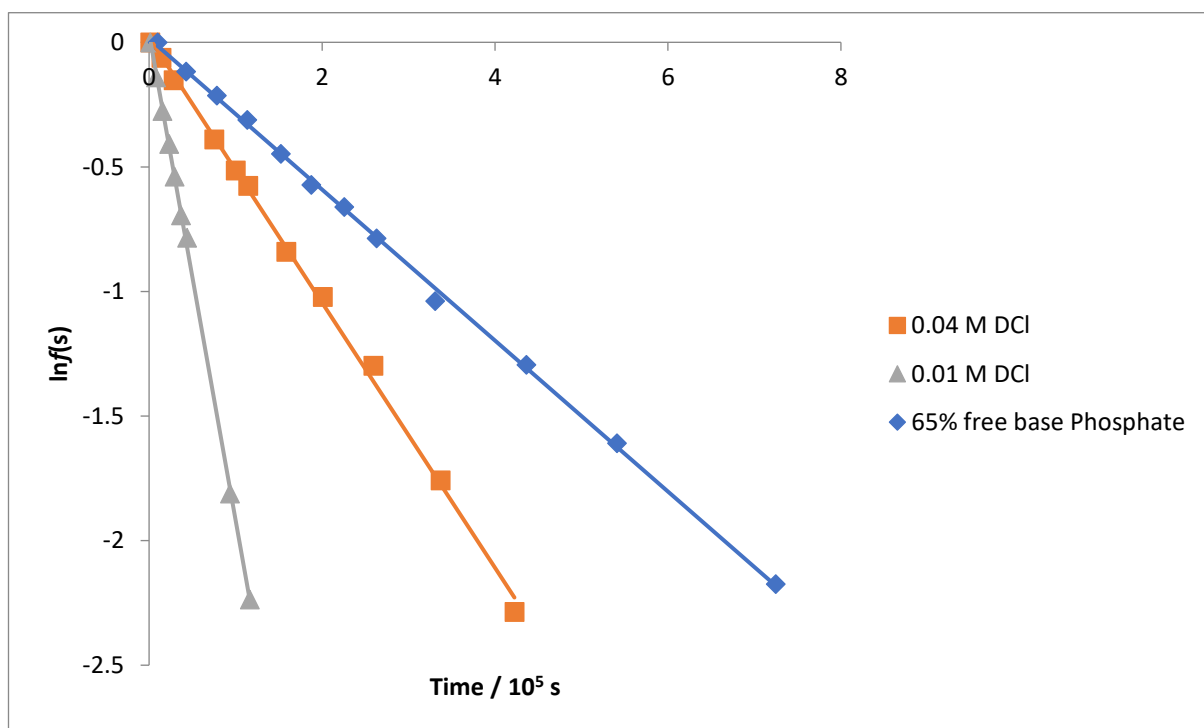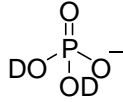
Figure 2.39   Semilogarithmic plots of the fraction of unexchanged substrate against time for the deuterium exchange reactions of **33** in solutions of DCl in D_2O at 25 ˚C and $I = 1.0$ (KCl).

### 2.5.1.d 2-(3-Chlorophenyl)-6,7-dihydro-5*H*-pyrrolo[2,1-c][1,2,4]triazol-2-ium tetrafluoroborate in buffered solutions

Pseudo-first-order rate constants for the deuteroxide ion-catalysed exchange of the C(3)-H of triazolium ion **142** to form the corresponding deuterated triazolium ion **142-D** in buffered solutions of D_2O were determined by ^{1}H HMR spectroscopy (400 MHz and 500MHz). General base catalysis has been previously shown to be negligible with triazolium derived catalysts[1].

Table 2.5: Reaction data and pseudo-first-order rate constants for exchange k_{ex} (s^{-1}) of the C(3)-H of triazolium ion 142 for deuterium in buffers solutions of D_2O at 25 °C, [buffer]$_{tot}$^{a} = 0.10 M, and I = 1.0 (KCl)

Buffer	[DO]$^-$, M^b	time, s	f(s)^c	ln f(s)	k_{ex}, s^{-1d}
		600	1.000	0.000	
		3900	0.822	-0.196	
		7440	0.669	-0.402	
154		10980	0.523	-0.648	
Monobasic phosphate		14820	0.416	-0.876	
	4.14 x 10^{-13}	18240	0.327	-1.118	6.09 x 10^{-5}
	(pD = 2.35)	21840	0.254	-1.371	
f_B 65%		25740	0.216	-1.531	
		29220	0.168	-1.785	
		32700	0.148	-1.908	
		36300	0.114	-2.170	

Monobasic phosphate, f_B 75%	6.41×10^{-13} (pD = 2.54)	540	1.000	0.000	1.05×10^{-4}
		3840	0.692	-0.368	
		7620	0.479	-0.736	
		11100	0.323	-1.131	
		14760	0.213	-1.548	
		18300	0.143	-1.943	
		21900	0.102	-2.278	
		25500	0.076	-2.583	
Monobasic phosphate, f_B 85%	1.28×10^{-12} (pD = 2.84)	720	1.000	0.000	1.81×10^{-4}
		3780	0.570	-0.562	
		7440	0.302	-1.198	
		11220	0.139	-1.976	
		14700	0.088	-2.435	
		18060	0.041	-3.193	
Formate, f_B 10%	3.29×10^{-12} (pD = 3.25)	600	1.000	0.000	5.06×10^{-4}
		780	0.922	-0.081	
		960	0.827	-0.189	
		1140	0.756	-0.280	
		1320	0.691	-0.369	
		1680	0.578	-0.548	
		1860	0.537	-0.623	
		2220	0.432	-0.840	
		2580	0.368	-1.000	

3120	0.273	-1.298
3840	0.201	-1.606
4740	0.123	-2.093

(a) Total concentration of buffer $[O_2PO_2D^-K^+]+[O_2PO_2D_2]$, $[HCOO^-K^+]+[HCOOD]$ as applicable; (b) Concentration of deuteroxide ion calculate using **Equation 2.3**, where γ_{DO} = 0.73; (c) Fraction of unexchanged substrate remaining, $f(s)$, calculated using **Equation 2.2**; (d) Pseudo-first-order rate constant for exchange, k_{ex} (s⁻¹), obtained from the slope of the plot of $\ln f(s)$ against time in **Figure 2.37**
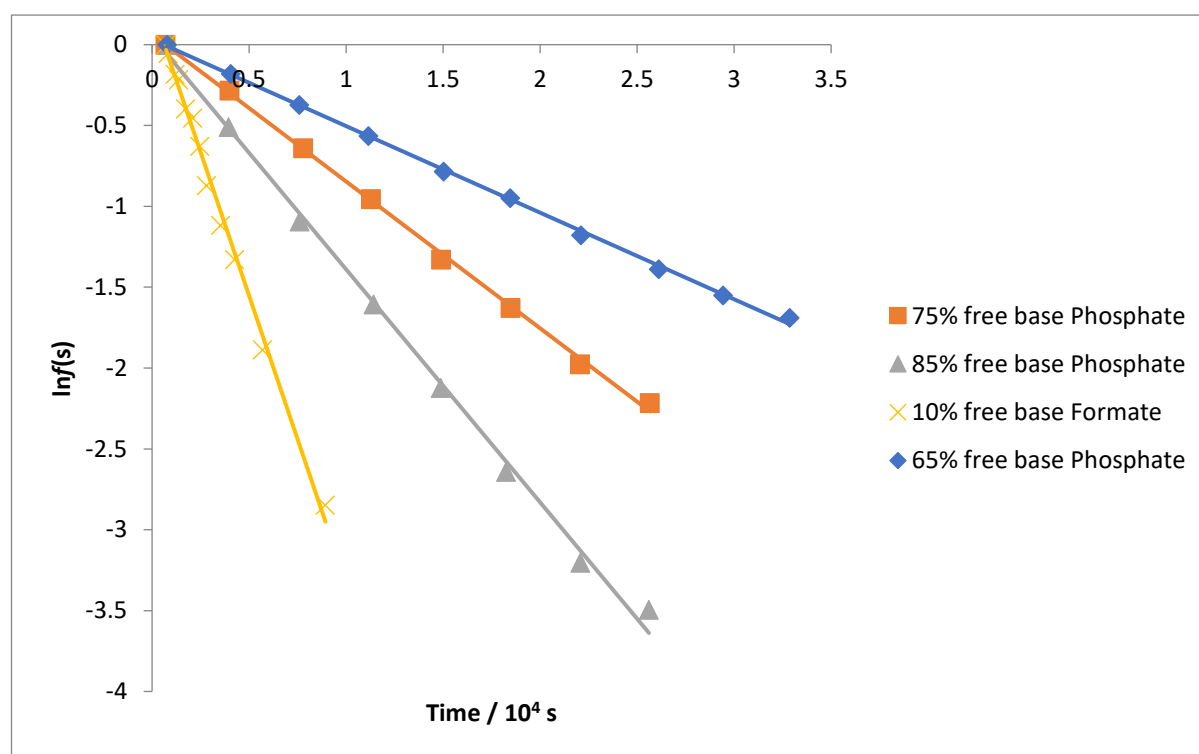
Figure 2.40 Semilogarithmic plots of the fraction of unexchanged substrate against time for the H/D-exchange of the triazolium ion **142** in monobasic phosphate buffer solutions and formic acid buffer solution at buffer base concentration 0.1 M in D_2O at 25 °C and I = 1.0 (KCl).

2.5.1.e 2-(4-Bromophenyl)-6,7-dihydro-5*H*-pyrrolo[2,1-c][1,2,4]triazol-2-ium tetrafluoroborate in buffered solutions

Pseudo-first-order rate constants for the deuteroxide ion-catalysed exchange of the C(3)-H of triazolium ion **144** to form the corresponding deuterated triazolium ion **144-D** in buffered solutions of D_2O were determined by ^{1}H HMR spectroscopy (400 MHz and 500MHz).

Table 2.6: Reaction data and pseudo-first-order rate constants for exchange k_{ex} (s^{-1}) of the C(3)-H of triazolium ion 144 for deuterium in buffers solutions of D_2O at 25 °C, [buffer]$_{tot}$ = 0.10 M, and I = 1.0 (KCl)

Buffer	[DO]⁻, M	time, s	f(s)	ln f(s)	k_{ex}, s⁻¹
		780	1.000	0.000	
		4080	0.834	-0.181	
		7620	0.690	-0.372	
		11160	0.569	-0.565	
Monobasic	4.33×10^{-13}	15060	0.456	-0.784	
phosphate,		18480	0.387	-0.949	5.36×10^{-5}
f_B 65%	(pD = 2.37)	20940	0.308	-1.177	
		26160	0.250	-1.388	
		29460	0.212	-1.551	
		32880	0.185	-1.690	
Monobasic	7.19×10^{-13}	720	1.000	0.000	
phosphate,		4020	0.753	-0.284	9.08×10^{-5}
f_B 75%	(pD = 2.59)	7800	0.527	-0.640	

		11340	0.385	-0.955	
		14940	0.265	-1.328	
		18540	0.196	-1.628	
		22080	0.138	-1.977	
		25680	0.109	-2.215	
		900	1.000	0.000	
		3960	0.602	-0.508	
		7620	0.335	-1.094	
Monobasic phosphate, f_B 85%	1.31×10^{-12} (pD = 2.85)	11460	0.201	-1.606	1.44×10^{-4}
		14940	0.120	-2.123	
		18300	0.071	-2.642	
		22080	0.041	-3.205	
		25620	0.030	-3.495	
		720	1.000	0.000	
		900	0.948	-0.053	
		1260	0.834	-0.182	
		1440	0.805	-0.217	
		1800	0.673	-0.396	
Formate, f_B 10%	3.29×10^{-12} (pD = 3.25)	2160	0.636	-0.453	3.55×10^{-4}
		2520	0.533	-0.629	
		2880	0.418	-0.872	
		3600	0.327	-1.117	
		4320	0.265	-1.328	
		5760	0.152	-1.887	

8940   0.058   -2.847
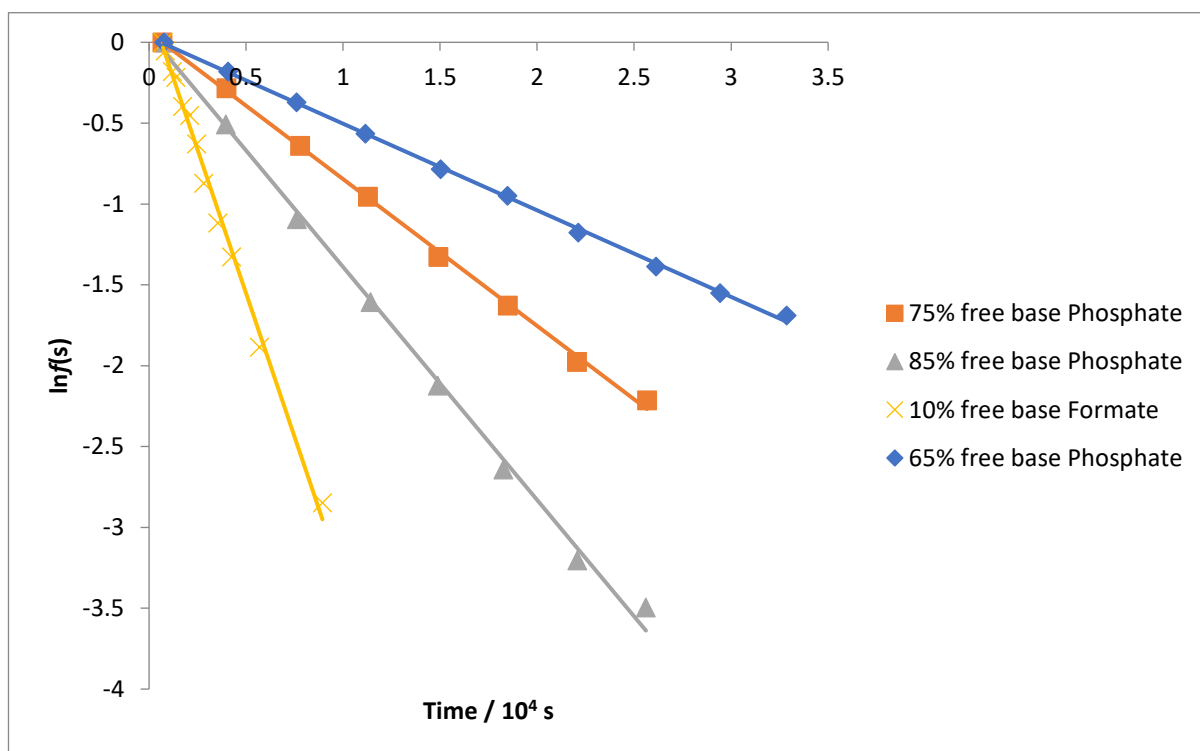
Figure 2.41 Semilogarithmic plots of the fraction of unexchanged substrate against time for the H/D-exchange of the triazolium ion **144** in monobasic phosphate buffer solutions and formic acid buffer solution at buffer base concentration 0.1 M in D_2O at 25 ˚C and $I =$ 1.0 (KCl)

### 2.5.1.f   2-Phenyl-6,7-dihydro-5*H*-pyrrolo[2,1-c][1,2,4]triazol-2-ium tetrafluoroborate in buffered solutions

Pseudo-first-order rate constants for the deuteroxide ion-catalysed exchange of the C(3)-H of triazolium ion **33** to form the corresponding deuterated triazolium ion **33-D** in buffered solutions of D_2O were determined by ^1H HMR spectroscopy (400 MHz and 500MHz).

Table 2.7:   **Reaction data and pseudo-first-order rate constants for exchange k_{ex} (s^{-1}) of the C(3)-H of triazolium ion 33 for deuterium in buffers solutions of D_2O at 25 ˚C, [buffer]$_{tot}$ = 0.10 M, and I = 1.0 (KCl)**

Buffer	[DO]$^-$, M	time, s	f(s)	ln f(s)	k_{ex}, s^{-1}
		1020	1.000	0.000	
		4320	0.889	-0.118	
		7860	0.807	-0.215	
		11400	0.732	-0.312	
		15300	0.639	-0.448	
Monobasic phosphate, f_B 65%	4.43 x 10^{-13} (pD = 2.38)	18780	0.564	-0.573	3.03 x 10^{-5}
		22620	0.516	-0.661	
		26340	0.455	-0.788	
		33120	0.354	-1.039	
		43680	0.274	-1.295	
		54120	0.200	-1.609	
		72480	0.114	-2.175	
Monobasic phosphate,	7.53 x 10^{-13} (pD = 2.61)	960	1.000	0.000	5.39 x 10^{-5}
		4200	0.863	-0.147	

f_B 75%		8040	0.692	-0.369
		11520	0.590	-0.528
		15180	0.466	-0.763
		18720	0.382	-0.961
		22320	0.324	-1.126
		25920	0.261	-1.344
		29520	0.217	-1.526
		33120	0.182	-1.702
		36720	0.142	-1.954
		40200	0.119	-2.131
		1140	1.000	0.000
		4200	0.746	-0.294
Monobasic		7860	0.549	-0.599
phosphate,	1.31×10^{-12}	11640	0.402	-0.912	8.79×10^{-5}
f_B 85%	$(pD = 2.85)$	15120	0.278	-1.282
		18480	0.208	-1.572
		22320	0.152	-1.886
		25860	0.117	-2.148
		840	1.000	0.000
		1200	0.923	-0.080
Formate,	3.29×10^{-12}	1380	0.884	-0.123	2.97×10^{-4}
f_B 10%	$(pD = 3.25)$	1740	0.778	-0.251
		2100	0.697	-0.361
		2640	0.600	-0.510

3180	0.519	-0.655
3720	0.431	-0.842
4440	0.356	-1.032
5340	0.267	-1.322
6420	0.194	-1.638
8040	0.121	-2.114
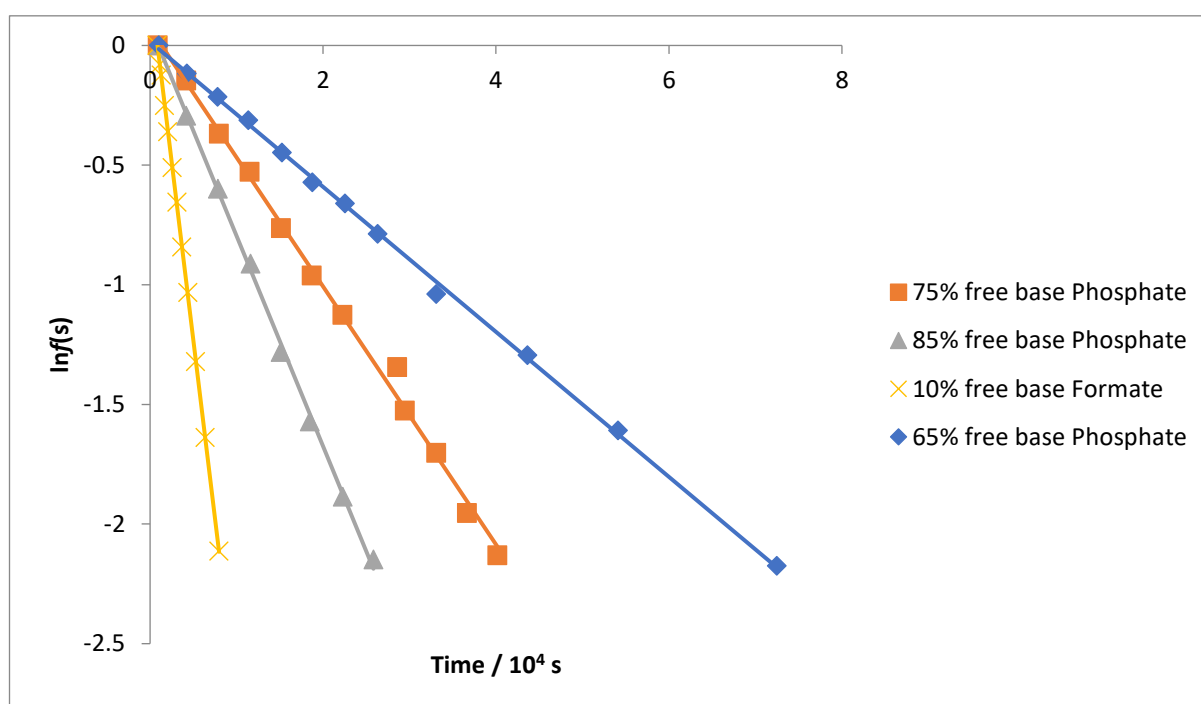
Figure 2.42 Semilogarithmic plots of the fraction of unexchanged substrate against time for the H/D-exchange of the triazolium ion 18 in monobasic phosphate buffer solutions and formic acid buffer solution at buffer base concentration 0.1 M in D$_2$O at 25 ˚C and I = 1.0 (KCl)
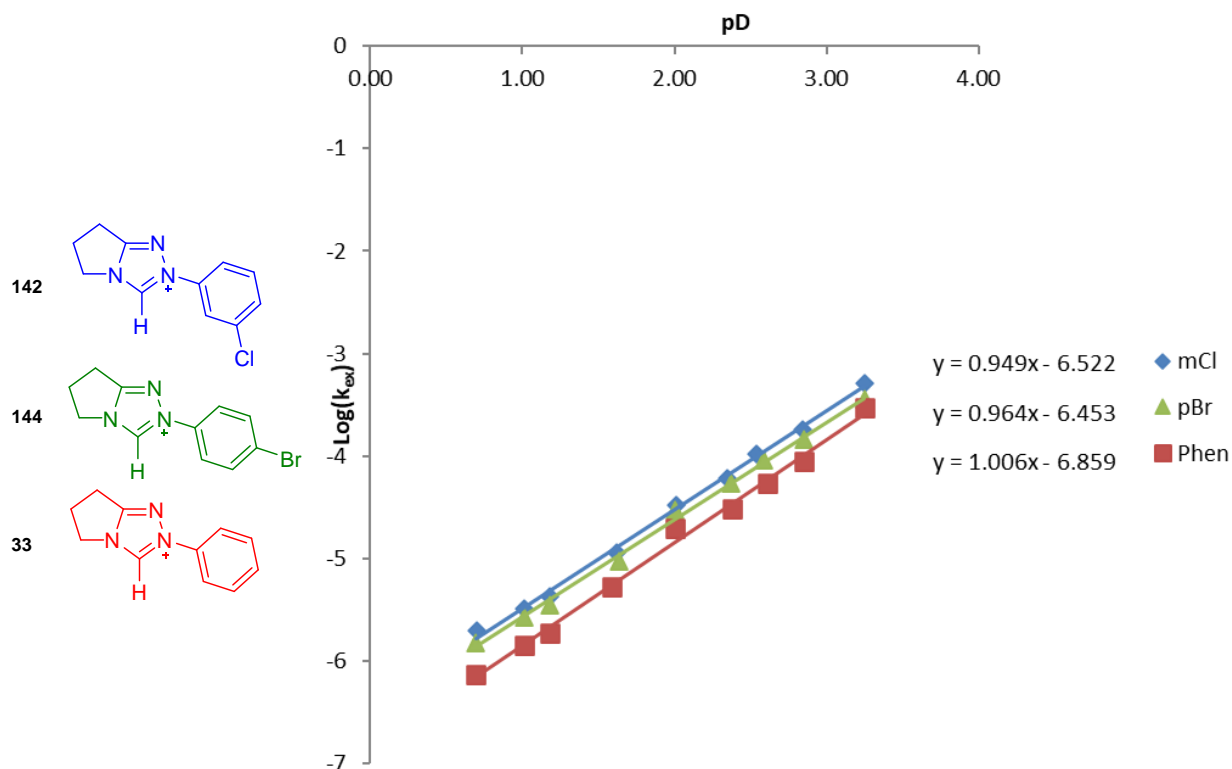
Figure 2.43   p*H*-rate profiles for the exchange of the C(3)-H of triazolium ions **142**, **144**, and **33** for deuterium in D$_2$O at 25 °C and I = 1.0 (KCl).

For triazolium ions **33**, **142**, and **144**, values of log k_{ex} were found to increase with p*D* in the range 0.69 – 3.25. The lines-of-best-fit through the p*D*-rate profiles for the triazolium ions **33**, **142**, and **144** show the fit of these data to **Equation 2.4**, derived from **Equation 2.5**, where k_{DO} is the second-order rate constant for deuteroxide ion-catalysed exchange, K_W = 10$^{-14.87}$ is the ionic product for D$_2$O at 24 °C, and γ_{DO} is the activity coefficient for deuteroxide ion determined under these reaction conditions. These fits are linear and of slope close to unity, which is consistent with deuteroxide ion-catalysed exchange *via* the following pathway **Scheme 2.10** as the dominant mechanism for H/D-exchange.

$$\log k_{ex} = \log\left(\frac{k_{\text{DO}}K_{\text{W}}}{\gamma_{\text{DO}}}\right) + \text{p}D \qquad\qquad \textbf{Equation 2.4}$$

$$k_{ex} = k_{\text{DO}}[\text{DO}^-] \qquad\qquad \textbf{Equation 2.5}$$
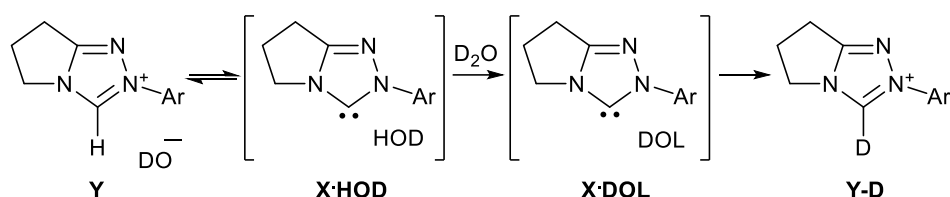
Scheme 2.10 Generalised pathway for deuterium exchange of triazolium salts **Y** to deuterated form **Y-D**.

In this pathway, deprotonation of triazolium ion **Y** by deuteroxide ion gives **X·HOD**, an intimately bound complex of the triazolylidene **Y-D** and a molecule of HOD. Solvent reorganisation results in the replacement of the molecule of HOD with a molecule of DOL (where L is H or D) to form **X·DOL**, where the molecule of DOL is in a position to deuterated the C(3) position. This solvent reorganisation step could either be rotation of the original molecule of HOD within the complex to yield **X·DOL** (L = H), or alternatively, the rotation could be accompanied by transfer of the proton with the bulk solvent (L = D). As the concentration of D_2O is present in vast excess in comparison to the protonated substrate (10 mM), deuteration to form the deuterated product **Y-D** is essentially irreversible.

2.6 Estimation of pK_a

Previous research from our group has shown that the pathway in **Scheme 2.10** is the dominant pathway for deuterium exchange in triazolium salts such as **33**[26]. This is assumed

104

to also be true of triazolium salts **142**, and **144** in the following section, as structurally and electronically they are similar to other triazolium salts that follow this mechanism.

$$pK_a = pK_w + \log\frac{k_{HOH}}{k_{HO}}$$

Equation 2.6

In **Equation 2.6**, derived from **Scheme 2.11**, K_w is the equilibrium constant for autoionization of water. Values for k_{HO} for the deprotonation of triazolium ions at C(3) by a hydroxide ion can be estimated from the corresponding experimental values obtained for k_{DO} values for deuteroxide-catalysed C(3)-H/D exchange *via* **Scheme 2.11**.
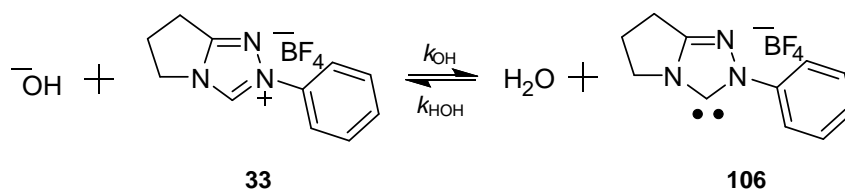
Scheme 2.11 Rate constants for deprotonation of triazolium salt **33**.

The rate of proton transfer from neat alcohol solvent to singlet diphenylcarbenes is controlled by solvent reorganisation, as shown by femtosecond transient absorbance spectroscopy[73]. There is evidence that this is also true of triazolyl carbenes[26], and that this occurs with limiting rate constant of the rate of solvent reorganisation $k_{reorg} = k_{HOH} = 1 \times 10^{11}$ s^{-1}. The value for k_{DO} is obtained from experimental results of $k_{ex} - pD$ shown graphically in **Figure 2.43**, using **Equation 2.4**, derived from **Equation 2.5**. The value for pK_a can then be obtained using the relationship $k_{DO}/k_{HO} = 2.4$, and with **Equation 2.6**. The values experimentally obtained for both k_{DO} and pK_a are displayed in **Table 2.8**. In **Figure 2.43** it can be seen that there is no deviation from linearity in the rate profile**.**

Triazolium salt	k_{DO} (M⁻¹s⁻¹)	pK_a
142	1.53×10^8	17.2
144	1.07×10^8	17.3
33	8.87×10^7	17.4
33 with BF$_4$⁻[26]	6.82×10^7	17.6
33 with Cl⁻[26]	5.84×10^7	17.6

Table 2.8   Experimentally-obtained values for k_{DO} and pK_a for triazolium salts **33**, **142**, and **144**, with reference literature values.

Our value for the k_{DO} of the N-phenyl triazolium salt **33** are ~ 30.1% different, and the pK_a are ~1.1% different from our previously published values for this salt with a tetrafluoroborate counterion[26]. This is outside of experimental error in k_{DO} (~10%), thus is it possible that complete exchange of counterion had not occurred. However, the k_{DO} value is reasonably close to give confidence in relative k_{DO} values for **142**, **144**, and **33**. The values obtained for the pK_a of the *para*-bromo **144** and *meta*-chloro **142** triazolium salts are similar to the pK_a values for **33**. Values of k_{DO} for **142** and **144** are higher than for **33** consistent with the presence of electron-withdrawing halogens on the N-aryl rings. As inductive effects dominate for halogens, the k_{DO} value for *meta*-chloro substituted **142** is highest, owing to the closer proximity of the former to the central triazolium ring, as inductive effects decrease with increased distance.

3 Conclusions

3.1 Conclusions

2-Trimethylsilyl benzaldehyde, **109**, was prepared and purified with the intent to study the 2-substituent effect on the cross-benzoin condensation with a Lewis acidic *ortho*-substituent. The synthetic route to **109** was refined, with reaction time and column residence time identified as important to the yield of product.

Initial experiments into the homo-benzoin condensation of **109** identified no clear formation of silylated homo-benzoin products, which was expected of this reaction. However, in the case of the pentafluorophenyl **26**, phenyl **33** and *para*-fluorophenyl **132** NHC catalysts, there was significant formation of multiple species that could not be easily identified on the basis of homo-benzoin studies alone with the 2-trimethylsilylaldehyde **109**. This persisted through the cross-benzoin condensation studies of benzaldehyde, however, it was possible to assign products based on the established chemical shifts of the homo-benzoin reaction of benzaldehyde with the three catalysts studied. Evidence of the first silylated hydroxyaryl adduct intermediate (**A**, **Figure 2.17**) was obtained with the N-mesityl triazolium salt. Attempts were made to isolate this hydroxyaryl adduct species, though this appeared to be unstable in acetonitrile.

Though the desired hydroxyaryl adduct between 2-trimethylsilyl benzaldehyde and the relevant NHC was believed to form based on the data, there was little evidence of onwards reaction to form a silylated homo- or cross-benzoin product. This could be because deprotonation to give the Breslow intermediate is slow, though is more likely because the onwards reaction of the Breslow intermediate is slow.

It also appears, from the mesityl cross-benzoin studies, that there is not selective formation of the silyl aldehyde NHC adduct compared to the benzaldehyde NHC adduct (**A** and **B**, **Figure 2.17**) as greater quantities of the latter are observed. This is in contrast to the established 2-substituent effect for Lewis basic and alkyl substituents where the hydroxyaryl adduct is formed selectively from the 2-substituted aldehyde.

Furthermore, normally 2-substituted aldehydes preferentially react with the benzaldehyde-derived Breslow intermediate, to give a cross rather than homo-benzoin outcome. However in the case of 2-trimethylsilylbenzaldehyde this is not the case, and the benzaldehyde homo-benzoin reaction can progress normally. In the cases of the N-mesityl and N-parafluorophenyl cross studies, the only observed benzoin product is the homo-benzoin product from benzaldehyde. In the case of the N-pentafluorophenyl cross study, there is an unidentified peak at 6.41 ppm that could either be the hydroxyaryl adduct species for 2-trimethylsilyl benzaldehyde, or an alternative benzoin product. However less of this is formed than the homo-benzoin product observed at 6.12 ppm. Thus, the unusual 2-substituent effect is not observed for 2-trimethylsilyl benzaldehyde, and this is possibly true of other 2-silyl substitutions of benzaldehyde. Interestingly, this highlights clear differences between Lewis acidic and basic substituents from the perspective of NHC catalysis.

Two triazolium salts, **142** and **144**, were prepared. These were the *meta*-chloro phenyl triazolium salt, **142**, and *para*-bromo phenyl triazolium salt, **144**, respectively. These were used to probe the stability of triazolium salts, to organolithiation and the formation of a Grignard reagent respectively. This was done in the hope of silylation of the triazolium salts to examine the effects of steric interactions on the N-aryl ring. These initial studies suggest the triazolium salts are not stable in the presence of these reagents.

During the deuterium exchange studies of the *meta*-chloro **142** and *para*-bromo **144** triazolium salts it was noted that these species had a similar pK_a than to published values for the N-phenyl triazolium salt[26] **109** and lower than the observed pK_a for this salt. The values for these two halogenated triazolium salts are consistent with what is expected for limited effects of the subsitutents on the N-aryl group. Both **142** and **144** have higher k_{DO} and lower pK_a values than for **109** though this effect is within an order of magnitude for the value of k_{DO} indicating a minor effect of the substituent.

The work presented in this thesis indicates that silyl groups present challenges for examining the benzoin condensation. Interestingly, the 2-silyl substituent effect differs from other 2-heteroatoms examined to date, although further work is necessary to explore the origin of this difference in behaviour. There are further avenues of research in the future to mitigate the effect of problems experienced with silyl groups, and other potential Lewis acidic groups to be explored in this reaction. There is still much work that can be done into silylation in the benzoin condensation, with many possible avenues to pursue in the future.

3.2   Future work

The continuation of the synthetic procedures for the formation of silylated catalysts could use two main alternative strategies. First, the formation of the triazolium ions could be attempted from precursors with the use of protecting groups and less reactive reagents to prevent reactions at the C(3) acidic position of the triazolium ion. A possible candidate for this would be deuteration of the C(3) proton, with the hope that the reduced lability would direct the magnesium towards the second site in the Grignard approach. Alternatively, the use of a C(3) benzyl group to protect the triazolium and prevent formation of the carbene could be effective, with tuning of the benzyl group to allow mild

deprotonation conditions. This would also allow for later orthogonal removal, without compromising the silyl group.

Second, it is possible that the N-aryl substituent could be silylated before formation of the amidrazone, **149**, or ring closure, though there is the potential for steric interactions to hinder these steps.

This would involve forming a silylated aromatic species, followed by conversion to the desired silylated aryl hydrazine. One method would be to use butyl lithium to deprotonate a silylated benzene derivative. The highly reactive organolithiate species formed would be reacted in-situ with di-tert-butyl diazene-1,2-dicarboxylate (DBAD) to form the protected hydrazine. The protecting carboxyl groups on this hydrazine would then require cleavage with acid to form the desired hydrazine. This is a well-known method of accessing unstable hydrazines[10]. Proto-desilylation is a potential problem in the final step.
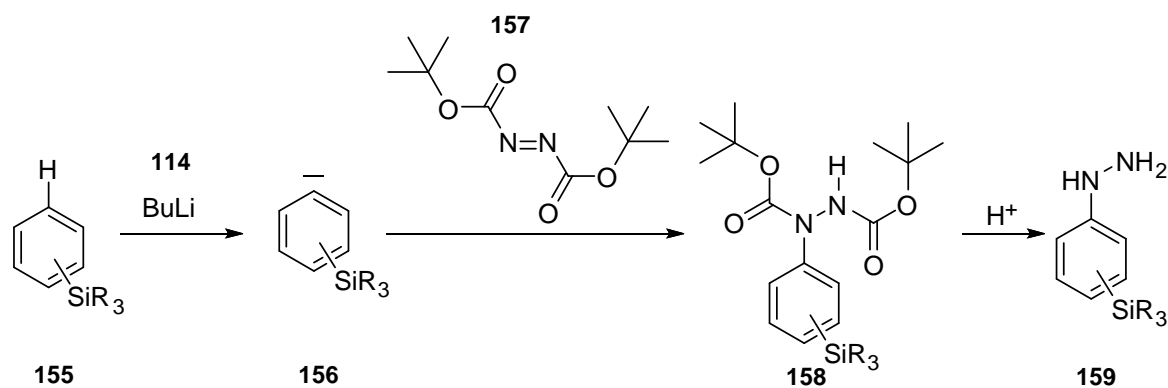
Scheme 3.1   A potential route for the formation of silylated arylhydrazines through lithiation of silylated benzene derivatives followed by reaction with DBAD. The carboxyl protecting groups can then be removed with acid.

Another possible route would be to silylate the halogenated aniline, **160** and **164**, before the formation of the hydrazines **163** and **167**, **Scheme 3.1**. From there, the

triazolium salt could be formed from this species, though it is unclear how the steric bulk of the silyl group would affect other steps in the reaction, such as ring closure and amidrazone formation. The relevant hydrazine, **163** and **167**, could be accessed through the formation of the relevant diazonium cation species, **162** and **166**. Protodesilylation could occur under conditions for diazonium formation. It is also uncertain whether the conditions of the hydrazine formation, particularly a tin chloride reduction, would interact with the silyl group. It is possible that, due to the radical nature of this reduction, there may be interactions between the tin chloride and the silyl group, though this could be mitigated by a prudent choice of silyl alkyl or aryl substituent.
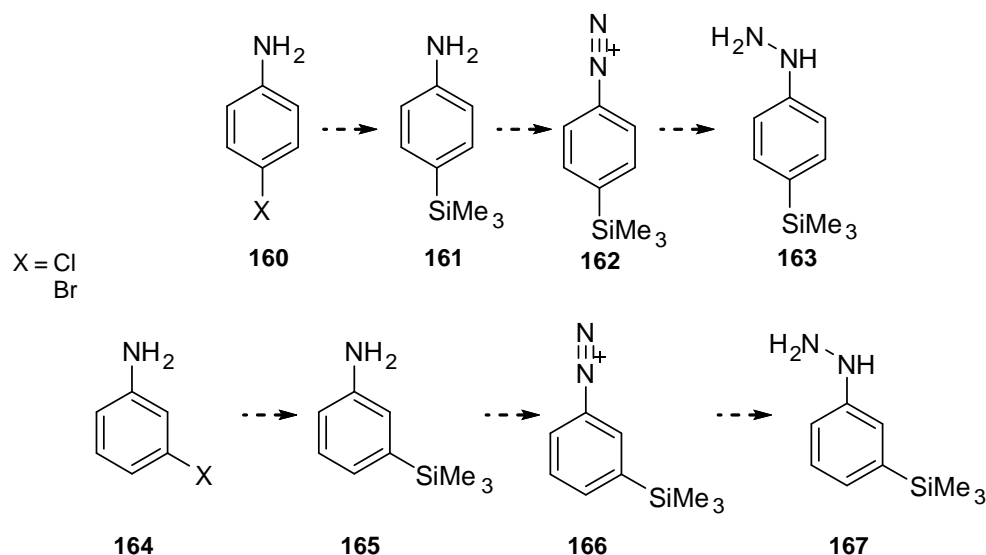
Scheme 3.2 Potential formation of silylated hydrazine derivatives formed from corresponding silylated aniline. This would be done by formation of the diazonium species, followed by tin chloride reduction to the hydrazine.

Additionally, further work could be carried out to isolate the postulated C(3) silylated triazolium salts, which are thought to form as a side reaction in the lithiation process. This would use modified N-aryl groups to stabilise the triazolium structure during the lithiation. Tuned reaction conditions would be required to reduce the possibility of ring

111

opening, as well as a substrate that reduces substitution at other points on the molecule to reduce possible side product formation.

Silicon was identified as being problematic in the benzoin condensation as there is a possibility of an entropically favoured migration of the silyl group onto the hydroxyl group. This was implied by the results of the experiments into the benzoin condensation with 2-trimethylsilyl benzaldehyde. The reduced yield in the formation of the 2-trimethylsilylbenzaldehyde with longer column times suggests there were also issues with the lability of silicon bonds in silicon containing molecules. This caused some degeneration of the silyl species when in contact with column surfaces. With this difficulty in using silicon, it was postulated that other heteroatoms may be good choices for probing the 2-substituent effect, such as boryl groups.

There are potential ways to work around the lability of the silyl groups, such as protecting groups on the oxygen to prevent migration, or altering the groups of the silyl group to reduce the ability for migration, though both of these may be difficult as they are likely to inhibit the progression of the benzoin condensation and pose solubility problems for kinetic analysis in deuteriomethanol and D_2O. With this in mind it is difficult to choose a protecting group that would allow for examination of the reaction. While benzyl, **168**, or silyl ethers, **169**, are conventional protecting groups for hydroxyl groups, their large steric bulk seems likely to interfere with the reaction. In the case of a silyl protecting group, the conditions used to remove the protecting group would also abstract the silyl group from the molecule. Another potential avenue to examine is the use of triazolium salts which inhibit the silyl migration, similar to what was observed herein for the mesityl catalyst in the cross benzoin studies.
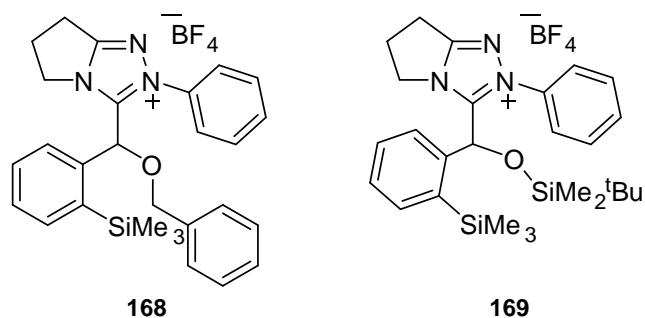
Figure 3.1 Potential hydroxyaryl adducts with protecting groups on the hydroxyl group, showing both the benzyl and *tert*-butyldimethylsilyl protecting groups

Boryl groups would allow for a similarly neutrally charged substituent as a silyl group, though it would not bond with oxygen to the same degree due to a lower affinity for oxygen. There is the potential that boryl groups would not experience a shift onto the oxygen in the hydroxyaryl adduct that appeared to have happened with silyl groups. A possible starting point for a borylated benzaldehyde derivative would be the formation of 2-pinacolatoboryl benzaldehyde **170**. This would be a good candidate for initial testing and would allow for manipulation of the R-groups of the boryl group, as bispinacolatoboron is a commonly used borylating agent.
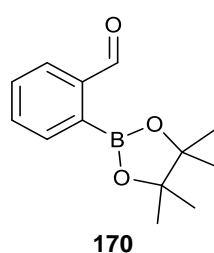
Figure 3.2 Structure of 2-pinacolatoboryl benzaldehyde.

There are some potential solutions to the difficulties experienced with silyl migration that is thought to have occurred during the benzoin conditions. There is potential in optimising either the substrate or the reaction conditions in a way that may prevent this

interaction. With experimentation into different N-aryl salts, it may be possible to affect

the stabilisation of the molecule and prevent migration, though reducing the lability of the

silyl group. From our data, the N-mesityl group is more promising for this than the penta-

or *para*-fluorophenyl groups. It may also be possible to modify the R-groups of the silyl

group to reduce the lability of this group. By extending the time length of the silyl

migration, it would be possible to examine the benzoin condensation of this molecule with

the effects of the migration being negligible. It may also be possible to prevent the silyl

migration entirely, through choice of R-group, though this would be more difficult, though

it may be possible to use sterically hindering alkyl groups such as isopropyl, *tert*-butyl, or

aryl groups.

R = Ar
R = ^{i}Pr
R = ^{t}Bu
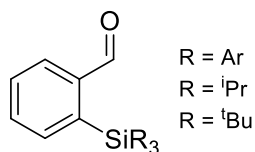
Figure 3.3 Potential R groups for the 2-silyl benzaldehyde that may prevent migration

onto oxygen during the benzoin condensation

4 Experimental

4.1 General instrumentation

NMR: NMR samples were prepared in acetonitrile-d_3, chloroform-d_1, deuterium oxide-d_2 and, methanol-d_4. ^{1}H and ^{13}C NMR chemical shifts are reported relative to residual solvent peaks as stated in **Table 4.1**[74].

Table 4.1:   **NMR solvents and reference signals**

Solvent	δ_H, ppm	δ_C, ppm
acetonitrile-d_3	1.94	1.3
chloroform-d_1	7.26	77.2
deuterium oxide-d_2	4.79	-
methanol-d_4	3.31	49.0

Data are presented as follows: chemical shift (ppm), integration, multiplicity (s = singlet, t = triplet, q = quintet, m = multiplet), coupling constants (Hz), and assignment. NMR spectra at 400, 500, and 700 MHz were recorded on Varian Mercury-400, Bruker Avance-400, Varian Inova-500, and Varian VNMR-700 instruments.

Elemental analyses were obtained from the Microanalytical Unit (Department of Chemistry, Durham University), and performed on an Exeter CE-440 Elemental Analyser.

Low resolution mass spectrometry was performed on a Waters *TQD* mass spectrometer and a Shimadzu *QP2010-Ultra* mass spectrometer. High resolution mass spectrometry was performed using a Thermo-Finnigan *LTQ FT* mass spectrometer.

Thin layer chromatography was performed using Machery Nagel TLC 40 X 80 mm plates purchased from Fisher Scientific. Column Chromatography was performed using silica gel.

4.2 Materials

NMR Solvents: Deuterium oxide-d$_2$ (99.9 atom % D), acetonitrile-d$_3$ (99.8 atom % D) and methanol-d$_4$ (99.8 atom % D) were purchased from Cambridge Isotope Laboratories Inc. Chloroform-d$_1$ (99.8 atom % D) was purchased from Sigma-Aldrich.

Other reagents: Benzaldehyde, triethylamine, and chlorotrimethylsilane were purchased from Sigma-Aldrich and were distilled prior to use. Reactions involving air- or moisture-sensitive reagents were performed under an argon atmosphere using oven-dried glassware. Solvents were dried prior to use.

4.3 Synthetic procedures

4.3.1 Synthesis of substituted aldehyde substrate

4.3.1.a 2-Trimethylsilyl benzaldehyde
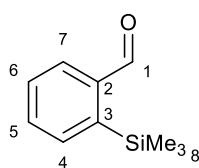
109

N-Butyl lithium **114** (2.5 M, 5.0 ml) was added dropwise to a solution of $N^1N^1N^2$-trimethylethylene-1,2-diamine **113** (1.15 g, 11.3 mmol) in hexane (30 ml) at -78 °C. Freshly distilled benzaldehyde **46** (1.00 g, 9.42 mmol) was added dropwise at -78 °C. N-butyl lithium **114** (2.5 M, 7.5 ml) was added dropwise at -78 °C. The solution was warmed to 4 °C for 15 h. Chlorotrimethylsilane **171** (6.13 g, 56.4 mmol) was added dropwise at -78

°C. The solution was stirred for 2 h at -78 °C, and then stirred for 45 minutes at r.t. Hydrochloric acid (2.5 M, 12.5 ml) was added to the solution. The organic phase was separated from the aqueous phase and was washed with diethyl ether (2 x 10 ml). The organic phases were dried using sodium sulphate; the solvent was then removed under reduced pressure to yield the crude product. The crude product was purified by column chromatography (9 : 1, hexane : ethyl acetate) to yield the pure title compound **109** as a yellow oil (0.18 g, 11%); **^{1}H NMR** (400 MHz, CDCl$_3$) δ_H: 0.36 (9H, s, Si(C^{8}H$_3$)$_3$), 7.53-7.54 (1H, m, C^{5}H), 7.56-7.61 (1H, m, C^{6}H), 7.73-7.74 (1H, m, C^{4}H), 7.91.7.93 (1H, m, C^{7}H), 10.17 (1H, s, C^{1}H); **^{13}C NMR** (175 MHz, CDCl$_3$); δ_C: 0.24 (SiCH$_3$), 129.3 (CHCHCH), 132.4 (C^6), 133 (CHCHCH), 135.5 (C^3), 193.6 (C^7); **^{29}Si NMR** (700 MHz, CDCl$_3$) δ_{Si}; -3.2 (CSi(CH$_3$)$_3$); **MS** *m/z* 163 ([M-CH$_3$]$^+$, 100%), 164 (15), 165 (4). All spectroscopic data was in good agreement with literature reports [69]

Solvent	Quenching agent	Column Conditions (hexane : ethyl acetate)	Butyl lithium equivalents	Pure yield (%)
THF	HCl	9 : 1	2.5	57

4.3.2 Synthesis of 1,2,4-triazolium salt

4.3.2.a 6,7-Dihydro-2-pentafluorophenyl-5H-pyrrolo[2,1-c]-1,2,4-triazolium tetrafluoroborate
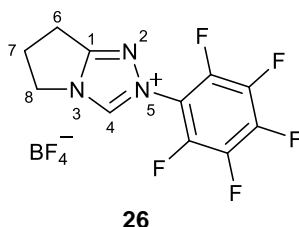
26

Based on a procedure by Rovis *et al.*[68], trimethyloxonium tetrafluoroborate **172** (3.22 g, 22.0 mmol) and 2-pyrrolidinone **146** (1.85 g, 22.0 mmol) in dry dichloromethane (50 mL) were stirred for 24 h at r.t. under argon. Pentafluorophenyl hydrazine **173** (4.33 g, 22.0 mmol) was added, and the solution was stirred for 48 h at r.t. under an inert atmosphere. The solvent was removed under reduced pressure. Triethyl orthoformate **174** (44.6 g, 300 mmol) was added to the residue. The solution was refluxed for 24 h. The solvent was removed under reduced pressure. The precipitate was washed with ethyl acetate to yield the pure title compound **26** as a pale yellow solid. (5.18 g, 66%); **EA** (Found: C, 36.3; H, 1.9; N, 11.6. $C_{11}H_7BF_9N_3$ requires C, 36.4; H 1.9; N 11.6); **^{1}H NMR** (400 MHz, CD_3CN) δ_H: 2.79 (2H, q, *J* 7.4, C^7H_2), 3.19 (2H, t, *J* 7.5, C^6H_2), 4.44 (2H, t, *J* 7.4, C^8H_2), 9.59 (1H, s, C^4H); **^{13}C NMR** (100 MHz, CDCN) δ_C: 22.7 (C^7), 27.5 (C^6), 49.4 (C^8), 143.6 (C^1), 165.8 (C^4); **^{19}F NMR** (400 MHz, CDCN) δ_F: -146.9 (2F, m, ArF), -149.4 (F, tt, *J* 20.8, 4.0, ArF), -151.9 (s, BF_4), -161.4 (2F, m, ArF); **MS** *m/s* 276 (M^+, 38), 277 ($[M + H]^+$, 100). All spectroscopic data was in good agreement with literature reports [28]

4.3.2.b 6,7-Dihydro-2-(4-fluorophenyl)-5H-pyrrolo[2,1-c]-1,2,4-triazolium tetrafluoroborate
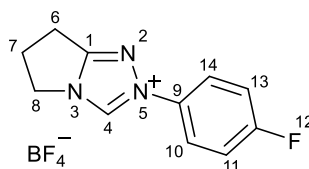
122

Based on a procedure by Rovis *et al.*[68], trimethyloxonium tetrafluoroborate **172** (3.22 g, 22.0 mmol) and 2-pyrrolidinone **146** (1.85 g, 22.0 mmol) in dry dichloromethane (50 mL) were stirred for 24 h at r.t. under argon. Parafluorophenyl hydrazine **175** (4.33 g, 22.0 mmol) was added, and the solution was stirred for 48 h at r.t. under an inert atmosphere. The solvent was removed under reduced pressure. Triethyl orthoformate **174** (44.6 g, 300 mmol) was added to the residue. The solution was refluxed for 24 h. The solvent was removed under reduced pressure. The precipitate was washed with ethyl acetate to yield the pure title compound **122** as a pale yellow solid (3.33 g, 52%); **EA** (Found: C, 45.0; H, 3.8; N, 14.5. $C_{11}H_{11}BF_5N_3$ requires C, 45.4; H, 3.8; N, 14.4); **^{1}H NMR** (400 MHz, CDCl$_3$) δ_H: 2.90 (2H, q, J 7.6, C^7H_2), 3.27 (2H, t, J 7.8, C^6H_2), 4.65 (2H, t, J 7.4, C^8H_2), 7.25-7.26 (2H, m, $C^{11}H$-C^{12}-$C^{13}H$), 7.84-7.85 (1H, m, $C^{10}H$-C^9-$C^{14}H$), 10.18 (1H, s, C^4H); **^{19}F NMR** (400 MHz, CDCN) δ_F: -108.3 (1F, s, CF), -151.9 (4F, s, BF_4^-). All spectroscopic data was in good agreement with literature reports [75]

4.3.2.c 6,7-Dihydro-2-(3-chlorophenyl)-5H-pyrrolo[2,1-c]-1,2,4-triazolium tetrafluoroborate

142
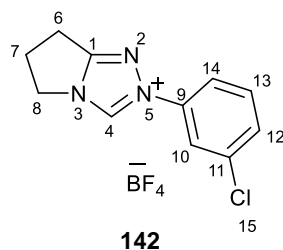
Based on a procedure by Rovis *et al.*[68], trimethyloxonium tetrafluoroborate **172** (2.25 g, 15.0 mmol) and 2-pyrrolidinone **146** (1.18 g, 14.0 mmol) in dry dichloromethane (50 mL) were stirred for 24 h at r.t. under argon. *m*-chlorophenyl hydrazine hydrochloride **176** (3.56 g, 20.0 mmol) was dissolved in aqueous NaOH 1 M and extracted into dichloromethane. The solution was immediately added to the reaction mixture, and the solution was stirred for a further 48 h at r.t. under an inert atmosphere. The solvent was removed under reduced pressure. To the residue, methanol (15 mL) and triethyl orthoformate **174** (40 mL, 238 mmol) were added. The solution was refluxed for 48 h. The solvent was removed under reduced pressure. The precipitate was washed with ethyl acetate to yield the pure title compound **142** as a pale yellow solid (3.83 g, 83%); **^{1}H NMR** (700 MHz, CD$_3$CN) δ_H: 2.82 (2H, q, *J* 7.6, C^{7}H$_2$), 3.21 (2H, t, J 7.6, C^{6}H$_2$), 4.43 (2H, t, J 7.4, C^{8}H$_2$), 7.42-7.49 (2H, m, C^{12}HC^{13}H), 7.56-7.58 (1H, m, C^{14}H), 7.73-7.74 (1H, m, C^{10}H), 9.65 (1H, s, C^{4}H); **^{13}C NMR** (175 MHz, CDCN) δ_C: 21.5 (C^6), 26.6 (C^7), 47.7 (C^8), 119.9 (C^{14}), 121.4 (C^{10}), 130.8 (C^{13}), 131.7 (C^{12}), 135.2 (C^{11}), 136.6 (C^9), 137.6 (C^1), 163.8 (C^4); **HMRS** (ES+): [M-BF$_4$]$^+$ C$_{11}$H$_{11}$N$_3$Cl requires 220.0642, found 220.0657.

4.3.2.d 6,7-Dihydro-2-(4-bromophenyl)-5H-pyrrolo[2,1-c]-1,2,4-triazolium tetrafluoroborate
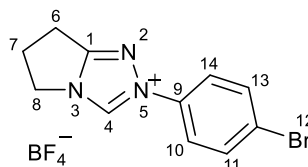
144

Based on a procedure by Rovis *et al.*[68], trimethyloxonium tetrafluoroborate **172** (3.22 g, 22.0 mmol) and 2-pyrrolidinone **146** (1.85 g, 22.0 mmol) in dry dichloromethane (50 mL) were stirred for 24 h at r.t. under argon. *p*-bromophenyl hydrazine **177** (4.33 g, 22.0 mmol) was added, and the solution was stirred for 48 h at r.t. under an inert atmosphere. The solvent was removed under reduced pressure. To the residue, triethyl orthoformate **174** (44.6 g, 300.0 mmol), and HCl in dioxane (4 N, 2 mL) were added. The solution was refluxed for 48 h. The solvent was removed under reduced pressure. The precipitate was washed with ethyl acetate to yield the pure title compound **144** as a pale yellow solid. (4.41 g, 57%); **EA** (Found: C, 37.2; H, 3.1; N, 11.8. $C_{11}H_{11}BF_4BrN_3$ requires C, 37.6; H, 3.2; N, 11.9); **^{1}H NMR** (400 MHz, CD_3CN) δ_H: 2.83 (2H, q, J 7.6, C^7H_2), 3.21 (2H, t, J 7.7, C^6H_2), 4.43 (2H, t, J 7.5, C^8H_2), 7.54-7.57 (2H, m, $C^{11}H$-C^{12}-$C^{13}H$), 7.65-7.67 (2H, m, $C^{10}H$-C^9-$C^{14}H$), 9.59 (1H, s, C^4H). All spectroscopic data was in good agreement with literature reports [75].

4.3.2.e 5-(2-(4-Bromophenyl)hydrazinyl)-3,4-dihydro-2H-pyrrol-1-ium
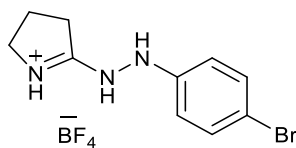
149' (X = 4Br)

Trimethyloxonium tetrafluoroborate **172** (3.22 g, 22.0 mmol) and 2-pyrrolidinone **146** (1.85 g, 22.0 mmol) in dry dichloromethane (50 mL) were stirred for 24 h at r.t. under argon. *p*-bromophenyl hydrazine **175** (4.33 g, 22.0 mmol) was added, and the solution was stirred for 48 h at r.t. under an inert atmosphere. The solvent was removed under reduced pressure to yield the pure title compound **149'** (X = 4-Br) as a white solid (5.71 g, 76%); **¹H NMR** (600 MHz, CD₃CN) δ_H: 2.30 (2H, q, *J* 7.7), 2.99 (2H, t, *J* 8.1), 3.67 (2H, t, *J* 7.2), 6.76-7.80 (2H, m), 7.02 (1H, s), 7.36-7.40 (2H, m), 8.40 (1H, s), 7.03 (1H, s); **¹³C NMR** (150 MHz, CDCN); δ_C: 20.5, 28.7, 47.3, 113.7, 115.7, 132.1, 144.7, 172.27.

4.3.2.f Synthesis of benzaldehyde from 2-trimethylsilylbenzaldehyde

109   **46**
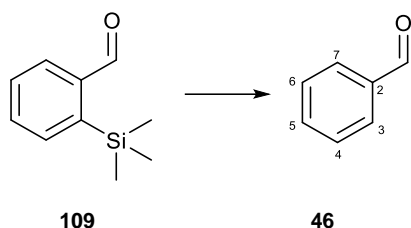
2-Trimethylsilylbenzaldehyde **109** (0.200 g, 1.12 mmol) was added to a solution of tetrabutylammonium fluoride **119** (0.88 g, 3.37 mmol) in THF (3.36 mL). The solution was stirred for 24 h at r.t. The solvent was removed under reduced pressure. The resulting oil was dissolved in DCM (5 ml). The solution was washed with water (3 x 5 mL). The organic phase was dried with sodium sulphate. The solvent was removed under reduced pressure to yield the title compound **46**. (0.11 g, 91%); **^{1}H NMR** (400 MHz, CD_3CN) δ_H: 7.55-7.56 (2H, m, C^4H-C^5-C^6H), 7.65-7.67 (1H, m, C^5H), 7.90-7.91 (2H, m, C^3H-C^2-C^7H), 10.04 (1H, s, C^1H). All spectroscopic data was in good agreement with literature reports [76].

4.4 X-ray crystallography

4.4.1 2-Trimethylsilyl benzoic acid

For data, see **Appendix 1**.

4.4.2 6,7-Dihydro-2-(3-chlorophenyl)-5H-pyrrolo[2,1-c]-1,2,4-triazolium tetrafluoroborate

For data, see **Appendix 2**.

4.4.3 6,7-Dihydro-2-(4-bromophenyl)-5H-pyrrolo[2,1-c]-1,2,4-triazolium tetrafluoroborate

For data, see **Appendix 2**.

4.5 Preparations of Solutions

4.5.1 Studies of the NHC-catalysed benzoin condensation of 2-trimethylsilylbenzaldehyde

Solutions of triethylamine buffer in methanol-d_4 were prepared from distilled triethylamine and dried triethylamine hydrochloride. Solutions were prepared immediately prior to use.

4.5.2 Buffer preparation

Stock solutions of buffers were produced in advance of the kinetic experiments. The required amount of deuterium chloride or monobasic phosphate was added to volumetric flasks (5 mL). The remaining volume of solution of the volumetric flask was filled with d_4-methanol. The flask was sealed airtight and stored in a desiccator until use.

4.6   Kinetic methods

Buffer and DCl solutions for kinetic methods were prepared in stock solutions in advance of the kinetic experiments for all concentrations of deuterium chloride, and of monobasic phosphate. The benzaldehyde and triazolium salt for each desired reaction was dissolved in the relevant solvent, and 0.800 ml of this solution was pipetted into an NMR tube. The NMR tube was incubated at 25 °C and the progression of the reaction was followed by ^{1}H NMR spectroscopy

4.6.1   NMR conditions

For studies of the benzoin condensation, ^{1}H NMR spectra were recorded on an Oxford Varian Inova 500 spectrometer thermostated at 25 °C, with a relaxation delay of 5 s, sweep width of 10,000 Hz, acquisition time of 2 s and 45° pulse angle. Spectra were run with 32 transients (total running time ~4 min). Measurement times were taken from the start of the acquisition.

In all cases, ^{1}H NMR spectral baselines were subject to a first–order drift correction before integration of the peak areas.

5   References

1.   Hine, J. S. *Divalent Carbon*. (Ronald Press Co New York, 1964).

2.   Vasiliu, M., Peterson, K. A., Arduengo, A. J. & Dixon, D. A. Characterization of Carbenes via Hydrogenation Energies, Stability, and Reactivity: What's in a Name? *Chem. Weinh. Bergstr. Ger.* **23**, 17556–17565 (2017).

3.   Arduengo, A. J., Harlow, R. L. & Kline, M. A stable crystalline carbene. *J. Am. Chem. Soc.* **113**, 361–363 (1991).

4.   Igau, A., Grutzmacher, H., Baceiredo, A. & Bertrand, G. Analogous Alpha,alpha'-Bis-Carbenoid Triply Bonded Species - Synthesis. *J. Am. Chem. Soc.* **110**, 6463–6466 (1988).

5.   Martin, D., Melaimi, M., Soleilhavoup, M. & Bertrand, G. A Brief Survey of our Contribution to Stable Carbene Chemistry. *Organometallics* **30**, 5304–5313 (2011).

6.   Pötter, B. & Seppelt, K. Trifluoroethylidynesulfur Trifluoride, F3C☐C☐SF3. *Angew. Chem. Int. Ed. Engl.* **23**, 150–150 (1984).

7.   Despagnet-Ayoub, E. *et al.* (Phosphino)(aryl)carbenes: effect of aryl substituents on their stabilization mode. *J. Am. Chem. Soc.* **125**, 124–130 (2003).

8.   Baceiredo, A. *et al.* Phosphinocarbene-phosphaalkene rearrangement and intramolecular Wittig-like reaction involving a phosphorus vinyl ylide. *J. Am. Chem. Soc.* **108**, 7868–7869 (1986).

9.   Breslow, R. On the Mechanism of Thiamine Action .4. Evidence from Studies on Model Systems. *J. Am. Chem. Soc.* **80**, 3719–3726 (1958).

10. Flanigan, D. M., Romanov-Michailidis, F., White, N. A. & Rovis, T. Organocatalytic Reactions Enabled by N-Heterocyclic Carbenes. *Chem. Rev.* **115**, 9307–9387 (2015).

11. Stetter, H. Catalyzed Addition of Aldehydes to Activated Double Bonds—A New Synthetic Approach. *Angew. Chem. Int. Ed. Engl.* **15**, 639–647 (1976).

12. Chow, K. Y.-K. & Bode, J. W. Catalytic generation of activated carboxylates: direct, stereoselective synthesis of beta-hydroxyesters from epoxyaldehydes. *J. Am. Chem. Soc.* **126**, 8126–8127 (2004).

13. Murry, J. A. *et al.* Synthesis of alpha-amido ketones via organic catalysis: thiazolium-catalyzed cross-coupling of aldehydes with acylimines. *J. Am. Chem. Soc.* **123**, 9696–9697 (2001).

14. Noonan, C., Baragwanath, L. & Connon, S. J. *Tetrahedron Lett* **49**, 4003–4006 (2008).

15. Mattson, A. E., Bharadwaj, A. R. & Scheidt, K. A. The thiazolium-catalyzed Sila-Stetter reaction: conjugate addition of acylsilanes to unsaturated esters and ketones. *J. Am. Chem. Soc.* **126**, 2314–2315 (2004).

16. Mattson, A. E., Bharadwaj, A. R., Zuhl, A. M. & Scheidt, K. A. Thiazolium-catalyzed additions of acylsilanes: a general strategy for acyl anion addition reactions. *J. Org. Chem.* **71**, 5715–5724 (2006).

17. Bourissou, D., Guerret, O., Gabbai, F. P. & Bertrand, G. Stable carbenes. *Chem. Rev.* **100**, 39–91 (2000).

18. Mitsch, R. Difluorodiazirine .3. Synthesis of Difluorocyclopropanes. *J. Am. Chem. Soc.* **87**, 758- (1965).

19. Moss, R. & Mallon, C. Characterization of Carbene Selectivity - Applications to Difluorocarbene. *J. Am. Chem. Soc.* **97**, 344–347 (1975).

20. Moss, R., Wlostowski, M., Shen, S., Kroghjespersen, K. & Matro, A. Dimethoxycarbene - Direct Observation of an Archetypal Nucleophilic Carbene. *J. Am. Chem. Soc.* **110**, 4443–4444 (1988).

21. Du, X. M. *et al.* Reactions of dimethoxycarbene and fluoromethoxycarbene with hydroxyl compounds. Absolute rate constants and the heat of formation of dimethoxycarbene. *J. Am. Chem. Soc.* **112**, 1920–1926 (1990).

22. Wang, J., Toscano, J., Platz, M., Nikolaev, V. & Popik, V. Dicarbomethoxycarbene - a Laser Flash-Photolysis Study. *J. Am. Chem. Soc.* **117**, 5477–5483 (1995).

23. Visser, P., Zuhse, R., Wong, M. W. & Wentrup, C. Reactivity of carbenes and ketenes in low-temperature matrices. Carbene. *J. Am. Chem. Soc.* **118**, 12598–12602 (1996).

24. Berndt, A. Classical and Nonclassical Methyleneboranes. *Angew. Chem.-Int. Ed.* **32**, 985–1009 (1993).

25. Moss, R. A., Mallon, C. B. & Ho, C.-T. The correlation of carbenic reactivity. *J. Am. Chem. Soc.* **99**, 4105–4110 (1977).

26. Massey, R. S., Collett, C. J., Lindsay, A. G., Smith, A. D. & O'Donoghue, A. C. Proton transfer reactions of triazol-3-ylidenes: kinetic acidities and carbon acid pKa values for twenty triazolium salts in aqueous solution. *J. Am. Chem. Soc.* **134**, 20421–20432 (2012).

27. Higgins, E. M. *et al.* pKas of the conjugate acids of N-heterocyclic carbenes in water. *Chem. Commun. Camb. Engl.* **47**, 1559–1561 (2011).

28. Li, Z., Li, X. & Cheng, J.-P. An Acidity Scale of Triazolium-Based NHC Precursors in DMSO. *J. Org. Chem.* **82**, 9675–9681 (2017).

29. Dunn, M. H., Konstandaras, N., Cole, M. L. & Harper, J. B. Targeted and Systematic Approach to the Study of pKa Values of Imidazolium Salts in Dimethyl Sulfoxide. *J. Org. Chem.* **82**, 7324–7331 (2017).

30. O'Donoghue, A. C. & Massey, R. S. Acid–Base Chemistry of Carbenes. in *Contemporary Carbene Chemistry* 75–106 (Wiley-Blackwell, 2013).

31. Tucker, D. E. *et al.* Proton transfer reactions of N-aryl triazolium salts: unusual ortho-substituent effects. *J. Phys. Org. Chem.* **28**, 108–115 (2015).

32. Collett, C. J. *et al.* Rate and Equilibrium Constants for the Addition of N-Heterocyclic Carbenes into Benzaldehydes: A Remarkable 2-Substituent Effect. *Angew. Chem. Int. Ed Engl.* **54**, 6887–6892 (2015).

33. Delany, E. G. & Connon, S. J. Highly chemoselective intermolecular cross-benzoin reactions using an ad hoc designed novel N-heterocyclic carbene catalyst. *Org. Biomol. Chem.* **16**, 780–786 (2018).

34. Luo, Y.-R. *Comprehensive Handbook of Chemical Bond Energies*. (CRC Press, 2007).

35. Brook, A. G., Abdesaken, F., Gutekunst, B., Gutekunst, G. & Kallury, R. K. A solid silaethene: isolation and characterization. *J. Chem. Soc. Chem. Commun.* 191–192 (1981).

36. Wiberg, N., Niedermayer, W., Noth, H. & Warchhold, M. Compounds of silicon. 146 [1] Unsaturated silicon compounds. 59 [2] On the way to a disilyne -Si Si-: Formation of RHSi=SiHR and indication of the intermediate formation of RSi SiR (R = SiH(SitBu(3))(2)). *Z. Anorg. Allg. Chem.* **627**, 1717–1722 (2001).

37. Miracle, G. E., Ball, J. L., Powell, D. R. & West, R. The first stable 1-silaallene. *J. Am. Chem. Soc.* **115**, 11598–11599 (1993).

38. KIRA, M. Reactions of a stable dialkylsilylene and their mechanisms. *J. Chem. Sci.* **124**, 1205–1215 (2012).

39. Arrington, C. A., Petty, J. T., Payne, S. E. & Haskins, W. C. K. The reaction of dimethylsilylene with carbon monoxide in low-temperature matrices. *J. Am. Chem. Soc.* **110**, 6240–6241 (1988).

40. Mattson, A. E., Bharadwaj, A. R. & Scheidt, K. A. The Thiazolium-Catalyzed Sila-Stetter Reaction: Conjugate Addition of Acylsilanes to Unsaturated Esters and Ketones. *J. Am. Chem. Soc.* **126**, 2314–2315 (2004).

41. Mattson, A. E., Bharadwaj, A. R., Zuhl, A. M. & Scheidt, K. A. Thiazolium-Catalyzed Additions of Acylsilanes: A General Strategy for Acyl Anion Addition Reactions. *J. Org. Chem.* **71**, 5715–5724 (2006).

42. Labarre-Lainé, J., Beniazza, R., Desvergnes, V. & Landais, Y. Convergent Access to Bis-spiroacetals through a Sila-Stetter–Ketalization Cascade. *Org. Lett.* **15**, 4706–4709 (2013).

43. Labarre-Lainé, J., Periñan, I., Desvergnes, V. & Landais, Y. Synthesis of the C10–C24-Bis-Spiroacetal Core of 13-Desmethyl Spirolide C Based on a Sila-Stetter-Acetalization Process. *Chem. – Eur. J.* **20**, 9336–9341 (2014).

44. Dhara, D. *et al.* NHC-stabilized 1-hydrosilaimine: synthesis, structure and reactivity. *Chem. Commun. Camb. Engl.* **53**, 8592–8595 (2017).

45. Tanaka, H., Ichinohe, M. & Sekiguchi, A. An isolable NHC-stabilized silylene radical cation: synthesis and structural characterization. *J. Am. Chem. Soc.* **134**, 5540–5543 (2012).

46. Li, Y. *et al.* Trapping a Silicon(I) Radical with Carbenes: A Cationic cAAC-Silicon(I) Radical and an NHC-Parent-Silyliumylidene Cation. *Angew. Chem. Int. Ed Engl.* **56**, 7573–7578 (2017).

47. Wendel, D. *et al.* Silicon and Oxygen's Bond of Affection: An Acyclic Three-Coordinate Silanone and Its Transformation to an Iminosiloxysilylene. *J. Am. Chem. Soc.* **139**, 17193–17198 (2017).

48. Mondal, K. C., Roy, S. & Roesky, H. W. Silicon based radicals, radical ions, diradicals and diradicaloids. *Chem. Soc. Rev.* **45**, 1080–1111 (2016).

49. Ahmad, S. U., Szilvási, T. & Inoue, S. A facile access to a novel NHC-stabilized silyliumylidene ion and C-H activation of phenylacetylene. *Chem. Commun. Camb. Engl.* **50**, 12619–12622 (2014).

50. Sarkar, D. *et al.* Chalcogen-atom transfer and exchange reactions of NHC-stabilized heavier silaacylium ions. *Dalton Trans. Camb. Engl. 2003* **46**, 16014–16018 (2017).

51. Chan, Y.-C. *et al.* A Dimeric NHC-Silicon Monotelluride: Synthesis, Isomerization, and Reactivity. *Angew. Chem. Int. Ed Engl.* **56**, 11565–11569 (2017).

52. Hadlington, T. J., Szilvási, T. & Driess, M. Silylene-Nickel Promoted Cleavage of B-O Bonds: From Catechol Borane to the Hydroborylene Ligand. *Angew. Chem. Int. Ed Engl.* **56**, 7470–7474 (2017).

53. Dhara, D. *et al.* Assembly of NHC-stabilized 2-hydrophosphasilenes from Si(iv) precursors: a Lewis acid-base complex. *Dalton Trans. Camb. Engl. 2003* **45**, 19290–19298 (2016).

54. Lee, K., Zhugralin, A. R. & Hoveyda, A. H. Efficient C-B bond formation promoted by N-heterocyclic carbenes: synthesis of tertiary and quaternary B-substituted carbons through metal-free catalytic boron conjugate additions to cyclic and acyclic alpha,beta-unsaturated carbonyls. *J. Am. Chem. Soc.* **131**, 7253–7255 (2009).

55. Kleeberg, C. *et al.* Spectroscopic and structural characterization of the CyNHC adduct of B2pin2 in solution and in the solid state. *J. Org. Chem.* **77**, 785–789 (2012).

56. Wu, H., Radomkit, S., O'Brien, J. M. & Hoveyda, A. H. Metal-free catalytic enantioselective C-B bond formation: (pinacolato)boron conjugate additions to α,β-unsaturated ketones, esters, Weinreb amides, and aldehydes promoted by chiral N-heterocyclic carbenes. *J. Am. Chem. Soc.* **134**, 8277–8285 (2012).

57. Eck, M. *et al.* B-B bond activation and NHC ring-expansion reactions of diboron(4) compounds, and accurate molecular structures of B2(NMe2)4, B2eg2, B2neop2 and B2pin2. *Dalton Trans. Camb. Engl. 2003* **46**, 3661–3680 (2017).

58. Watanabe, T., Geib, S. J., Curran, D. P. & Taniguchi, T. N-Heterocyclic Carbene

    Boranes are Hydrogen Donors in Masamune-Bergman Reactions of

    Benzo[3,4]cyclodec-3-ene-1,5-diynes. *J. Org. Chem.* **82**, 13034–13042 (2017).

59. Patra, A. *et al.* N-Heterocyclic-Carbene-Catalyzed Umpolung of Imines. *Angew.*

    Chem. Int. Ed Engl. **56**, 2730–2734 (2017).

60. Mahatthananchai, J., Kaeobamrung, J. & Bode, J. W. Chiral N-Heterocyclic Carbene

    Catalyzed Annulations of Enals and Ynals with Stable Enols: A Highly

    Enantioselective Coates-Claisen Rearrangement. *ACS Catal.* **2**, 494–503 (2012).

61. Movassaghi, M. & Schmidt, M. A. N-heterocyclic carbene-catalyzed amidation of

    unactivated esters with amino alcohols. *Org. Lett.* **7**, 2453–2456 (2005).

62. Binanzer, M., Hsieh, S.-Y. & Bode, J. W. Catalytic kinetic resolution of cyclic

    secondary amines. *J. Am. Chem. Soc.* **133**, 19698–19701 (2011).

63. Ema, T., Nanjo, Y., Shiratori, S., Terao, Y. & Kimura, R. Solvent-Free Benzoin and

    Stetter Reactions with a Small Amount of NHC Catalyst in the Liquid or Semisolid

    State. *Org. Lett.* **18**, 5764–5767 (2016).

64. Fleige, M. & Glorius, F. α-Unsubstituted Pyrroles by NHC-Catalyzed Three-

    Component Coupling: Direct Synthesis of a Versatile Atorvastatin Derivative. *Chem.*

    Weinh. Bergstr. Ger. **23**, 10773–10776 (2017).

65. Patra, A. *et al.* Synthesis of 4-Difluoromethylquinolines by NHC-Catalyzed Umpolung

    of Imines. *Org. Lett.* **20**, 1086–1089 (2018).

66. Di Carmine, G. *et al.* Synthesis of functionalized imidazolidine-2-thiones via

    NHC/base-promoted aza-benzoin/aza-acetalization domino reactions. *Org. Biomol.*

    Chem. **15**, 8788–8801 (2017).

67. Kang, B. *et al.* Site-selective benzoin-type cyclization of unsymmetrical dialdoses catalyzed by N-heterocyclic carbenes for divergent cyclitol synthesis. *Chem. Commun. Camb. Engl.* **53**, 4469–4472 (2017).

68. Kerr, M. S., de Alaniz, J. R. & Rovis, T. An efficient synthesis of achiral and chiral 1,2,4-triazolium salts: Bench stable precursors for N-heterocyclic carbenes. *J. Org. Chem.* **70**, 5725–5728 (2005).

69. Ye, B.-H. & Naruta, Y. A novel method for the synthesis of regiospecifically sulfonated porphyrin monomers and dimers. *Tetrahedron* **59**, 3593–3601 (2003).

70. Zhu, J. PhD Thesis. (2019).

71. DiRocco, D. A., Oberg, K. M., Dalton, D. M. & Rovis, T. Catalytic Asymmetric Intermolecular Stetter Reaction of Heterocyclic Aldehydes with Nitroalkenes: Backbone Fluorination Improves Selectivity. *J. Am. Chem. Soc.* **131**, 10872-+ (2009).

72. O'Brien, J. M. & Hoveyda, A. H. Metal-Free Catalytic C–Si Bond Formation in an Aqueous Medium. Enantioselective NHC-Catalyzed Silyl Conjugate Additions to Cyclic and Acyclic α,β-Unsaturated Carbonyls. *J. Am. Chem. Soc.* **133**, 7712–7715 (2011).

73. Peon, J., Polshakov, D. & Kohler, B. Solvent reorganization controls the rate of proton transfer from neat alcohol solvents to singlet diphenylcarbene. *J. Am. Chem. Soc.* **124**, 6428–6438 (2002).

74. Fulmer, G. R. *et al.* NMR Chemical Shifts of Trace Impurities: Common Laboratory Solvents, Organics, and Gases in Deuterated Solvents Relevant to the Organometallic Chemist. *Organometallics* **29**, 2176–2179 (2010).

75. Massey, R. S. *et al.* Kinetic and structure–activity studies of the triazolium ion-catalysed benzoin condensation. *Org. Biomol. Chem.* **19**, 387–393 (2021).

76. Lee, J. Y., Fan, W. Y., Mak, K. H. G. & Leong, W. K. The formation of aldehydes from the photochemically activated reaction of Cp*Ir(CO)(Cl)(CH2R) complexes with water. *J. Organomet. Chem.* **724**, 275–280 (2013).

Appendix 1

Structure 130

Table 1 Crystal data and structure refinement for 16srv119.	
Identification code	16srv119
Empirical formula	$C_{10}H_{14}O_2Si$
Formula weight	194.30
Temperature/K	120.0
Crystal system	monoclinic
Space group	$P2_1/c$
a/Å	18.3577(9)
b/Å	7.6985(4)
c/Å	16.5650(8)
α/°	90.00
β/°	114.2744(18)
γ/°	90.00
Volume/Å^3	2134.10(18)
Z	8
ρ_{calc}g/cm^3	1.209
μ/mm^{-1}	0.187
F(000)	832.0
Crystal size/mm^3	$0.37 \times 0.24 \times 0.16$
Radiation	MoKα (λ = 0.71073)
2Θ range for data collection/°	4.86 to 60

Index ranges	$-25 \leq h \leq 25, -10 \leq k \leq 10, -23 \leq l \leq 23$
Reflections collected	44163
Independent reflections	6212 [R_{int} = 0.0460, R_{sigma} = 0.0341]
Data/restraints/parameters	6212/0/249
Goodness-of-fit on F^2	1.032
Final R indexes [I>=2σ (I)]	R_1 = 0.0397, wR_2 = 0.0917
Final R indexes [all data]	R_1 = 0.0635, wR_2 = 0.1011
Largest diff. peak/hole / e Å^{-3}	0.37/-0.26

Table 2 Fractional Atomic Coordinates ($\times 10^4$) and Equivalent Isotropic Displacement Parameters ($Å^2 \times 10^3$) for 16srv119. U_{eq} is defined as 1/3 of of the trace of the orthogonalised U_{IJ} tensor.				
Atom	***x***	***y***	***z***	**U(eq)**
Si1	1136.7(2)	1754.3(5)	2492.3(2)	16.22(9)
O1	324.4(6)	3684.3(14)	853.5(6)	23.0(2)
O2	548.5(7)	3454.2(17)	-365.3(7)	32.9(3)
C1	960.6(8)	1132.2(19)	653.9(9)	18.9(3)
C2	1155.8(7)	484.9(18)	1515.7(9)	16.8(3)
C3	1434.3(8)	-1229.6(19)	1666(1)	22.9(3)
C4	1527.3(9)	-2237(2)	1017.1(11)	28.4(3)

C5	1358.7(9)	-1543(2)	192.7(11)	28.7(3)
C6	1072.2(8)	138(2)	6.5(10)	25.2(3)
C7	587.1(8)	2868.9(19)	398.2(9)	19.9(3)
C8	1666.8(9)	3883(2)	2656.2(10)	25.1(3)
C9	101.1(8)	1926.3(18)	2428.9(9)	20.5(3)
C10	1746.3(9)	475(2)	3507.8(10)	29.3(3)
Si2	3837.9(2)	3006.5(5)	6474.4(2)	18.05(9)
O3	4535.1(7)	1108.5(14)	5476.7(7)	29.9(3)
O4	4675.0(7)	1845.2(16)	4248.2(7)	31.5(3)
C11	4013.2(8)	3819.9(18)	4803.2(9)	19.3(3)
C12	3734.5(8)	4297.7(18)	5449.8(9)	18.8(3)
C13	3367.2(9)	5930(2)	5333.9(10)	25.4(3)
C14	3275.4(9)	7008(2)	4628.6(11)	30.2(3)
C15	3548.2(9)	6503(2)	4001.5(10)	29.1(3)
C16	3919.2(8)	4909(2)	4091.3(9)	24.0(3)
C17	4427.9(8)	2138.2(19)	4875.7(9)	20.6(3)
C18	3275.7(10)	911(2)	6208.6(10)	28.9(3)
C19	3345.4(9)	4309(2)	7063.8(10)	26.0(3)
C20	4908.3(8)	2785(2)	7260.5(9)	23.2(3)

Atom	U_{11}	U_{22}	U_{33}	U_{23}	U_{13}	U_{12}
Si1	15.94(17)	17.32(18)	14.82(17)	3.24(14)	5.75(14)	1.10(14)
O1	29.2(5)	24.9(5)	16.3(5)	4.5(4)	10.6(4)	6.3(4)
O2	41.1(7)	41.2(7)	22.9(5)	13.0(5)	19.8(5)	17.3(6)
C1	15.1(6)	23.1(7)	18.8(6)	-0.9(5)	7.2(5)	-1.6(5)
C2	11.7(6)	18.3(6)	21.3(6)	0.8(5)	7.7(5)	-1.4(5)
C3	22.1(7)	18.7(7)	31.1(8)	3.0(6)	14.1(6)	-0.7(5)
C4	25.5(7)	18.2(7)	45.3(9)	-4.9(7)	18.6(7)	-2.4(6)
C5	24.4(7)	29.8(8)	34.6(8)	-13.0(7)	15.0(7)	-4.7(6)
C6	21.5(7)	33.3(8)	21.0(7)	-4.8(6)	9.1(6)	-2.1(6)
C7	15.8(6)	27.9(8)	14.7(6)	2.7(5)	4.8(5)	-0.3(5)
C8	22.8(7)	24.7(8)	25.7(7)	-1.7(6)	7.9(6)	-4.9(6)
C9	21.0(6)	20.0(7)	23.3(7)	1.4(5)	11.9(6)	0.6(5)
C10	29.4(8)	34.1(9)	21.9(7)	10.1(6)	7.9(6)	7.1(7)
Si2	17.34(18)	18.38(19)	20.00(19)	-0.91(15)	9.27(15)	1.14(14)
O3	46.6(7)	23.5(6)	30.2(6)	5.2(5)	26.7(5)	11.8(5)

Table 3 Anisotropic Displacement Parameters ($\text{Å}^2 \times 10^3$) for 16srv119. The Anisotropic displacement factor exponent takes the form: $-2\pi^2[h^2a^{*2}U_{11}+2hka^*b^*U_{12}+\ldots]$.

O4	44.9(7)	33.2(7)	23.4(5)	4.3(5)	21.0(5)	14.7(5)
C11	18.0(6)	20.0(7)	18.7(6)	-0.2(5)	6.2(5)	-0.4(5)
C12	15.5(6)	19.2(7)	20.8(7)	-0.2(5)	6.4(5)	0.5(5)
C13	23.3(7)	23.2(7)	29.9(8)	0.5(6)	10.9(6)	5.8(6)
C14	27.8(8)	22.0(8)	35.4(9)	5.4(6)	7.7(7)	6.1(6)
C15	29.2(8)	25.8(8)	26.4(8)	9.3(6)	5.6(6)	1.3(6)
C16	23.5(7)	26.2(8)	20.8(7)	2.7(6)	7.5(6)	-0.5(6)
C17	21.6(6)	23.0(7)	18.1(6)	-3.0(5)	9.0(5)	0.5(5)
C18	33.1(8)	26.3(8)	27.8(8)	-2.8(6)	13.0(7)	-7.0(6)
C19	20.5(7)	32.1(8)	28.2(8)	-3.4(6)	12.8(6)	3.4(6)
C20	19.9(7)	25.2(8)	25.0(7)	2.6(6)	9.8(6)	4.6(6)

Table 4 Bond Lengths for 16srv119.

Atom	Atom	Length/Å		Atom	Atom	Length/Å
Si1	C2	1.9027(14)		Si2	C12	1.9080(14)
Si1	C8	1.8680(15)		Si2	C18	1.8677(16)
Si1	C9	1.8651(14)		Si2	C19	1.8713(15)
Si1	C10	1.8719(15)		Si2	C20	1.8661(14)
O1	C7	1.2224(17)		O3	C17	1.2236(17)
O2	C7	1.3168(17)		O4	C17	1.3134(17)
C1	C2	1.4121(19)		C11	C12	1.4123(19)
C1	C6	1.3995(19)		C11	C16	1.3984(19)
C1	C7	1.483(2)		C11	C17	1.482(2)
C2	C3	1.4003(19)		C12	C13	1.402(2)
C3	C4	1.392(2)		C13	C14	1.386(2)
C4	C5	1.378(2)		C14	C15	1.382(2)
C5	C6	1.383(2)		C15	C16	1.381(2)

Table 5 Bond Angles for 16srv119.

Atom	Atom	Atom	Angle/°		Atom	Atom	Atom	Angle/°
C8	Si1	C2	112.56(6)		C18	Si2	C12	113.40(7)

141

C8	Si1	C10	104.35(7)		C18	Si2	C19	104.31(7)
C9	Si1	C2	111.30(6)		C19	Si2	C12	106.99(7)
C9	Si1	C8	113.82(7)		C20	Si2	C12	111.07(6)
C9	Si1	C10	107.87(7)		C20	Si2	C18	114.01(7)
C10	Si1	C2	106.30(7)		C20	Si2	C19	106.31(7)
C2	C1	C7	120.16(12)		C12	C11	C17	120.02(12)
C6	C1	C2	121.70(13)		C16	C11	C12	121.72(13)
C6	C1	C7	118.06(12)		C16	C11	C17	118.25(13)
C1	C2	Si1	126.34(10)		C11	C12	Si2	127.19(11)
C3	C2	Si1	117.77(10)		C13	C12	Si2	117.08(11)
C3	C2	C1	115.77(13)		C13	C12	C11	115.69(13)
C4	C3	C2	122.66(14)		C14	C13	C12	122.51(14)
C5	C4	C3	120.02(14)		C15	C14	C13	120.60(14)
C4	C5	C6	119.60(14)		C16	C15	C14	118.97(14)
C5	C6	C1	120.18(14)		C15	C16	C11	120.50(14)
O1	C7	O2	122.53(13)		O3	C17	O4	122.71(13)
O1	C7	C1	122.70(12)		O3	C17	C11	122.52(13)
O2	C7	C1	114.76(12)		O4	C17	C11	114.78(12)

<table>
<tr><td colspan="7" align="center">Table 6 Hydrogen Bonds for 16srv119.</td></tr>
<tr><td>**D**</td><td>**H**</td><td>**A**</td><td>**d(D-H)/Å**</td><td>**d(H-A)/Å**</td><td>**d(D-A)/Å**</td><td>**D-H-A/°**</td></tr>
<tr><td>O2</td><td>H2</td><td>O1[1]</td><td>0.93(3)</td><td>1.72(3)</td><td>2.6476(15)</td><td>175(2)</td></tr>
<tr><td>O4</td><td>H4A</td><td>O3[2]</td><td>0.93(2)</td><td>1.71(3)</td><td>2.6340(16)</td><td>175(2)</td></tr>
</table>

[1]-X,1-Y,-Z; [2]1-X,-Y,1-Z

A	B	C	D	Angle/°		A	B	C	D	Angle/°
C1	C2	Si1	C8	-48.85(13)		C11	C12	Si2	C18	-65.22(14)
C1	C2	Si1	C9	80.30(12)		C11	C12	Si2	C19	-179.67(12)
C1	C2	Si1	C10	-162.49(11)		C11	C12	Si2	C20	64.71(14)
C2	C1	C7	O1	-11.4(2)		C12	C11	C17	O3	0.9(2)
C2	C1	C7	O2	169.66(13)		C12	C11	C17	O4	-178.70(13)
C3	C2	Si1	C8	127.04(11)		C13	C12	Si2	C18	117.18(12)
C3	C2	Si1	C9	-103.81(11)		C13	C12	Si2	C19	2.73(13)
C3	C2	Si1	C10	13.39(12)		C13	C12	Si2	C20	-112.89(12)
C6	C1	C7	O1	165.40(13)		C16	C11	C17	O3	-179.95(14)
C6	C1	C7	O2	-13.57(18)		C16	C11	C17	O4	0.43(19)

Table 7 Selected Torsion Angles for 16srv119.

Table 8 Hydrogen Atom Coordinates ($\mathring{A}\times10^4$) and Isotropic Displacement Parameters ($\mathring{A}^2\times10^3$) for 16srv119.				
Atom	*x*	*y*	*z*	**U(eq)**
H3	1565	-1725	2234	27
H4	1707	-3404	1143	34
H5	1439	-2214	-245	34
H6	951	619	-563	30
H8A	2143	3749	2535	38
H8B	1826	4271	3269	38
H8C	1309	4746	2251	38
H9A	-233	2581	1898	31
H9B	114	2529	2955	31
H9C	-122	760	2400	31
H10A	1505	-673	3473	44
H10B	1762	1088	4033	44
H10C	2291	341	3548	44
H2	259(15)	4490(30)	-506(16)	69(7)
H13	3174	6312	5755	31
H14	3023	8105	4576	36

H15	3482	7240	3516	35
H16	4112	4549	3666	29
H18A	3540	92	5963	43
H18B	2728	1118	5773	43
H18C	3264	423	6750	43
H19A	2778	4460	6677	39
H19B	3603	5450	7219	39
H19C	3398	3700	7604	39
H20A	5156	3938	7396	35
H20B	5189	2067	6991	35
H20C	4942	2235	7808	35
H4A	4929(13)	770(30)	4343(15)	64(7)

Appendix 2

Structure 142

Table 1 Crystal data and structure refinement for 18srv431.	
Identification code	18srv431
Empirical formula	$C_{11}H_{11}N_3Cl$ x BF_4
Formula weight	307.49
Temperature/K	120.0
Crystal system	monoclinic
Space group	$P2_1/c$
a/Å	9.0461(9)
b/Å	8.0475(8)
c/Å	17.6103(17)
α/°	90
β/°	93.866(4)
γ/°	90
Volume/Å^3	1279.1(2)
Z	4
ρ_{calc}g/cm^3	1.597
μ/mm^{-1}	0.339
F(000)	624.0
Crystal size/mm^3	$0.34 \times 0.29 \times 0.06$
Radiation	MoKα (λ = 0.71073)
2Θ range for data collection/°	4.514 to 57.986
Index ranges	-12 ≤ h ≤ 12, -10 ≤ k ≤ 10, -24 ≤ l ≤ 24
Reflections collected	25412
Independent reflections	3398 [R_{int} = 0.0598, R_{sigma} = 0.0398]
Data/restraints/parameters	3398/0/225
Goodness-of-fit on F^2	1.025

Final R indexes [I>=2σ (I)]	$R_1 = 0.0462$, $wR_2 = 0.1087$
Final R indexes [all data]	$R_1 = 0.0703$, $wR_2 = 0.1213$
Largest diff. peak/hole / e Å^{-3}	0.51/-0.61

Table 2 Fractional Atomic Coordinates ($\times 10^4$) and Equivalent Isotropic Displacement Parameters (Å$^2 \times 10^3$) for 18srv431. U_{eq} is defined as 1/3 of of the trace of the orthogonalised U_{IJ} tensor.

Atom	*x*	*y*	*z*	U(eq)
Cl1	8802.6(6)	6379.7(8)	5660.8(4)	57.2(2)
N1	3649.3(16)	8938.0(18)	5753.8(8)	25.2(3)
N2	2216.3(18)	9212(2)	5468.2(9)	38.3(4)
N3	2655.6(16)	10370.3(18)	6589.9(8)	25.2(3)
C1	3904(2)	9637(2)	6429.1(10)	27.4(4)
C2	1653(2)	10090(3)	6000.1(11)	33.2(4)
C3	212(2)	10882(4)	6147.0(15)	51.9(6)
C4	642(2)	12058(3)	6809.6(14)	45.4(5)
C5	2066(2)	11354(3)	7203.3(12)	34.9(4)
C6	4668(2)	8006(2)	5331.1(10)	27.4(4)
C7	4220(3)	7434(2)	4610.5(11)	34.5(4)
C8	5216(3)	6505(2)	4221.5(12)	41.1(5)
C9	6613(3)	6161(2)	4533.1(12)	39.6(5)
C10	7037(2)	6778(3)	5251.6(12)	37.7(5)
C11	6071(2)	7703(2)	5660.5(11)	32.1(4)
F1	2824.5(12)	4992.2(13)	7872.9(6)	36.2(3)
F2	2058.2(12)	6368.1(15)	6784.8(6)	37.0(3)
F3	2820.0(14)	7796.6(14)	7842.6(7)	39.0(3)
F4	4488.6(12)	6372.1(15)	7197.8(7)	40.6(3)
B1	3031(2)	6387(2)	7418.9(11)	24.7(4)

Atom	U_{11}	U_{22}	U_{33}	U_{23}	U_{13}	U_{12}
Cl1	39.8(3)	64.2(4)	69.9(4)	-26.5(3)	20.1(3)	0.3(3)
N1	32.6(8)	24.1(7)	18.9(7)	1.0(6)	2.1(5)	-9.9(6)
N2	30.0(8)	59.3(11)	25.3(8)	-4.8(8)	-0.9(6)	-10.4(8)
N3	31.8(8)	20.4(7)	23.2(7)	0.8(6)	0.7(6)	-4.0(6)
C1	35.3(9)	20.1(8)	26.2(9)	-2.4(7)	-3.0(7)	-0.9(7)
C2	29.9(9)	43.9(11)	25.7(9)	1.1(8)	1.2(7)	-11.2(8)
C3	28.3(11)	83.8(19)	43.1(13)	-11.1(13)	-1.1(9)	-0.8(12)
C4	27.6(10)	57.2(15)	51.7(14)	-6.0(12)	4.0(9)	1.1(10)
C5	40.9(11)	29.3(10)	34.2(10)	-7.0(9)	-0.2(8)	5.1(9)
C6	42.2(10)	18.7(8)	22.4(8)	-0.4(6)	10.5(7)	-12.1(7)
C7	59.5(13)	23.4(9)	20.6(9)	2.2(7)	2.3(8)	-7.6(9)
C8	78.6(16)	25.3(10)	20.4(9)	-1.4(8)	11.0(9)	-11.0(10)
C9	67.6(14)	21.7(9)	32.7(10)	-2.6(8)	26.5(10)	-9.9(9)
C10	43.6(11)	30.9(10)	41.0(11)	-5.7(9)	19.0(9)	-11.5(8)
C11	37.9(10)	31.6(10)	28.1(9)	-8.6(8)	11.7(8)	-11.3(8)
F1	38.9(6)	28.3(6)	41.6(7)	13.1(5)	2.8(5)	-0.9(5)
F2	37.2(6)	46.5(7)	26.4(6)	0.7(5)	-4.1(4)	-0.1(5)
F3	52.0(7)	28.9(6)	36.8(6)	-6.5(5)	7.5(5)	-2.3(5)
F4	29.1(6)	51.4(7)	42.3(7)	15.0(6)	10.5(5)	7.0(5)
B1	27.5(9)	24.0(9)	22.7(9)	2.5(7)	2.9(7)	2.1(7)

Table 3 Anisotropic Displacement Parameters ($\text{Å}^2 \times 10^3$) for 18srv431. The Anisotropic displacement factor exponent takes the form: $-2\pi^2[h^2a^{*2}U_{11}+2hka^*b^*U_{12}+\ldots]$.

Table 4 Bond Lengths for 18srv431.						
Atom	**Atom**	**Length/Å**		**Atom**	**Atom**	**Length/Å**
Cl1	C10	1.737(2)		C6	C7	1.384(3)
N1	N2	1.376(2)		C6	C11	1.381(3)
N1	C1	1.322(2)		C7	C8	1.387(3)
N1	C6	1.434(2)		C8	C9	1.372(4)
N2	C2	1.304(3)		C9	C10	1.389(3)
N3	C1	1.322(2)		C10	C11	1.386(3)
N3	C2	1.351(2)		F1	B1	1.398(2)
N3	C5	1.468(2)		F2	B1	1.374(2)
C2	C3	1.490(3)		F3	B1	1.378(2)
C3	C4	1.533(4)		F4	B1	1.400(2)
C4	C5	1.530(3)				

Table 5 Bond Angles for 18srv431.							
Atom	**Atom**	**Atom**	**Angle/°**		**Atom**	**Atom**	**Atom**	**Angle/°**
N2	N1	C6	121.09(14)		C11	C6	N1	118.60(16)
C1	N1	N2	111.28(15)		C11	C6	C7	122.00(18)
C1	N1	C6	127.62(16)		C6	C7	C8	118.2(2)
C2	N2	N1	103.20(15)		C9	C8	C7	121.5(2)
C1	N3	C2	107.42(16)		C8	C9	C10	118.9(2)
C1	N3	C5	139.15(16)		C9	C10	Cl1	120.12(17)
C2	N3	C5	113.43(16)		C11	C10	Cl1	118.54(16)
N1	C1	N3	106.47(16)		C11	C10	C9	121.3(2)
N2	C2	N3	111.62(17)		C6	C11	C10	118.07(18)
N2	C2	C3	138.19(18)		F1	B1	F4	108.48(14)
N3	C2	C3	110.19(17)		F2	B1	F1	110.67(15)
C2	C3	C4	102.47(17)		F2	B1	F3	110.15(15)

C5	C4	C3	106.21(19)		F2	B1	F4	109.71(15)
N3	C5	C4	101.70(16)		F3	B1	F1	108.82(15)
C7	C6	N1	119.40(18)		F3	B1	F4	108.96(15)

Table 6 Selected Torsion Angles for 18srv431.									
A	**B**	**C**	**D**	**Angle/°**		**A**	**B**	**C**	**D**	**Angle/°**
C7	C6	N1	N2	2.8(2)		C11	C6	N1	N2	-177.00(16)
C7	C6	N1	C1	-176.80(17)		C11	C6	N1	C1	3.4(3)

Table 7 Hydrogen Atom Coordinates ($\text{Å}\times10^4$) and Isotropic Displacement Parameters ($\text{Å}^2\times10^3$) for 18srv431.				
Atom	*x*	*y*	*z*	**U(eq)**
H1	4770(20)	9620(30)	6728(13)	37(6)
H3A	-220(40)	11450(40)	5731(19)	76(10)
H3B	-430(30)	10020(40)	6287(17)	75(9)
H4A	-110(30)	12210(30)	7182(15)	52(7)
H4B	860(40)	13310(40)	6587(19)	94(11)
H5A	2710(30)	12190(30)	7354(14)	49(7)
H5B	1890(30)	10640(30)	7602(15)	51(7)
H7	3290(20)	7670(30)	4383(13)	34(6)
H8	4940(30)	6120(30)	3750(15)	51(7)
H9	7310(30)	5460(30)	4294(14)	49(7)
H11	6370(30)	8100(30)	6166(14)	48(7)

Structure 144

Table 1 Crystal data and structure refinement for 17srv303.	
Identification code	17srv303
Empirical formula	$C_{11}H_{11}BrN_3$ x BF_4
Formula weight	351.95
Temperature/K	120.0
Crystal system	monoclinic
Space group	$P2_1/n$
a/Å	7.0877(3)
b/Å	12.1656(5)
c/Å	15.7597(7)
α/°	90
β/°	100.3689(15)
γ/°	90
Volume/Å^3	1336.71(10)
Z	4
ρ_{calc}g/cm^3	1.749

μ/mm^{-1}	3.114
F(000)	696.0
Crystal size/mm^3	0.33 × 0.21 × 0.1
Radiation	MoKα (λ = 0.71073)
2Θ range for data collection/°	5.96 to 59.994
Index ranges	-9 ≤ h ≤ 9, -17 ≤ k ≤ 17, -22 ≤ 1 ≤ 22
Reflections collected	28802
Independent reflections	3866 [R_{int} = 0.0287, R_{sigma} = 0.0158]
Data/restraints/parameters	3866/0/181
Goodness-of-fit on F^2	1.036
Final R indexes [I>=2σ (I)]	R_1 = 0.0213, wR_2 = 0.0551
Final R indexes [all data]	R_1 = 0.0251, wR_2 = 0.0567
Largest diff. peak/hole / e Å^{-3}	0.51/-0.36

Table 2 Fractional Atomic Coordinates (×10^4) and Equivalent Isotropic Displacement Parameters (Å^2×10^3) for 17srv303. U_{eq} is defined as 1/3 of of the trace of the orthogonalised U_{IJ} tensor.				
Atom	*x*	*y*	*z*	**U(eq)**
Br1	1950.9(2)	4178.5(2)	4921.8(2)	23.85(5)
N1	9831.3(14)	2252.6(8)	6221.1(6)	15.32(19)
N2	10705.2(16)	2411.9(9)	7068.5(7)	20.4(2)
N3	12381.1(14)	1301.9(8)	6380.4(7)	16.77(19)
C1	10844.6(17)	1582.4(10)	5807.6(8)	16.6(2)
C2	12246.3(18)	1808.1(10)	7136.8(8)	19.4(2)
C3	13880(2)	1496.2(12)	7826.6(10)	28.3(3)
C4	14721(2)	497.9(14)	7411.8(10)	33.1(3)
C5	14090.2(18)	593.9(11)	6434.0(9)	22.5(3)
C6	7992.7(16)	2722.4(9)	5902.1(8)	15.1(2)
C7	7065.7(17)	3282.7(10)	6475.4(8)	17.9(2)
C8	5257.9(18)	3724.1(11)	6176.8(8)	19.9(2)
C9	4426.1(17)	3587(1)	5320.1(8)	18.0(2)
C10	5351.0(18)	3029.2(10)	4745.6(8)	20.3(2)
C11	7161.1(18)	2593.2(11)	5038.8(8)	19.5(2)
F1	7863.3(12)	-82.8(7)	5578.6(5)	27.26(17)
F2	9118.3(13)	66.4(7)	7010.5(5)	27.27(18)
F3	10426.4(13)	-1112.6(8)	6162.3(6)	29.28(18)
F4	7498.5(14)	-1475.5(8)	6498.9(6)	33.7(2)
B1	8709(2)	-653.0(12)	6316.8(9)	19.1(3)

Table 3 Anisotropic Displacement Parameters ($\text{Å}^2 \times 10^3$) for 17srv303. The Anisotropic displacement factor exponent takes the form: $-2\pi^2[h^2a^{*2}U_{11}+2hka^*b^*U_{12}+\dots]$.						
Atom	**U_{11}**	**U_{22}**	**U_{33}**	**U_{23}**	**U_{13}**	**U_{12}**
Br1	13.61(7)	24.06(7)	32.12(8)	3.44(5)	-0.63(5)	2.24(4)
N1	15.0(4)	15.3(4)	15.0(4)	-2.3(4)	0.8(3)	0.6(3)
N2	20.0(5)	21.6(5)	17.4(5)	-5.7(4)	-3.3(4)	3.6(4)
N3	14.0(4)	16.0(5)	20.7(5)	-1.5(4)	4.0(4)	0.0(4)
C1	15.1(5)	17.6(5)	17.7(5)	-0.6(4)	4.2(4)	0.4(4)
C2	18.0(5)	18.1(5)	20.7(6)	-4.3(4)	-0.5(4)	1.3(4)
C3	23.8(6)	29.7(7)	27.0(7)	-7.5(5)	-7.5(5)	9.2(5)
C4	29.5(7)	36.4(8)	31.3(7)	-1.1(6)	-0.6(6)	15.7(6)
C5	14.6(5)	23.2(6)	29.5(7)	-2.7(5)	3.6(5)	4.8(4)
C6	13.6(5)	13.7(5)	17.6(5)	-0.4(4)	1.6(4)	0.1(4)
C7	16.7(5)	20.5(5)	16.2(5)	-1.8(4)	2.0(4)	1.5(4)
C8	17.3(6)	21.4(6)	21.4(6)	-1.6(5)	5.0(4)	2.3(4)
C9	12.2(5)	16.7(5)	24.0(6)	2.2(4)	0.6(4)	0.1(4)
C10	19.2(6)	20.5(6)	19.4(6)	-2.5(4)	-1.7(4)	-0.1(4)
C11	19.8(6)	20.0(6)	17.9(6)	-3.9(4)	1.3(4)	1.6(4)
F1	29.8(4)	30.2(4)	21.5(4)	5.1(3)	3.8(3)	5.9(3)
F2	37.7(5)	25.4(4)	20.7(4)	-6.8(3)	10.6(3)	-7.3(3)
F3	28.4(4)	34.2(4)	26.2(4)	-0.7(3)	7.6(3)	9.7(4)
F4	42.1(5)	35.0(5)	24.8(4)	-0.7(4)	8.1(4)	-20.9(4)
B1	22.1(7)	19.7(6)	16.6(6)	-0.2(5)	6.8(5)	-1.4(5)

155

Table 4 Bond Lengths for 17srv303.						
Atom	**Atom**	**Length/Å**		**Atom**	**Atom**	**Length/Å**
Br1	C9	1.8956(12)		C6	C7	1.3879(16)
N1	N2	1.3809(14)		C6	C11	1.3908(16)
N1	C1	1.3318(15)		C7	C8	1.3909(17)
N1	C6	1.4289(15)		C8	C9	1.3827(18)
N2	C2	1.3046(16)		C9	C10	1.3869(18)
N3	C1	1.3279(16)		C10	C11	1.3883(17)
N3	C2	1.3603(16)		F1	B1	1.3939(16)
N3	C5	1.4763(16)		F2	B1	1.3896(16)
C2	C3	1.4876(18)		F3	B1	1.4002(17)
C3	C4	1.549(2)		F4	B1	1.3814(16)
C4	C5	1.530(2)				

Table 5 Bond Angles for 17srv303.							
Atom	**Atom**	**Atom**	**Angle/°**		**Atom**	**Atom**	**Atom**	**Angle/°**
N2	N1	C6	120.40(10)		C7	C6	C11	121.69(11)
C1	N1	N2	111.82(10)		C11	C6	N1	119.87(10)
C1	N1	C6	127.64(10)		C6	C7	C8	118.98(11)
C2	N2	N1	102.94(10)		C9	C8	C7	119.26(11)
C1	N3	C2	107.52(10)		C8	C9	Br1	118.95(9)
C1	N3	C5	138.84(11)		C8	C9	C10	121.86(11)
C2	N3	C5	113.60(10)		C10	C9	Br1	119.18(9)
N3	C1	N1	105.86(10)		C9	C10	C11	119.12(11)
N2	C2	N3	111.87(11)		C10	C11	C6	119.08(11)
N2	C2	C3	137.21(12)		F1	B1	F3	108.07(11)
N3	C2	C3	110.90(11)		F2	B1	F1	109.92(11)
C2	C3	C4	101.52(11)		F2	B1	F3	108.86(11)
C5	C4	C3	107.48(12)		F4	B1	F1	110.13(12)
N3	C5	C4	100.96(10)		F4	B1	F2	110.02(11)
C7	C6	N1	118.42(10)		F4	B1	F3	109.80(11)

Table 6 Selected Torsion Angles for 17srv303.									
A	**B**	**C**	**D**	**Angle/°**		**A**	**B**	**C**	**D**	**Angle/°**
C1	N3	C2	N2	-0.92(15)		C4	C5	N3	C1	-162.55(15)
C2	C3	C4	C5	22.49(17)		C4	C5	N3	C2	14.64(15)
C3	C2	N3	C1	177.54(11)		C5	N3	C2	N2	-178.98(11)
C3	C2	N3	C5	-0.52(16)		C7	C6	N1	N2	-3.79(16)
C3	C4	C5	N3	-22.54(15)		C7	C6	N1	C1	171.44(12)
C4	C3	C2	N2	164.19(17)		C11	C6	N1	N2	177.43(11)
C4	C3	C2	N3	-13.71(16)		C11	C6	N1	C1	-7.34(18)

Table 7 Hydrogen Atom Coordinates (Å×10^4) and Isotropic Displacement Parameters (Å^2×10^3) for 17srv303.

Atom	x	y	z	U(eq)
H1	10532.33	1352.27	5223.15	20
H3A	13435.19	1286.77	8364.84	34
H3B	14826.63	2099.53	7950.62	34
H4A	16138.31	500.23	7565.21	40
H4B	14238.35	-196.19	7621.54	40
H5A	15090.92	945.34	6161.38	27
H5B	13759.72	-132.31	6164.44	27
H7	7656.94	3363.45	7062.79	21
H8	4602	4115.33	6557.2	24
H10	4753.82	2946.59	4159.16	24
H11	7822.54	2211.96	4655.17	23